
Check for updates

organisms utilize Fe in its ferrous [Fe(II)] rather than ferric [Fe(III)] form. However, under aerobic conditions, Fe(II) is rapidly oxidized to Fe(III) and subsequently forms insoluble Fe(III) (hydr)oxides. Therefore, the concentration of bioavailable Fe in most aqueous phase is generally so low (a few nM) that Fe scarcity is frequently limiting biological production in ecosystems (Martin and Fitzwater, 1988; Kendall et al., 2012). Such Fe limitations are especially pronounced in the surface of the oceans, for instance, affecting marine life forms such as algae (Martin and Fitzwater, 1988; Rue and Bruland, 1997; Emerson et al., 2012). Iron deficiency may also develop in terrestrial systems, particularly at calcareous sites because Fe solubility and thus availability in these alkaline soils is extremely low (Chen and Barak, 1982). Nevertheless, many terrestrial plants and microbes have developed sophisticated strategies to enable the usage and metabolism of Fe needed for their survival (Weber et al., 2006; Briat et al., 2007; Melton et al., 2014).

The Fe cycle in terrestrial environment is not only driven by abiotic chemical reactions, but also involves microbially mediated processes (Weber et al., 2006; Melton et al., 2014). Iron is a redox-sensitive element. Consequently, the cycling of Fe is largely related to reduction and oxidation processes, and frequently coupled to the cycles of other elements such as carbon (C), nitrogen (N), phosphorus (P), sulfur (S), and manganese (Mn) (Straub et al., 1996; Weber et al., 2006; Raiswell and Canfield, 2012). Changes in the Fe cycle may thus be a sensitive indicator of overall changes in the biogeochemistry of terrestrial and aquatic ecosystems.

Primary rock minerals contain Fe in both reduced and oxidized forms, such as siderite ($FeCO_3$), magnetite (Fe_3O_4), and pyrite (FeS_2), as well as Fe-containing silicates like olivine or pyroxene. In addition to the dominant oxidative chemical weathering under the influence of O_2, water and acids, the primary Fe(II) minerals can be accessed by lithotrophic Fe(II) oxidizing bacteria under both aerobic and anaerobic conditions (Weber et al., 2006). Under anaerobic conditions, Fe(II) is used as a source of electrons by phototrophic bacteria in the present of light to fix CO_2 or by nitrate-reducing Fe oxidizers with simultaneous reduction of nitrates, and thus is closely linked with C and N cycles (Weber et al., 2006; Hedrich et al., 2011). The Fe(III) species comprise disordered ferrihydrite [$(Fe^{3+})_2O_3$•$0.5H_2O$], which ages to ferrimagnetic ferrihydrite (Michel et al., 2010), and other amorphous or crystalline forms of Fe such as goethite [FeO(OH)], lepidocrocite [γ-FeO(OH)] or hematite [Fe_2O_3], as well as Fe-containing silicates (Raiswell and Canfield, 2012). These minerals are strong adsorbents for anions, and promote aggregate stabilization and the sequestration of soil organic carbon (Patrick Jr and Khalid, 1974; Stucki, 1988; Bowell, 1994; Kiem and Kögel-Knabner, 2002; Peretyazhko and Sposito, 2005; Herbel and Fendorf, 2006; Eusterhues et al., 2011). Therefore, Fe transformations and translocations are key processes in soil formation, particularly under acidic conditions with improved Fe solubility (van Breemen and Buurman, 2002).

Several reduction processes reduce Fe(III) to Fe(II), thus closing the Fe cycle of the ecosystem, unless there is an Fe export by plant uptake, by riverbank or surface erosion, or simply by leaching. The latter processes include water transport of aqueous Fe species and Fe-containing nanoparticles (< 100 nm) or colloids (< 1 μm; Lead and Wilkinson, 2007; Raiswell and Canfield, 2012; Gottselig et al., 2014, 2017). These processes can be schematized for soil-plant-freshwater systems as outlined in Fig. 1, and each of the indicated processes may summate a range of specific biogeochemical reactions.

Biogeochemical processes often lead to Fe isotope fractionation, leaving behind an Fe isotopic fingerprint on the compartments of the systems (e.g., vegetation, topsoil, subsoil, parent rock, or different water reservoirs, Fig. 1). Variations of these isotopic signatures potentially permit the reconstruction of the dominating mechanisms in the modern Fe cycle, as best shown in studies on ancient and modern marine Fe cycle (Dauphas et al., 2017). However, whenever the origin of Fe is intended to be traced using stable isotopes, a correct assignment of Fe isotope data to the underlying environmental processes requires that the different fractionation factors are known for all major pathways and pools of the Fe cycle in terrestrial ecosystems. Previous extensive reviews, such as by Anbar (2004), Johnson et al. (2004), Dauphas and Rouxel (2006), Johnson et al. (2008) and Dauphas et al. (2017), already provide us with great insights into fundamental and state-of-the-art knowledge and methodology (see also SI1) in Fe isotope systematics in cosmo- and terrestrial geochemistry. The present work thus mainly focuses on the current knowledge on Fe isotopic signatures of different compartments of terrestrial ecosystems (different soil orders, higher plants and freshwater bodies). In addition, the main Fe transformation processes that have to date been analyzed for changes in Fe isotope compositions are outlined to illustrate Fe isotope variations in above-mentioned ecosystem compartments.

2. Iron isotope fractionation processes

Naturally occurring Fe consists of four stable isotopes, ^{54}Fe (abundance 5.845%), ^{56}Fe (91.754%), ^{57}Fe (2.119%) and of ^{58}Fe (0.282%). Natural variation of Fe isotope composition is mostly due to mass dependent isotope fractionation, as a result of slight differences in efficiency of these isotopes in participating in chemical reactions and/or physical processes (Bigeleisen and Mayer, 1947; Schauble, 2004; Vanhaecke and Degryse, 2012). These differences in efficiency are related to a slight difference in thermodynamics for each different isotope (equilibrium effect) or in the rate at which the isotopes participate in a process or reaction (kinetic effect) (Bigeleisen and Mayer, 1947; Schauble, 2004; Vanhaecke and Degryse, 2012). Mass-independent isotope fractionation might also occur in nature, though in rare cases, such as during magnetite biomineralization by magnetotactic bacteria as recently suggested from a laboratory experiment by Amor et al. (2016, 2018).

Iron isotope composition in an unknown sample is commonly expressed as $\delta^{56}Fe$ (or sometimes $\delta^{57}Fe$) as the difference relative to the Fe isotopic standard IRMM-014:

$$\delta^{56}Fe = (({}^{56}Fe/{}^{54}Fe)_{sample}/({}^{56}Fe/{}^{54}Fe)_{IRMM-014} - 1) \times 1000\ (‰).$$

To describe the extent of the mass fractionation as a result of a process, the fractionation factor, or the α notation, is usually used:

$$\alpha_{B-A} = R_B/R_A$$

where R is the isotope ratio of $^{56}Fe/^{54}Fe$ or $^{57}Fe/^{54}Fe$, and A and B can either be the product and the substrate in a kinetically controlled process or the two phases in an equilibrium process. The apparent difference between the isotope composition of B and A is described by:

$$\Delta = \delta_B - \delta_A$$

and can often be converted to α using:

$$\Delta \approx 1000 \ln \alpha_{B-A}$$

For mass-dependent isotope fractionation, the relation between the fractionation factor α of the isotope ratio $^{56}Fe/^{54}Fe$ and that of $^{57}Fe/^{54}Fe$ can be described by the exponential law:

$$\alpha_{{}^{56}Fe/{}^{54}Fe} = (\alpha_{{}^{57}Fe/{}^{54}Fe})^{\beta}$$

where the scaling factors β for kinetic and equilibrium fractionation, respectively, are:

$$\beta_{kin} = ln\left(\frac{54}{56}\right)/ln\left(\frac{54}{57}\right)$$

$$\beta_{equil} = \left(\frac{1}{54} - \frac{1}{56}\right)/\left(\frac{1}{54} - \frac{1}{57}\right)$$

For mass-dependent isotope fractionation, $\delta^{57}Fe$ of a sample is about 1.5 times that of $\delta^{56}Fe$. Details on stable isotope fractionation laws are provided by Wiederhold (2015), Dauphas and Schauble (2016)

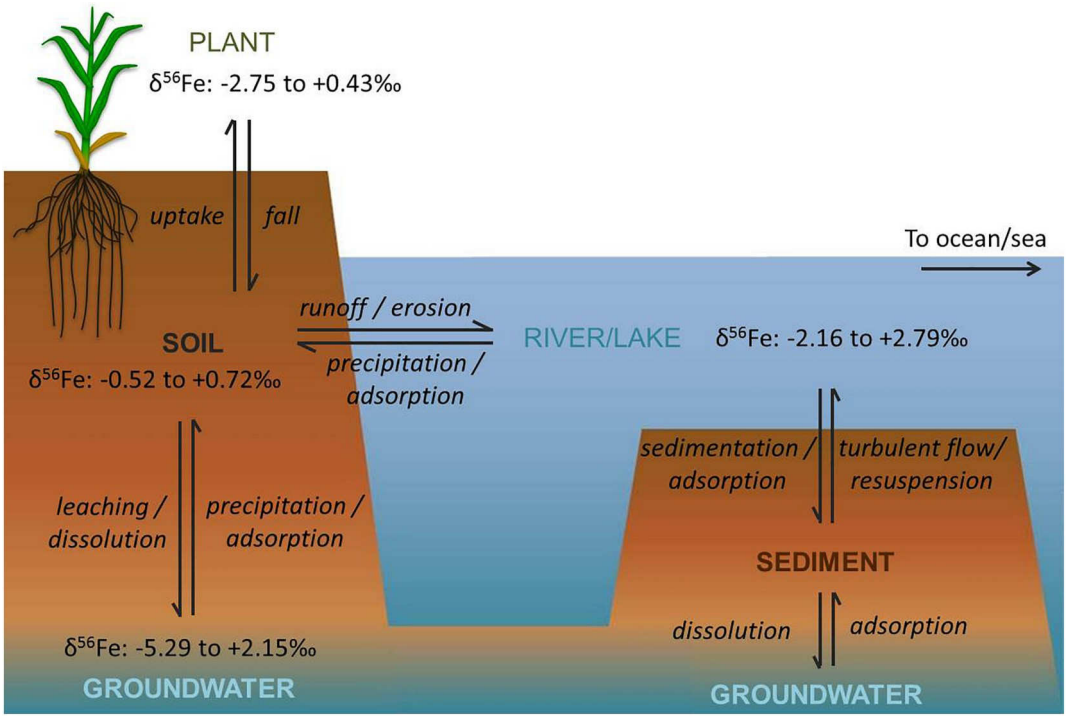

Fig. 1. Schematic view of main processes of Fe cycles in soil-plant-freshwater ecosystems. Iron isotope compositions of the ecosystem compartments that are reviewed in this paper are given with the range of Fe isotope compositions (expressed as δ^{56}Fe values, relative to Fe isotopic standard IRMM-014, see Section 2) of bulk soil, plant roots and aboveground tissues, and freshwaters including all particle size fractions, respectively. Due to limited isotopic data on freshwater sediments and different extraction methods employed to produce these data, the Fe isotope composition of freshwater sediments is not given. Note that in each ecosystem compartment, parts of the bioavailable Fe may be frequently cycled by biota, which is not explicitly illustrated in this figure.

and Dauphas et al. (2017). In the present review, we focus on mass-dependent Fe isotope fractionation and report δ^{56}Fe values of soils, plants and freshwaters, some of which are calculated from the δ^{57}Fe values in the literature based on the above-mentioned scaling factor.

Some of the largest isotope fractionations of Fe (up to 3.0‰) occur among changes between reduced and oxidized Fe forms (Johnson et al., 2002; Anbar et al., 2005), where oxidized Fe species are usually enriched in heavy Fe isotopes relative to their reduced counterparts (Johnson and Beard, 2006). While primary parent materials such as igneous rocks or Fe-containing minerals can display Fe isotopic variations (Poitrasson and Freydier, 2005; Teng et al., 2008; also see review article by Dauphas et al., 2017), pedogenic processes may further fractionate Fe isotopes leading to differed Fe isotope composition of the weathering products compared with their respective parent materials. Dissolved Fe leached from soils and particulate Fe from mechanical weathering, showing varied Fe isotope compositions between themselves, are important Fe inputs to water bodies and may implicate changes in the Fe isotopic signature of the water. Depending on Fe absorption pathway of the plant, as well as Fe availability in the growth media, the uptake of Fe by plants can result in large Fe isotope fractionation. The following sections summarize in detail the underlying processes leading to Fe isotope fractionation.

2.1. General description

Rock weathering and pedogenic processes take place continuously, leading to consecutive elemental transformation and translocation within and from the soil and sediment into other environmental compartments. In the case of Fe, dissolution of primary and secondary Fe minerals, transformation between Fe(II) and Fe(III), adsorption and precipitation of Fe species, changes of Fe-binding ligands, uptake by and translocation within plants, and microbial activities, are often accompanied by Fe isotope fractionation (e.g. Brantley et al., 2001, 2004; Guelke and von Blanckenburg, 2007; Teutsch et al., 2005; von Blanckenburg et al., 2009; Wiederhold et al., 2006). Iron isotope fractionation can be due to either kinetic or equilibrium fractionation effects, or a combination of both (Beard and Johnson, 2004; Johnson et al., 2004; Wiederhold et al., 2006).

In soil, Fe isotope fractionation is usually a result of several abiotic and biotic processes. However, certain processes can be dominant in specific soil profiles. For instance, in the absence of O_2, reductive dissolution of minerals by dissimilatory Fe reducing (DIR) bacteria preferentially releases light Fe isotopes into soil solution. The dissolved Fe (II) can be isotopically lighter by up to ~3‰ in δ^{56}Fe than the reactive Fe(III) on the mineral surface (e.g. hematite, goethite) determined under laboratory conditions (Crosby et al., 2005; Wu et al., 2010). This isotopically light Fe pool is easily leached, resulting in zonation in the soil profile with different Fe concentrations as well as Fe isotope compositions (Wiederhold et al., 2007b). It is worth noting that the extent in Fe isotope fractionation in soil may differ from that obtained in the laboratory studies due to differences in Fe pool sizes and studied phases between the soil and the laboratory settings (Wiederhold et al., 2007b). Nevertheless, both laboratory data and field studies have identified a series of processes that result in Fe isotope variations.

Table 1 provides a comprehensive, yet possibly incomplete, overview of the processes that have been investigated so far, either by laboratory experiments or field studies, for their Fe isotope fractionation potential. Although the processes in Table 1 are grouped into different categories, many of them are interlinked. For instance, precipitation of Fe(III) (hydr)oxides happens unavoidably after Fe(II) is oxidized to Fe (III). This precipitation is then followed by adsorption of aqueous Fe(II) [$Fe(II)_{aq}$] onto these newly formed precipitates. Table 1 attempts to present individual processes that lead to either significant or no apparent Fe isotope fractionation. Biogeochemical processes that happen in soil-plant and freshwater ecosystems are presented in Figs. 2 and 3, respectively, revealing that many of these processes are interlinked, thus making exact source assignment frequently difficult, especially as identifying kinetically-controlled or equilibrium-controlled processes is

Table 1
Iron isotope fractionation processes and the extent of the fractionation expressed either as $10^3\alpha_{B\text{-}A}$ or as $\Delta^{56}Fe_{B\text{-}A}$.*

Process			Isotope fractionation	$10^3\alpha_{B\text{-}A}$ or $\Delta^{56}Fe_{B\text{-}A}$ (‰)	Remarks	Reference
Species A	Species B	Condition				
Kinetic and equilibrium fractionation between Fe(II) and other Fe species						
$[Fe(II)(bipy)_3]^{2+}$	$Fe(III)_{aq}$		$[Fe(II)(bipy)_3]^{2+}$ heavier than $Fe(III)_{aq}$	up to −12	Rayleigh kinetic fractionation factor ~1.010; complexation of Fe(II) as $[Fe(II)(bipy)_3]^{2+}$ and separated from Fe(III) by anion exchange chromatography, kinetic fractionation during dissociation and breakdown of $[Fe(II)(bipy)_3]^{2+}$;	Matthews et al., 2001
$Fe(II)_{aq}$	$Fe(III)_{aq}$	22 °C, initial pH 2.5	$Fe(III)_{aq}$ heavier than $Fe(II)_{aq}$	+2.75 ± 0.15	Equilibrium fractionation; species separation by complete precipitation of Fe(III) through direct $BaCO_3$ addition (contribution to fractionation < 0.10‰) with no Fe(II) precipitation	Johnson et al., 2002
$Fe(II)_{aq}$	$Fe(III)_{aq}$	22 °C 0 °C	$Fe(III)_{aq}$ heavier than $Fe(II)_{aq}$	~ +2.8 ~ +3.5	Equilibrium fractionation; fractionation is temperature dependent but Cl concentration independent; separation by carbonate precipitation; corrected for the effects of incomplete separation and partial re-equilibrium during separation, Δ were + 3.0‰ and + 3.6‰ at 22 °C and 0 °C respectively	Welch et al., 2003
$Fe(II)_{aq}$	$Fe(III)_{aq}$	22 °C	$Fe(III)_{aq}$ heavier than $Fe(II)_{aq}$	~ +3.0	Theoretical predicted equilibrium fractionation factor	Anbar et al., 2005
$Fe(II)_{aq}$	Goethite	microrods nanorods pH = 7.5; 22 °C	goethite heavier	+1.05 ± 0.08 +1.22 ± 0.08	Microrods: 590 × 42 nm nanorods: 81 × 11 nm equilibrium fractionation factor; surface area effect largely controlled the fractionation	Beard et al., 2010 see also Frierdich et al., 2014 and Reddy et al., 2015
$Fe(II)_{aq}$	Goethite surface Fe(III)	microrods nanorods	$Fe(II)_{aq}$ lighter than surface Fe(III)	+1.68 ± 0.08 +2.10 ± 0.48	See above	Beard et al., 2010
$Fe(II)_{aq}$	Mackinawite	pH = 4, 25 °C 2 °C	mackinawite heavier	+0.33 ± 0.12 +0.52 ± 0.16	Equilibrium fractionation	Guilbaud et al., 2011b
$Fe(II)_{aq}$	Mackinawite	Fe:S: 10:1; pH 7 or 8 Fe:S: 1:1 (free sulfide added); pH 7, 20 °C	mackinawite heavier	+0.32 ± 0.29 +0.64 ± 0.36	Equilibrium fractionation; little effect of temperature and pH on the isotopic fractionation when aqueous Fe is dominated by $Fe(H_2O)_6^{2+}$	Wu et al., 2012a
$Fe(II)_{aq}$	Oceanic amorphous Fe(III)–Si coprecipitates	Fe:Si 1:2 Fe:Si 1:3 circum-nuetral pH	Fe(III)-Si heavier at equilibrium	+3.51 ± 0.20 +3.99 ± 0.17	Equilibrium fractionation	Wu et al., 2012b
Equilibrium fractionation between Fe(III) species						
$Fe(III)_{aq}$	Hematite	98 °C, through slow precipitation	No significant fractionation	+0.10 ± 0.20	Equilibrium fractionation	Skulan et al., 2002
$Fe(III)_{aq}$ loaded on the column	Fe(III)-chloro complexes	$Fe(III)_{aq}$ in HCl passing through anion exchange resin	heavier Fe eluded first, lighter Fe at last		Equilibrium effect during exchange of Fe(III) – chloro complexes; $\delta^{56}Fe$ range of the eluted solution: +3.6‰ to −3.4‰	Anbar et al., 2000; Roe et al., 2003
Inorganic $Fe(III)_{aq}$	Fe-DFOB	pH = 2, 25 °C	Fe-DFOB heavier	+0.60 ± 0.15	Equilibrium fractionation; species separation by precipitation of inorganic Fe(III) through carbonate addition; independent of the proportion of the two species	Dideriksen et al., 2008
$Fe(III)_{aq}$	$[Fe(III)Cl_4]^-$ in ether	$[Cl^-]$ from 0.5 to 5 M	$Fe(III)_{aq}$ heavier, but dependent on $[Cl^-]$	from ~ − 0.8 ($[Cl^-]$ = 0.5 M) to ~0 ($[Cl^-]$ = 5 M)	Equilibrium fractionation; dependent on chlorinity	Hill et al., 2009
$Fe(III)_{aq}$ & $Fe(II)_{aq}$	$[Fe(III)Cl_4]^-$ in ether	$[Cl^-]$ from 1.5 to 5 M	With Fe(II)aq (redox reaction) aqueous phase lighter	from ~ +0.1 to +2.4	Equilibrium fractionation; fractionation dependent on both chlorinity and $Fe(II)_{aq}/Fe(III)_{aq}$ ratio; increased chlorinity resulted in a decrease in the redox fractionation at rate of ~0.3‰/M $[Cl^-]$	Hill et al., 2010
Fe-DFOB	Fe-EDTA		No significant fractionation	−0.02 ± 0.11	equiLibrium fractionation; strong positive correlation between measured fractionation factors and the Fe-binding affinity of the ligands	Morgan et al., 2010
Fe-DFOB	Fe-oxalate		Fe-oxalate lighter	−0.2 ± 0.11	See above	Morgan et al., 2010
Oxidation of $Fe(II)_{aq}$						

(*continued on next page*)

Table 1 (*continued*)

Process			Isotope fractionation	$10^3\alpha_{B\text{-}A}$ or $\Delta^{56}Fe_{B\text{-}A}$ (‰)	Remarks	Reference
Species A	Species B	Condition				
$Fe(II)_{aq}$	Ferrihydrite	Abiotic	Ferrihydrite heavier	+0.9 ± 0.2	Preferential partition of relatively heavy Fe isotopes into intermediate complexes (e.g. $Fe(II)(OH)_x$) before oxidation; fractionation factor between ferrihydrite and Fe(II)aq depends on the relative proportions of the coexisting aqueous Fe species (Bullen et al., 2001); *updated explanation*: most likely caused by a combination of aqueous redox equilibrium and kinetic fractionation during precipitation (Dauphas and Rouxel, 2006)	Bullen et al., 2001
$Fe(II)_{aq}$	Ferrihydrite	With photoautotrophic bacteria (anoxic)	Fe(III) hydroxides heavier	~ +1.5 ± 0.2	Independent of the rate of photoautotrophic Fe(II)-oxidation, comparable to DIR of Fe(III) (hydr)oxides; equilibrium isotope exchange between Fe(II) and Fe(III) bound to biological ligands together with kinetic isotope effect of rapid ferrihydrite precipitation	Croal et al., 2004
$Fe(II)_{aq}$	$Fe(III)_{aq}$	Biotic oxidation	$Fe(III)_{aq}$ heavier	~ +2.2	Rayleigh type kinetic fractionation	Balci et al., 2006
$Fe(II)_{aq}$	$Fe(III)_{aq}$	Abiotic oxidation	$Fe(III)_{aq}$ heavier	~ +3.4	Rayleigh type kinetic fractionation	Balci et al., 2006
$Fe(II)_{aq}$ as Fe-citrate	Fe(III) complexed by ligands on cell	With N fixation bacteria	Cell-associated Fe heavier than Fe in the growth media	+1.1	Rayleigh fractionation factor, kinetic fractionation mixed with equilibrium fractionation possibly between different Fe complexes	Wasylenki et al., 2007
$Fe(II)_{aq}$	Fe(II/III) intermediate species	With marine photoferrotroph	Intermediate fe species heavier	+0.4 to +1.5	As ε based on Rayleigh fit; these intermediated species included organically bound, sorbed and/or colloidal Fe(II) and Fe(III) formed in the course of Fe(II) oxidation and Fe(III) precipitation by an FeOB	Swanner et al., 2015
Precipitation						
$Fe(II)_{aq}$	Mackinawite	2–40 °C	Mackinawite lighter and then became heavier	−0.85 ± 0.30	Significant kinetic isotope fractionation effect in the absence of a redox process with kinetic fractionation factor $\alpha_{Fe(II)\text{-}FeS}$ = 1.0009 ± 0.0003; fractionation during inner sphere ligand exchange between hexaqua Fe(II) and aqueous sulfide complexes	Butler et al., 2005
$Fe(II)_{reservoir}$	Pyrite	40 and 100 °C, abiotic, anoxic	Pyrite lighter	−1.7 to −3.0 ± 0.1	Kinetic fractionation factor $\alpha_{Fe(II)reservoir\text{-}pyrite}$ = 1.0022 ± 0.0007	Guilbaud et al., 2011a
$Fe(II)_{aq}$	Siderite	Abiotic, 20 °C, fast precipitation	No obvious isotopic fractionation	~0	Kinetic fractionation	Wiesli et al., 2004
		Slow precipitation	Siderite is lighter	~ − 0.5	As kinetic Rayleigh distillation fractionation factor $10^3\alpha_{siderite\text{-}Fe(II)}$	
$Fe(II)_{aq}$	$Fe_2(SO_4)_3$	With acidophilic Fe(II)-oxidizing bacteria	Precipitates heavier	+0.91 to +4.42	Kinetic fractionation	Balci et al., 2006
$Fe(II)_{aq}$	$FeCl_3$	With acidophilic Fe(II)-oxidizing bacteria	Precipitates heavier	+1.40 to +3.03	Kinetic fractionation	Balci et al., 2006
$Fe(III)_{aq}$	$Fe_2(SO_4)_3$	With acidophilic Fe(II)-oxidizing bacteria	Precipitates lighter	−1.67 to +0.53	Kinetic fractionation	Balci et al., 2006
$Fe(III)_{aq}$	$FeCl_3$	With acidophilic Fe(II)-oxidizing bacteria	Precipitates lighter	−0.81 to +0.15	Kinetic fractionation	Balci et al., 2006
$Fe(II)_{aq}$	$Fe_2(SO_4)_3$	Abiotic	Precipitates heavier	+1.84, +2.23	Kinetic fractionation	Balci et al., 2006
$Fe(III)_{aq}$	$Fe_2(SO_4)_3$	Abiotic	Precipitates slightly heavier	+0.10, +0.16	Kinetic fractionation	Balci et al., 2006
$Fe(II)_{aq}$	$Fe(OH)_3$ precipitates	Nitrate-reducing Fe(II)-oxidizing bacteria	$Fe(OH)_3$ precipitates heavier	+1.8 to +4.0	At low extent of oxidation, the isotope fractionations are not strongly dependent on closed-system equilibrium or Rayleigh fractionation models	Kappler et al., 2010
$Fe(II)_{aq}$	Fe(III) precipitates	With marine photoferrotroph	Fe(III) precipitates heavier	+1.2 to +2.2	As ε based on Rayleigh kinetic fractionation fit	Swanner et al., 2015
$Fe(II)_{aq}$	Fe(III) precipitates	With oxygen-producing marine Cyanobaterium	Fe(III) precipitates heavier	~ +3.1 to +4.2	As apparent different of $\delta^{56}Fe$ values; kinetic fractionation; complete equilibrium between the two species not reached due to partially suppressed electron and atom exchanged between $Fe(II)_{aq}$ and organic-coated Fe(III) precipitates	Swanner et al., 2017

(*continued on next page*)

Table 1 (*continued*)

Process			Isotope fractionation	$10^3\alpha_{B\text{-}A}$ or $\Delta^{56}Fe_{B\text{-}A}$ (‰)	Remarks	Reference
Species A	Species B	Condition				
$Fe(III)_{aq}$	Hematite	98 °C, fast precipitation	Hematte lighter	−1.32 ± 0.12	Kinetic fractionation; as Rayleigh distillation fractionation factor $10^3\alpha_{Fe(III)aq\text{-}Hematite}$	Skulan et al., 2002
Adsorption						
$Fe(II)_{aq}$	$Fe(II)_{sorbed}$ on goethite	Biotic, anoxic	Sorbed $Fe(II)_{aq}$ heavier than remaining $Fe(II)_{aq}$	+4.07	Equilibrium factor ~1.0041 Rayleigh type kinetic fractionation factor 1.0035	Icopini et al., 2004
$Fe(II)_{aq}$	$Fe(II)_{sorbed}$ on goethite	Abiotic, anoxic	Sorbed $Fe(II)_{aq}$ heavier than remaining $Fe(II)_{aq}$	+2.05	Equilibrium factor ~1.0021 Rayleigh type kinetic fractionation factor 1.0016	Icopini et al., 2004
$Fe(II)_{aq}$	$Fe(II)_{sorbed}$ on goethite	During dissolution of goethite by DIR bacteria	Sorbed $Fe(II)_{aq}$ heavier than remaining $Fe(II)_{aq}$	+0.86 ± 0.17 +0.87	Much smaller than $\Delta Fe(II)_{aq}\text{-}Fe(III)_{surface}$, thus sorption of Fe (II) on Fe(III) substrate cannot account for Fe isotope fractionation during the dissolution of oxides by DIR bacteria	Crosby et al., 2005, 2007
$Fe(II)_{aq}$	$Fe(II)_{sorbed}$ on goethite	Abiotic, anoxic, without strong Fe(III) chelator DFAM	Sorbed $Fe(II)_{aq}$ heavier than source $Fe(II)_{aq}$	+0.26 to +1.51		Jang et al., 2008
$Fe(II)_{aq}$	$Fe(II)_{sorbed}$ on goethite	Abiotic, anoxic, with strong Fe(III) chelator DFAM	Sorbed $Fe(II)_{aq}$ lighter than source $Fe(II)_{aq}$	−0.71 to −0.27		Jang et al., 2008
$Fe(II)_{aq}$	Incorporated Fe(II) in to goethite	Abiotic, anoxic, with or without strong Fe(III) chelator DFAM	Incorporated $Fe(II)_{aq}$ becomes heavier along adsorption time	−0.81 to +0.92	Incorporation of partial Fe(II) in to goethite structure during adsorption	Jang et al., 2008
$Fe(II)_{aq}$	$Fe(II)_{sorbed}$ on goethite-loaded quartz	Abiotic, anoxic	Sorbed $Fe(II)_{aq}$ heavier than Fe $(II)_{aq}$ at equilibrium	+0.85 ± 0.08	Equilibrium fractionation factor	Mikutta et al., 2009
$Fe(II)_{aq}$	$Fe(II)_{sorbed}$ on goethite	Abiotic, anoxic	Sorbed $Fe(II)_{aq}$ heavier than Fe $(II)_{aq}$ at equilibrium	+2.01 ± 0.08 +0.73 ± 0.24	Equilibrium fractionation factor without consideration of atom exchange with consideration of atom exchange; atom exchange superimposed sorption-induced isotope fractionation	Mikutta et al., 2009
$Fe(II)_{aq}$	$Fe(II)_{sorbed}$ on goethite	Abiotic	Sorbed $Fe(ii)_{aq}$ heavier than remaining $fe(ii)_{aq}$	+1.24 ± 0.14	equilibrium fractionation factor; fractionation regardless particle size of the goethite	Beard et al., 2010
$Fe(II)_{aq}$	Goethite	Abiotic, 22 °C	Goethite heavier	+1.04 ± 0.08 to +1.22 ± 0.11	equilibrium fractionation; isotope exchange rate dependent on surface area of the substrate; the extent of isotopic exchange between $Fe(II)_{aq}$ and goethite positively correlated with pH where the least amount of exchange occurred at lowest pH (2.5)	Frierdich et al., 2014 Reddy et al., 2015
$Fe(II)_{aq}$	$Fe(II)_{sorbed}$ on hematite	During dissolution of hematite with dir bacteria	Sorbed Fe(ii) heavier	+0.38 ± 0.10 +0.30 −0.49 ± 0.09	combined with small proportion of sorbed Fe(II), insignificant isotopic effects is due to sorption of Fe(II)	Crosby et al., 2005, 2007 Wu et al., 2009
$Fe(II)_{aq}$	$Fe(II)_{sorbed}$ on hematite	Abiotic	Sorbed Fe(ii) heavier	+0.49 ± 0.15	equilibrium fractionation	Wu et al., 2010
$Fe(II)_{aq}$	Fe(II) on cells	Cyanobacteria, ph 6	Heavier Fe(ii) sorbed on cell	+2.66 ± 0.14	equilibrium fractionation	Mulholland et al., 2015b
$Fe(III)_{aq}$	Fe(III) on cells	Cyanobacteria, ph 3	Heavier Fe(iii) sorbed on cell	+0.97 ± 0.19	equilibrium fractionation	Mulholland et al., 2015b
Oxidative dissolution of Fe minerals						
Sulphide-rich rocks	Fe leachate	pH = 2 pH = 5	Fe leached heavier initially and became the same as the rocks lighter in leached	+1.25 to ~0 −1.7	Fe leachate included both $Fe(II)_{aq}$ and $Fe(III)_{aq}$, $Fe(II)_{aq}$ was generally within 10% of the total Fe Fe isotopic composition in solution controlled by the precipitation of Fe(III)-oxide	Fernandez and Borrok, 2009
Chalcopyrite	Fe(III) leachate from electrochemical or oxic bioleaching	45 °C, pH 1.5	No significant fractionation at earlier stage, the leachate became heavier compared to the substrate at the end of leaching	~0 to ~ +0.1	Similar fractionation with or without microorganism; mainly regulated by the formation of secondary minerals such as jarosite enriched in heavier Fe isotopes	Rodríguez et al., 2015
Pyrite from multiple petrogenetic environments	Leachate	Abiotic	Leachate lighter than bulk pyrite	Up to ~ − 1	The fractionation consistent in direction, but not magnitude, with equilibrium isotope fractionation, with possible second order effects from isotopic heterogeneity of the pyrites	Wolfe et al., 2016
Reductive dissolution of Fe minerals						

(*continued on next page*)

Table 1 (*continued*)

Process			Isotope fractionation	$10^3\alpha_{B\text{-}A}$ or $\Delta^{56}Fe_{B\text{-}A}$ (‰)	Remarks	Reference
Species A	Species B	Condition				
Goethite	$Fe(II)_{aq}$	Abiotic, by oxalate acid in present of light, initial ph 3	Lighter Fe isotopes dissolved first; later became heavier in solution	−1.7 to +0.1	Kinetic fractionation	Wiederhold et al., 2006
Goethite	$Fe(II)_{aq}$	With DIR bacteria, anaerobic, 27 °C	Dissolved $Fe(II)_{aq}$ lighter	~ − 1.2	In equilibrium	Icopini et al., 2004
Goethite	$Fe(II)_{aq}$	With DIR bacteria	Dissolved $Fe(II)_{aq}$ lighter	initially −0.95, then to −0.65, and later stage to −1.55	fractionation is controlled by coupled electron and Fe atom exchange between Fe(II) and Fe(III) at iron oxide surfaces independent of the substrate	Crosby et al., 2005, 2007
Reactive goethite surface Fe (III)	$Fe(II)_{aq}$	With DIR bacteria	Dissolved $Fe(II)_{aq}$ lighter than surface Fe(III)	~ − 3	see above	Crosby et al., 2005, 2007
Hematite	$Fe(II)_{aq}$	With DIR bacteria	Dissolved $Fe(II)_{aq}$ lighter	initially −2, gradually change to −1 −1.27 ± 0.14	see above	Crosby et al., 2005, 2007 Beard et al., 2003
Reactive hematite surface Fe(III)	$Fe(II)_{aq}$	With DIR bacteria	Dissolved $Fe(II)_{aq}$ lighter than surface Fe(III)	~ − 3	see above	Crosby et al., 2005, 2007
Reactive hematite surface Fe(III)	$Fe(II)_{aq}$	Abiotic, ph 7, no Si	Dissolved $Fe(II)_{aq}$ lighter than surface Fe(III)	−2.81 ± 0.12 −2.87 ± 0.19	no significant change along with the time (25 days); regardless to the times of agitation	Wu et al., 2010
Reactive hematite surface Fe(III)	$Fe(II)_{aq}$	Abiotic, ph 7, with Si	Dissolved $Fe(II)_{aq}$ lighter than surface Fe(III)	−2.22 ± 0.24 to −3.21 ± 0.50	surface Fe(III) became heavier along with the time (25 days); constant agitation slightly enhanced fractionation	Wu et al., 2010
Reactive hematite surface Fe(III)	$Fe(II)_{aq}$	Abiotic, ph 8.7, with Si	Dissolved $Fe(II)_{aq}$ lighter than surface Fe(III), less fractionated at later stage	~ − 2.5 to ~ − 1.6	the fractionation moved away from Fe(II)aq-hematite equilibrium fractionation (−3.1‰), but towards Fe(II)aq-goethite equilibrium fractionation (−1.0‰), reflecting distortion of Fe—O bonds, and formation of Si-Fe-O bonds	Wu et al., 2010
Ferrihydrite	$Fe(II)_{aq}$	With DIR bacteria	Lighter in dissolved $Fe(II)_{aq}$	−1.3 ± 0.1	closed system Rayleigh distillation fractionation	Beard et al., 1999
Magnetite reduced from ferrihydrite	$Fe(II)_{aq}$	With DIR bacteria, low reduction rate	Lighter in dissolved solution	−1.3	equilibrium fractionation	Johnson et al., 2005
Siderite reduced from ferrihydrite	$Fe(II)_{aq}$	With DIR bacteria, low reduction rate	No significant fractionation	~0	equilibrium fractionation	Johnson et al., 2005
Ca-substituted siderite reduced from ferrihydrite	$Fe(II)_{aq}$	With DIR bacteria, low reduction rate	Heavier in dissolved $Fe(II)_{aq}$	+0.9	equilibrium fractionation	Johnson et al., 2005
Structure Fe(III) on nontronite	$Fe(II)_{aq}$	Abiotic	During rapid dissolution stage structure fe(iii) heavier, in 2nd stage lighter than $fe(ii)_{aq}$	−0.81 to +0.78	Stage 1: rapid reduction of a finite Fe(III) pool along the edges of the clay particles with a limited release of Fe(II) into solution; electron transfer and atom exchange between edge-bound Fe (II) and structural Fe(III) and between $Fe(II)_{aq}$ and structural Fe(III) via a transient sorbed Fe(II), stage 2, abiotic reduction continued, finally isotope composition of structural Fe(III) similar to that of edge-bound Fe(II)	Shi et al., 2016
Structure Fe(III) on nontronite	$Fe(II)_{aq}$	With DIR bacteria	During rapid dissolution stage structure Fe(III) heavier, in 2nd stage less pronounced fractionation	−1.17 to +0.06	during stage 2, microbial reduction inhibited, no further electron transfer and atom exchange between $Fe(II)_{aq}$ and structural Fe(III)	Shi et al., 2016
Proton-promoted dissolution of Fe minerals						
Goethite	Fe in solution	By 0.5 M hcl, ph 0.3	No significant fractionation	~0.0		Wiederhold et al., 2006
Granite	Fe in solution	By 0.5 M hcl	Lighter in dissolved solution, less fractionated at later stage	−1.85 to −0.55	alteration of biotite to chlorite followed by dissolution of chlorite likely the dominant processes; modeled steady-state Fe release of $\Delta^{56}Fe$ ~ −0.14‰	Chapman et al., 2009
Basalt	Fe in solution	By 0.5 M hcl	Lighter in dissolved solution, less fractionated at later stage	−1.5 to ~ − 0.4	dissolution of pigeonite was likely the Fe source	Chapman et al., 2009

(*continued on next page*)

Table 1 (*continued*)

Process			Isotope fractionation	$10^3\alpha_{B\text{-}A}$ or $\Delta^{56}Fe_{B\text{-}A}$ (‰)	Remarks	Reference
Species A	Species B	Condition				
Granite (biotite, chlorite)	Fe in solution	Anoxic, initial ph 2 or 4; by hcl, different K concentrations	Lighter in dissolved solution, less fractionated at later stage	initial −0.55 later −0.4 (no K, no pre-reaction)	kinetic, 1.6% of total Fe dissolved after 100 days; pre-reaction of O2-saturated water significantly influenced Fe isotope evolution in the early dissolution steps; addition of K to initial solutions dramatically enhanced the preferential release of light Fe isotopes	Kiczka et al., 2010a
Ligand-controlled dissolution						
Granite (biotite, chlorite)	Fe in solution	By oxalate in absence of light; 5 mm initial ph 4.5; different K concentrations	Dissolve lighter Fe first, then less light at the later stage	initial −0.4 later −0.1	kinetic and $\Delta^{56}Fe_{solution\text{-}granite}$ reached a constant level between −0.1 to −0.2‰, faster than dissolution by HCl; 20.6% of total Fe dissolved after 100 days; K addition had no effect on Fe isotope fractionation;	Kiczka et al., 2010a
Granite	Fe in solution	By oxalate in absence of light	Dissolve lighter fe first, then less light at the later stage	~ − 1.4 to ~ − 1	relative stable Δ after ~20 h dissolution	Chapman et al., 2009
Basalt	Fe in solution	By oxalate in absence of light	Dissolve lighter fe first, then less light at the later stage	~ − 0.8 to ~ − 0.5	relative stable Δ after ~20 h dissolution	Chapman et al., 2009
Hornblende	Fe in solution	By organic acids, abiotic	Lighter in dissolved solution	−1.2 to −0.3	kinetic fractionation; stronger chelates preferentially extract lighter Fe; predominantly due to retention of ^{56}Fe in an altered surface layer	Brantley et al., 2001, 2004
Hornblende	Fe in solution	By siderophore (DFAM), abiotic	Lighter in dissolved solution	−0.8 to −0.3	see above	Brantley et al., 2001, 2004
Hornblende	Fe in solution	With siderophore producing bacteria	Lighter in dissolved solution	−0.56 ± 0.19		Brantley et al., 2004
Goethite	Fe in solution	By siderophore (DFAM), abiotic	No significant fractionation or slightly heavier in solution	+0.21 ± 0.16	due to lack of altered layer	Brantley et al., 2004
Goethite	Fe in solution	By siderophore producing bacteria	Lighter in dissolved solution	−1.44 ± 0.16		Brantley et al., 2004
Goethite	Fe in solution	By oxalate acid, absent of light, initial ph 3	Lighter Fe isotopes dissolved first; later stage heavier in solution	early stage −1.3 to ~ +0.3	kinetic fractionation, at the end reached equilibrium	Wiederhold et al., 2006
Biomineralization by magnetotactic bacteria						
$Fe(III)_{aq}$ as $FeCl_3$	Intracellular magnetite (Fe_3O_4) produced by magnetotactic bacteria	4–35 °C	No significant fractionation	< 0.3	the passive binding of Fe ions to the external cell surface was the rate-limiting step for Fe_3O_4 formation and the bound Fe was totally consumed in the crystallization process leading to no significant fractionation	Mandernack et al., 1999
Fe(II)-ascorbate	Bacterial lysates	30 °C, pH 7.5, in darkness	Bacterial lysates heavier	~ +0.8		Amor et al., 2016
Fe(II)-ascorbate	Magnetite produced by magnetotactic bacteria	30 °C, pH 7.5, in darkness	Bacterial lysates heavier	~ − 1.4		Amor et al., 2016
Fe(III)-quinate	Bacterial lysates	30 °C, pH 7.5, in darkness	Bacterial lysates heavier	~ +0.5		Amor et al., 2016
Fe(III)-quinate	Magnetite produced by magnetotactic bacteria	30 °C, pH 7.5, in darkness	Produced magnetite lighter	~ − 2.2	mass independent isotope fractionation occurred with ~ + 0.23‰ in $\delta^{57}Fe$ heavier than mass-dependent fractionation; the mass independent isotope fractionation was only observed in(Garnier et al., 2017)Fe, but not in others	Amor et al., 2016, 2018
Diffusion						
$Fe(II)_{aq}$	Diffused $Fe(II)_{aq}$	20 °C, 10 mg L-1 $Fe(NO_3)_2$ in 0.33 M HNO_3	Lighter Fe diffused	can be < −0.3		Rodushkin et al., 2004
$FeCl_2$	Electrpoplated	During electroplating	Lighter Fe preferentially electroplated	up to −4.8 ± 0.02	kinetic fractionation; depending on observed plating current and the mass-transport limited current	Kavner et al., 2005, 2009
Plant uptake and redistribution						
	Fe in plant root (strategy I)		most take up lighter Fe	−0.58 to +0.18	as $\delta^{56}Fe$ values relative to IRMM-014; depends on not only the uptake strategy but also the Fe availability in the growth media	e.g. Kiczka et al., 2010b; Guelke-Stelling and von Blanckenburg, 2012

(*continued on next page*)

Table 1 (*continued*)

Process			Isotope fractionation	$10^3\alpha_{B\text{-}A}$ or $\Delta^{56}Fe_{B\text{-}A}$ (‰)	Remarks	Reference
Species A	Species B	Condition				
	Fe in plant root (strategy II)		no significant fractionation or take up heavier Fe	−0.14 to +0.49	see above, fractionation due to uptake must be referred to plant available Fe in the growth media	e.g. Kiczka et al., 2010b; Guelke-Stelling and von Blanckenburg, 2012
	Fe in abovegound tissues		lighter in leaves and flowers	−2.75 (strategy I leaf) to +0.27 (strategy II leaf)	as δ^{56}Fe values relative to IRMM-014	e.g. Kiczka et al., 2010b; Guelke-Stelling and von Blanckenburg, 2012

* It is important to note that the $\Delta^{56}Fe_{B\text{-}A}$ values (‰) of isotope fractionation in Table 1 between two Fe species A and B are either 1) those directly reported in the respective literature references wherever given, or 2) reported in the references as $10^3\alpha_{A\text{-}B}$, or 3) calculated assuming $\Delta^{56}Fe_{B\text{-}A} \approx 10^3\alpha_{A\text{-}B}$ when the reference only gave α, or 4) for plant uptake and translocation processes, the δ^{56}Fe values of the plant tissues instead of $\Delta^{56}Fe_{B\text{-}A}$, due to limited data on source Fe isotope composition (e.g. plant available Fe in growth medium). For kinetic isotope fractionation in some experiments, if the kinetic fractionation factor was not reported, then $\Delta^{56}Fe_{B\text{-}A}$ was calculated as $\delta^{56}Fe_B - \delta^{56}Fe_A$ without weighting/pooling and was given as a range of this $\Delta^{56}Fe_{B\text{-}A}$ usually along the experiment time. The readers are strongly encouraged to refer to the original experiments of individual studies to learn more about experiment conditions, isotope fractionation and the interpretation.

difficult in natural ecosystems.

In soil-plant systems (Fig. 2), it is not one individual process that causes shifts in Fe species, but rather multiple chemical reactions and cycling steps until Fe really leaves the soil or sediment system. Therefore, the Fe isotope signatures in plants and groundwater rarely reflect the Fe isotope fractionation caused by initial mineral dissolution (Table 1, Fig. 1).

In contrast to the soil-plant system that is dominated by the role of Fe(III) mineral phases as intermediate to Fe(II) releases, Fe transformations in rivers and lakes show a much pronounced zonation of isotope fractionation. The supply of oxygen in the epilimnion controls the residence time of $Fe(II)_{aq}$ and thus the fate of overall Fe in the system. In contrast, Fe(II) cycling processes dominate in the hypolimnion and are associated with sedimentary phases at low oxygen level (Fig. 3).

Spectroscopy data and ab-initio modelling show that Fe(III) compounds are preferentially enriched in heavy Fe isotopes compared with Fe(II)-bearing species, except for the Fe(II) and Fe(III) hexacyano complexes (Schauble et al., 2001). Aqueous ferrous Fe [$Fe(II)_{aq}$] is isotopically lighter than aqueous ferric Fe [$Fe(III)_{aq}$] and other Fe(III) species, yet heavier than some (but not all) Fe(II) species such as siderite (e.g. Polyakov, 1997; Schauble et al., 2001; Johnson et al., 2002; Welch et al., 2003; Anbar et al., 2005). Aqueous Fe(II) is reported to be isotopically lighter than Fe(II) sorbed on goethite (Beard et al., 2010; Crosby et al., 2005, 2007; Icopini et al., 2004; Jiang et al., 2008). The fractionation in this sorption process is more pronounced than adsorption on hematite (Crosby et al., 2005, 2007), indicating that the extent of Fe isotope fractionation during adsorption process depends on the sorption substrate.

In addition, the direction and the extent of isotope fractionation may change along the progression of a process. For instance, Fe(II) sulfide (FeS) precipitated from $Fe(II)_{aq}$ is isotopically lighter than Fe $(II)_{aq}$ at the beginning of the precipitation. Along with the precipitation process, FeS becomes isotopically heavier and at equilibrium FeS is heavier than $Fe(II)_{aq}$ (Butler et al., 2005; Wu et al., 2012a). The temporal changes of the Fe isotope composition of the precipitates reflect isotopic re-equilibration due to the aggregation of precipitated particles after an initial kinetic isotope fractionation during rapid FeS precipitation. As a result, different Fe minerals exhibit different Fe isotopic signatures owing to various Fe sources, the formation processes, as well as likely to mineral age and thus crystallinity.

For Fe minerals, the general trend with respect to their isotope composition is (from isotopically light to heavy): pyrite (with a wide range of δ^{56}Fe, Guilbaud et al., 2011a), ankerite, siderite, mackinawite, magnetite, [Fe(III)-organic ligands,] poorly crystalline Fe oxides, goethite, hematite, and Fe in silicate minerals (Johnson et al., 2003). Particle size of the Fe minerals may have an effect on the proportions of Fe species in the system and isotope fractionation in processes that take place at the mineral surface, such as in sorption and dissolution (Beard et al., 2010). An equilibrium experiment by Beard et al. (2010) demonstrated that the proportion of mineral surface Fe(III) was negatively related to particle size of the mineral (e.g. goethite), where the isotope fractionation between $Fe(II)_{aq}$ and surface Fe(III) was very high. The authors therefore assumed that the isotope composition of natural (water) systems could be significantly influenced by nanoparticulate Fe minerals in the system (Beard et al., 2010).

2.2. Redox transformations

An apparent pathway in which Fe isotope fractionation is expected to occur is redox transformation. In the presence of oxygen, the oxidation process leaves a solution enriched in light Fe isotopes, while heavier $Fe(III)_{aq}$ is rapidly precipitated as ferrihydrite (Table 1). The overall fractionation at equilibrium of this process shows that the isotopic signature of the ferrihydrite is about 1‰ heavier than the Fe(II) in solution, as a result of the combination of $Fe(III)_{aq}$-$Fe(II)_{aq}$ equilibrium fractionation (~3‰) and a kinetic isotope effect favoring light Fe

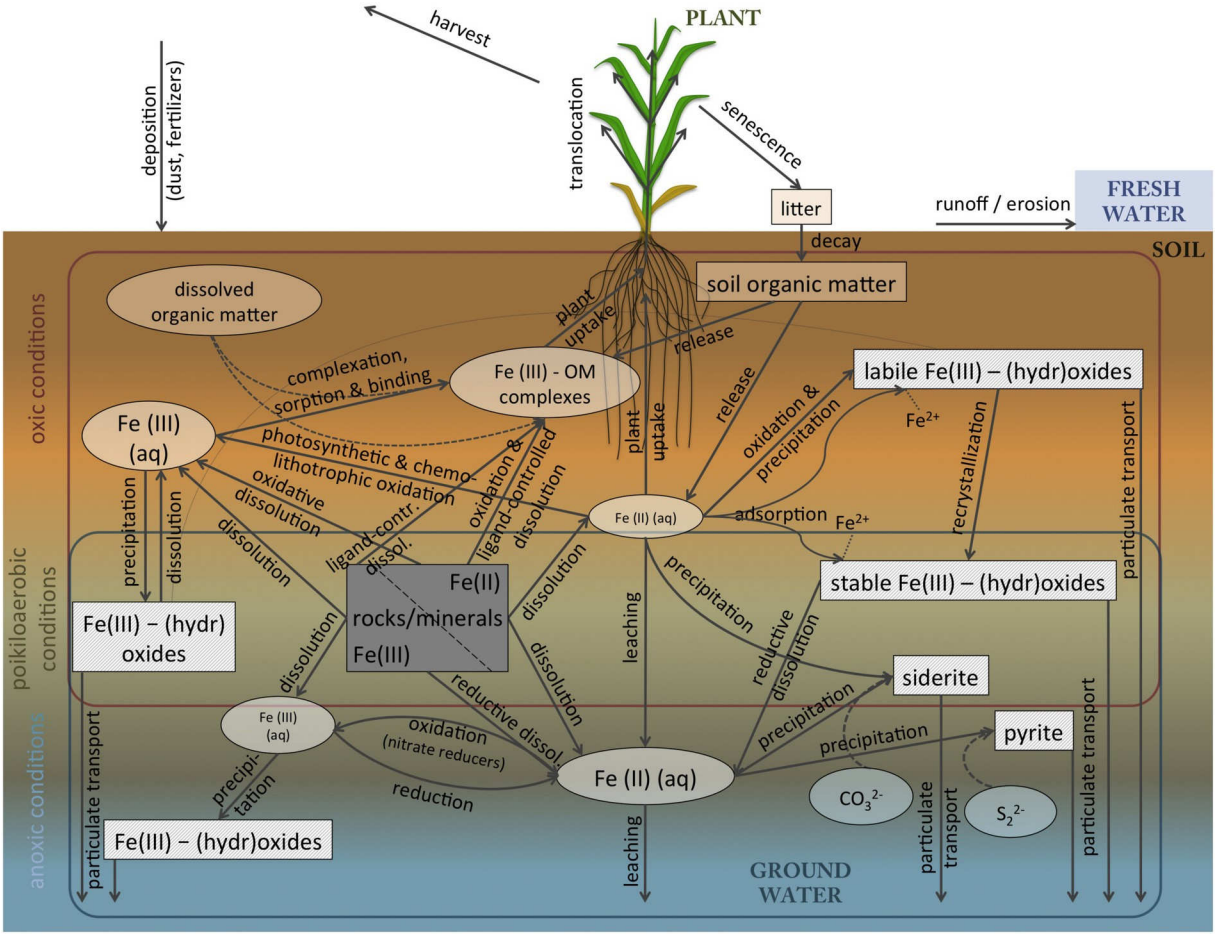

Fig. 2. Iron phases and possible transformation processes in soil-plant systems. Square boxes represent solid phases, while oval boxes represent dissolved species. Processes are grouped according to oxic/anoxic conditions, the latter being arranged from top to bottom with the red box encompassing the oxic conditions, the blue box the anoxic conditions and their overlap representing alternating (poikiloaerobic) conditions. We would like to point out at that although this is a logical progression of oxic conditions in soils, subsoils are not generally anoxic and the dominant Fe species throughout most soil profiles is Fe(III). The reader is hence cautioned not to equate this arrangement of conditions with soil depth. The figure is not complete in terms of all biotic processes that accompany many of the transformation reactions.

isotopes to precipitate as ferrihydrite from $Fe(III)_{aq}$ (Anbar et al., 2005; Bullen et al., 2001; Dauphas and Rouxel, 2006; Johnson et al., 2002; Welch et al., 2003). Skulan et al. (2002) found a correlation between Fe isotopic fractionation and the rate of precipitation, indicating a kinetic isotope effect during precipitation. In addition, $Fe(II)_{aq}$ can be adsorbed on the surface of the newly formed Fe(III) (hydr)oxides, which also favors heavy Fe isotopes, thus producing an isotopically very light Fe (II) in solution (Icopini et al., 2004; Teutsch et al., 2005). The isotope fractionation ($\sim -0.5‰$) between $Fe(II)_{aq}$ and sorbed Fe(II) is similar under abiotic and biotic condition and relatively constant in different experimental settings (e.g. different pH, with or without soluble Si; Crosby et al., 2007; Wu et al., 2009; Wu et al., 2010). Jang et al. (2008) additionally identified an Fe(II) pool that was incorporated into the structure of goethite during adsorption of $Fe(II)_{aq}$ due to electron transfer from sorbed Fe(II) to structural Fe(III) of goethite driven by equilibrium isotope effect between Fe(II) and Fe(III). When oxygen is absent, Fe(II) can be transformed via anaerobic photoautotrophic Fe(II) oxidation. This oxidation process also favors heavy Fe isotopes leaving relatively light $Fe(II)_{aq}$ compared with the precipitated poorly crystalline ferrihydrite (Croal et al., 2004). A recent study showed that UV photo-oxidation of Fe(II) at a pH of 7.3 resulted in Fe isotope fractionation between the precipitated Fe(III)-bearing lepidocrocite and $Fe(II)_{aq}$ with a fractionation factor for $^{56}Fe/^{54}Fe$ of $+1.2‰$ (Nie et al., 2017).

In terrestrial systems microorganisms play an important role in Fe redox transformation either utilizing the energy produced during oxidation by Fe-oxidizing bacteria (known as FeOB, Emerson et al., 2010) or using Fe(III) as terminal electron acceptor during Fe(III) reduction by DIR bacteria (Lovley et al., 2004). The processes mediated by these two types of bacteria including those of nitrate-reducing Fe(II) oxidizing bacteria have been shown to induce Fe isotope fractionation (e.g. Crosby et al., 2005, 2007; Croal et al., 2004; Kappler et al., 2010; Swanner et al., 2015). Both inorganic and microbially mediated redox transformations between Fe(II) and Fe(III) show a preferential removal of heavy Fe isotope from the solution. The fractionation extent in both cases is also similar, on the order of 1 to 2‰ in $\delta^{56}Fe$, which have been observed both in lab experiments (Beard et al., 1999; Bullen et al., 2001; Johnson et al., 2004; Wu et al., 2011) and in field studies (Rouxel et al., 2018). For further insights on Fe isotope fractionation in redox transformations, we kindly refer the readers to the excellent reviews by Johnson et al. (2004), Anbar (2004) and Dauphas and Rouxel (2006).

2.3. Dissolution of iron minerals

Pedogenic processes involve the dissolution of Fe minerals, which can generate soluble mobile Fe(II) in the soil that can be transported by diffusive and advective processes until it is oxidized and subsequently reprecipitated as secondary Fe(III) (hydr)oxides (Wiederhold et al., 2006). Minerals containing Fe(II) can on the other hand undergo oxidative dissolution and release Fe(III)-containing leachates. It is worth

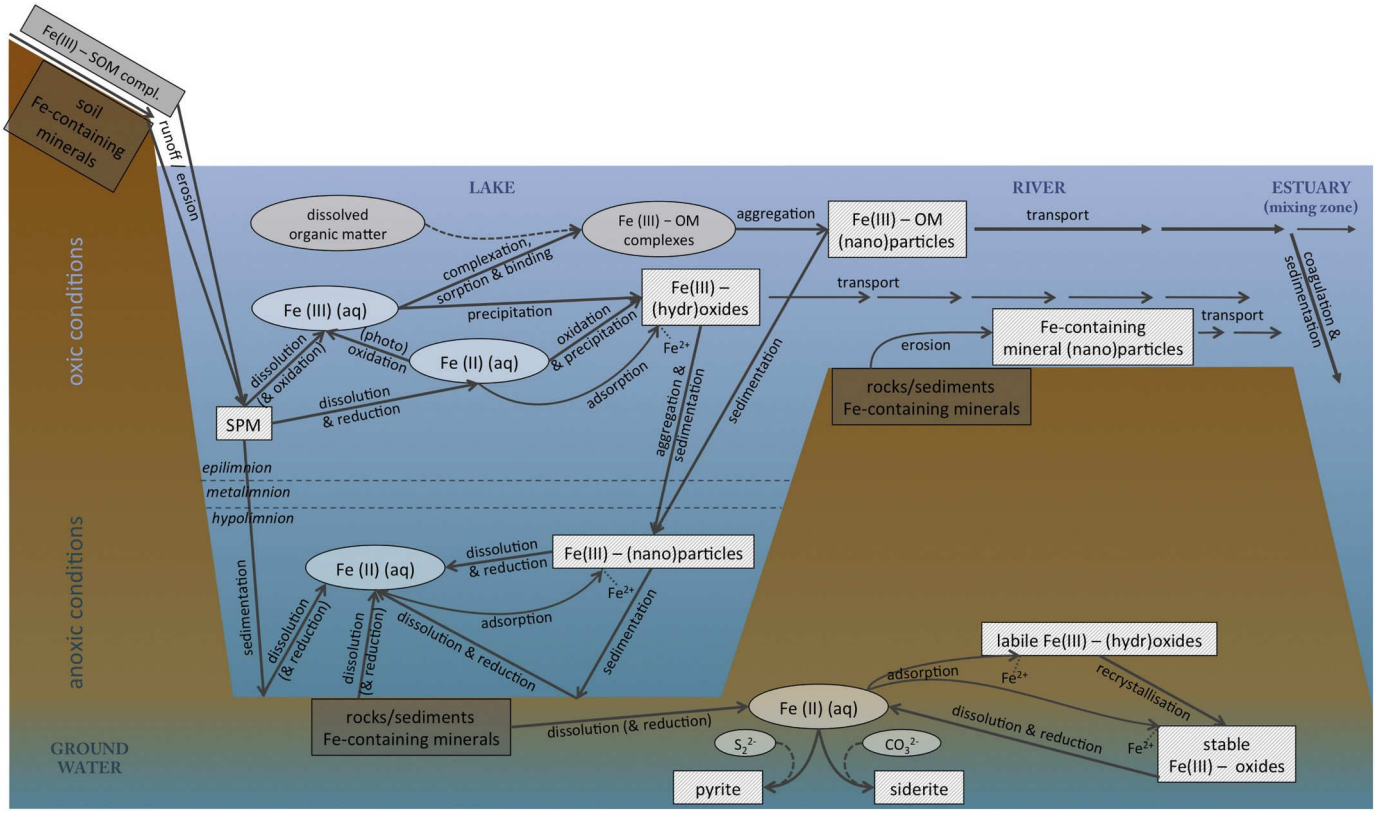

Fig. 3. Iron speciation, possible abiotic transformation processes and transportation in freshwater systems like lakes, rivers and groundwater. Square boxes represent solid phases, oval boxes represent dissolved species, SPM: suspended particulate matter. For reasons of clarity the figure does not display all biotic processes that accompany Fe-cycling and many of the transformation reactions. Exchanges between epi- and hypolimnion which occur during seasonal mixing are not considered either.

noting that only the mineral surface is actively dissolved (Wiederhold, 2015). Dissolution is governed by thermodynamic and kinetic constraints at the solid-solution interface (Stumm, 1992). This means that the kinetic fractionation effect is to some extent limited. When the light Fe isotope is preferentially released first, the newly-formed isotopically heavier mineral surface will sooner or later be dissolved and therewith enable the dissolution to continue, finally leading to a steady-state condition under which the extent of kinetic fractionation is limited (Wiederhold, 2015). However, kinetic fractionation effects can persist during long-term weathering in field systems and dominate Fe isotope fractionation in young weathering environments (Kiczka et al., 2011). Four major dissolution mechanisms of Fe minerals (proton-promoted, ligand-controlled, reductive and oxidative dissolution) have been demonstrated in laboratory experiments showing distinct isotope fractionation effects (Table 1).

2.3.1. *Reductive dissolution of iron minerals*

Reductive dissolution of Fe minerals is largely studied with the presence of DIR bacteria. The $Fe(II)_{aq}$ is commonly depleted in heavy Fe isotopes compared to the substrate where it is dissolved from (Table 1). The $\delta^{56}Fe$ value difference between $Fe(II)_{aq}$ and the reactive surface of Fe(III) minerals can vary by about −3‰ (Crosby et al., 2007; Table 1). This fractionation can remain constant over a long period and is independent of the Fe mineral substrate (e.g. hematite or goethite), indicating a common mechanism for Fe isotope fractionation during DIR of different substrates (Crosby et al., 2007). The dissolved $Fe(II)_{aq}$ can be partially resorbed onto the Fe mineral surface, subsequently undergoes interfacial electron transfer to Fe(III) in Fe (hydr)oxides and Fe (II)-Fe(III) atom exchange, producing a reactive layer of Fe(III) at the mineral surface (Crosby et al., 2007). This leads to changing proportions of Fe species within the system, which in turn results in variations of the absolute δ values for $Fe(II)_{aq}$, especially at the early stage of the reduction process. However, the fractionation between $Fe(II)_{aq}$ and Fe (III) on the reactive surface is identical within error to the equilibrium fractionation between $Fe(II)_{aq}$ and ferric oxide in abiological systems at room temperatures (Crosby et al., 2007). This was later confirmed by examination of Fe isotope fractionation (∼ −3‰) between $Fe(II)_{aq}$ and Fe(III) on the reactive surface of hematite which is independent of isotopic fractionations among other phases present in the system (Wu et al., 2010).

Reductive dissolution of ferrihydrite by DIR bacteria results not only in $Fe(II)_{aq}$ but also in biogenic Fe oxides and carbonates, such as magnetite and siderite, through reprecipitation or reaction with anions. The isotope fractionation between $Fe(II)_{aq}$ and ferrihydrite and related biogenic products is a function of Fe(III) reduction rates and pathways by which the biogenic minerals are formed (Table 1, Johnson et al., 2005). At high reduction rates, $Fe(II)_{aq}$ is significantly lighter in isotope composition than ferrihydrite, reflecting a kinetic fractionation effect that is related not only to dissolution, but also to fast sorption of Fe(II) to the ferrihydrite surface. The $\delta^{56}Fe$ values of $Fe(II)_{aq}$ can vary by −1.3‰ compared with that of ferrihydrite, while the difference in $\delta^{56}Fe$ between $Fe(II)_{aq}$ and biogenic Fe species reduced from ferrihydrite is variable during slow dissolution (Johnson et al., 2005). At equilibrium, $Fe(II)_{aq}$ can be enriched or depleted in light Fe isotopes or it might not show any significant fractionation from the biogenic Fe species (Johnson et al., 2005), which is in line with the predictions based on spectroscopy data (Polyakov, 1997; Polyakov and Mineev, 2000; Schauble et al., 2001) or observed natural isotopic variations of respective Fe minerals (Johnson et al., 2003).

2.3.2. *Proton-promoted dissolution of iron minerals*

Proton-promoted dissolution is due to the reaction of H with O and

hydroxyl groups (OH) at the mineral surface, which promotes Fe release from the mineral surface into solution (Cornell and Schwertmann, 2003). Under very acidic soil conditions, proton-promoted dissolution may play an important role in Fe mobilization, while under circumneutral pH conditions this dissolution mechanism cannot take place effectively, and thus its role in Fe mobilization is insignificant. Nevertheless, laboratory data indicate distinct isotope effects during proton-promoted dissolution that are related to the Fe oxide mineral form (Table 1). Proton-promoted dissolution of goethite (Wiederhold et al., 2006) and hematite (Skulan et al., 2002; Johnson et al., 2004) do not fractionate Fe isotopes, even when the dissolution is incomplete. However, proton-promoted dissolution of biotite and chlorite shows a preferential release of light Fe isotopes into solution by up to −1.4‰ in δ^{56}Fe compared with the bulk phyllosilicates, although the fractionation is less pronounced at the later stage of the dissolution (Kiczka et al., 2010a). Chapman et al. (2009) hypothesized that the dissolution process of biotite occurred in two steps: an alteration of biotite to chlorite followed by dissolution of chlorite. Such effects have to be considered when choosing a proper extraction agent for soil Fe pool analysis to avoid attacking an undesired Fe pool and maximize discretization of Fe pools (see Section 3.3; Guelke et al., 2010; Kiczka et al., 2011).

2.3.3. Ligand-controlled dissolution of iron minerals

Organic matter is an important C pool in soils and plays a significant role in nutrient cycling and water retention. Organic ligands in soils such as siderophores and low molecular weight organic acids are reported to participate in mineral dissolution (Brantley et al., 2001, 2004; Wiederhold et al., 2006) and in Fe uptake by plant roots (Takagi et al., 1984; Curie et al., 2001; Schaaf et al., 2004). Experimentally, the dissolution of Fe-bearing minerals (e.g. hornblende, goethite) by organic ligands (e.g. siderophores, oxalic acid) results in significant Fe isotope fractionation (Table 1, Brantley et al., 2001, 2004; Wiederhold et al., 2006; Chapman et al., 2009; Kiczka et al., 2010). The extent of this isotope fractionation is a function of the binding strength of the ligands (Brantley et al., 2004). Stronger Fe-binding chelates preferentially extract lighter Fe isotopes (Brantley et al., 2001, 2004).

Abiotic and biotic ligand-controlled dissolution of Fe minerals can lead to considerably different isotope fractionation effects (Table 1). Brantley et al. (2004) found that when goethite was dissolved by siderophores in the presence of bacteria, lighter Fe isotopes were preferentially dissolved, while no significant fractionation was observed without the mediation of bacteria. The authors explained that in the system with the presence of bacteria, oxygen became depleted due to the bacterial respiration, and thus $Fe(III)_{aq}$ was reduced. The equilibration between $Fe(II)_{aq}$ and $Fe(III)_{aq}$ created a pool of isotopically heavy Fe(III) that was assimilated by bacterial cells (Brantley et al., 2004).

During the ligand-controlled dissolution of goethite by oxalic acid in the dark, Wiederhold et al. (2006), Chapmen et al. (2009), and Kiczka et al. (2010a) all found that light Fe isotopes were preferentially released due to the kinetic isotope effect at the beginning of the dissolution, and thus the solution became lighter compared with the dissolving mineral (Table 1). At later stages the solution became enriched in heavier Fe isotopes, which was attributed to dissolution of a progressively heavier goethite surface resulting in an increasing release of heavier Fe isotopes (Wiederhold et al., 2006). Similar Fe isotope fractionation was also found during the reductive dissolution of goethite by oxalic acid in the presence of light via a photochemical reductive mechanism at a speed considerably higher than that of ligand-controlled dissolution (Wiederhold et al., 2006).

2.3.4. Oxidative dissolution of iron minerals

During abiotic oxidative leaching of iron-sulfide-bearing rocks (rich in pyrite, chalcopyrite, and sphalerite) under strongly acidic conditions (pH = 2), the isotope fractionation at the initial stage was found to be towards the accumulation of heavy Fe isotopes in the leachates, leaving behind a relatively light rock surface (Table 1, Fernandez and Borrok, 2009). As the leaching experiments progressed, the leachate became lighter until it reached the isotope composition of the rocks (Fernandez and Borrok, 2009). This phenomenon was explained by fractionation either through incongruent dissolution and/or through the dissolution of an already isotopically heterogeneous mineral or rock (Fernandez and Borrok, 2009). Interestingly, when the leaching was performed at pH = 5, the released Fe was consistently isotopically lighter than Fe in the rocks, which was due to the precipitation of Fe(III) (hydr)oxides at this pH (Table 1, Fernandez and Borrok, 2009).

2.4. Plant uptake and redistribution

As growing media for numerous species of plants on Earth, soils provide various mineral nutrients for plants' development. Plants have on the other hand evolved metabolic strategies to utilize the nutrients for their biological functions. The nutrient flows starting from the soil via the roots to aboveground shoots are continuously accompanied with transformation and redistribution of the elements. These processes consist of various linked series of chemical reactions catalyzed by enzymes, including reduction and oxidation, complexation and complex break-down, which have the potential to fractionate an element's isotopes. Plant tissues exhibit distinct Fe isotope compositions from the soil in which they grow (e.g. Guelke and von Blanckenburg, 2007; von Blanckenburg et al., 2009; Kiczka et al., 2010b). Iron isotope fractionation in plants depends not only on the metal uptake strategy of the plant but also on Fe availability in the growth substrate (Kiczka et al., 2010b; Guelke-Stelling and von Blanckenburg, 2012). Within the plant, Fe can be further fractionated showing more negative δ^{56}Fe values in leaves and flowers than in the roots (Kiczka et al., 2010b). Apart from higher plants, a recent study showed that uptake of Fe(II) by phytoplankton can also produce significant Fe isotope fractionation and that this fractionation is also dependent on growth media and intracellular Fe contents (Sun and Wang, 2018). We will explain the detailed Fe isotope composition in plants in Section 4.

2.5. Perspectives for Fe source assignment on the basis of δ^{56}Fe values

As shown in Figs. 2 and 3, multiple processes are involved in the release, transformation and translocation of Fe in soil-plant-freshwater systems, and, as indicated in Table 1, all of these processes exhibit different but overlapping extents of Fe isotope fractionation. Due to the relatively low number of studies in determination of fractionation factors for certain reactions and large variations in experimental conditions among the different studies, the true mean values of fractionation factors are still unconfirmed. Nevertheless, it appears that all reactions involved in the transformation to or immobilization as Fe(III) tend to shift the δ^{56}Fe values of the resulting product in a positive direction, whereas all processes related to a transformation to or dissolution of Fe (II) forms result in a product depleted in heavy Fe isotopes (Fig. 4). In this regard, Fe leaving a system can potentially be isotopically lighter than Fe remaining in the system.

Many plants also preferentially take up light Fe isotopes, indicating that losses and removal of plant biomass with harvest will result in the soils becoming depleted in light Fe isotopes. A clear obstacle in reconstructing Fe sources from isotope values occurs when Fe is not leaving a system as Fe(II) or in dissolved form, but as Fe nanoparticles, as recently shown by Gottselig et al. (2017). In this case, heavy Fe isotopes might also be lost from the system. A promising strategy to reconstruct the Fe cycle from remaining Fe isotopic signatures of different Fe pools in the system and known fractionation factors of the involved processes can benefit from reliable modelling of Fe loss pathways and speciation changes. However, one should bear in mind that pool sizes of the lost Fe and that remaining in the system may be significantly different, often leading to unremarkable variation in Fe isotope composition of the system. Therefore, one should always

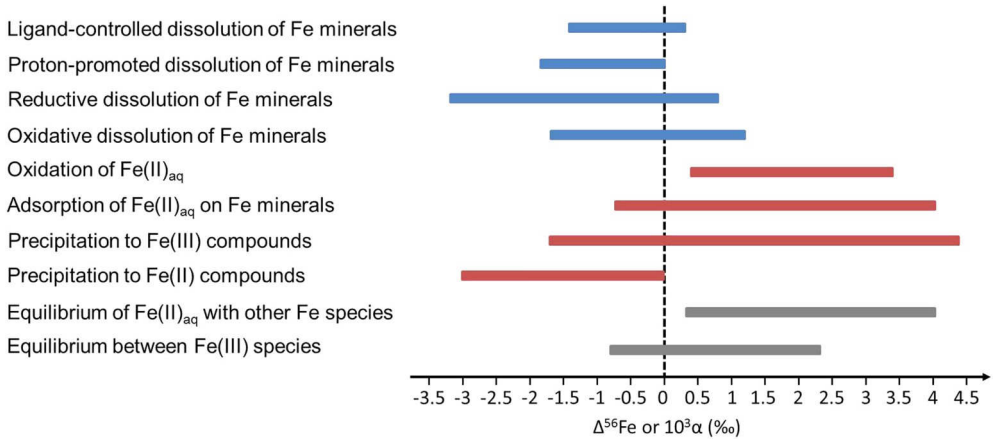

Fig. 4. Range of Fe isotope fractionations (Δ^{56}Fe or $10^3\alpha$) of main processes as assessed in the laboratory (see Table 1 for details). Blue bars: processes that mobilize Fe; red bars: processes that immobilize Fe; gray bars: equilibrium fractionation of Fe(II) and Fe(III) species. The footnote to Table 1 applies for this figure as well.

identify and interpret Fe isotope composition of one pool relative to another corresponding pool in the system. For instance, Fe isotope composition of plants should be interpreted relative to the plant available Fe pool in soil rather than the bulk Fe pool. Additionally, a main remaining challenge is the correct assignment of, usually mass-dependent, Fe fractionation factors to specific kinetic and equilibrium fractionation processes which are frequently hard to identify in natural systems.

3. Iron isotope fractionation in soils

The Fe isotope composition of bulk soils largely reflects that of the original parent material, altered by the impact of Fe isotope fractionation processes that occur with Fe transformation, redistribution within and/or losses from a soil profile and among the different diagnostic soil horizons. Though parent material vary in Fe isotope composition (e.g. Poitrasson and Freydier, 2005; Teng et al., 2008), most igneous rocks from the continental crust have limited Fe isotope variation (Poitrasson, 2006), referred by many studies as continental crust mean with δ^{56}Fe around 0.07‰ (Poitrasson, 2006) or around 0.09‰ (Beard et al., 2003). These two δ^{56}Fe values are identical within error, so we choose ~0.07‰ as the continental crust mean in the following sections. Details on the scale of Fe isotope fractionation in parent materials can be found in the papers of e.g. Rouxel et al. (2003) and Dauphas et al. (2017). Upon weathering and related pedogenic processes, such as eluviation of clay minerals with different particle sizes, formation and translocation of secondary Fe oxide minerals, or redoximorphosis, the spatial heterogeneity of Fe isotope composition in soil can increase. Once Fe is withdrawn from or added to a system, Fe isotope composition of the residue may be altered and become diagnostic for the degree and rates of Fe cycling within soil profiles, as well as in the related water catchments and soil-plant systems.

3.1. Iron isotope fractionation in soil profiles

Compared with laboratory experiments (Table 1), Fe isotopic studies of whole soils are still limited. To date only around 20 research papers have been published targeting soil profiles to identify Fe isotope compositions in terrestrial ecosystems. Moreover, most of these studies focus on forested or glacial soils, with the purposes to either unravel the geological development of the soils or to investigate specific pedogenic processes, which require such studies to take place in preferably pristine environments. Impacts of human agricultural activities on Fe cycling and related isotope fractionation processes have so far received very little attention. Only recently, a paddy soil (Anthrosol) irrigated with arsenic-enriched groundwater was studied with respect to Fe isotope fractionation in the soil-water-rice system (Garnier et al., 2017) and two paddy chronosequences in China were studied by using Fe isotope composition as a tool to investigate Fe transfer and redistribution caused by anthropedogenesis (Huang et al., 2018a, 2018b).

3.1.1. Major reference soil groups [according to IUSS (2014) classification]

During pedogenesis soils can develop a relatively wide range of Fe isotope compositions compared with their parent rocks. Compiling the Fe isotope data from different studies reveals that soils of different pedogenesis vary in their Fe isotope composition (Fig. 5, Figs. SI2). Within a given soil profile, the maximum change of δ^{56}Fe values is about 1‰ for the bulk soil (Fig. 5), which is much less than the full extent of the variations reported in the laboratory experiments for different processes involved in terrestrial Fe cycling (Table 1). This is due to the fact that Fe pool sizes in a natural ecosystem are different from those in laboratory settings. Furthermore, kinetically controlled processes may prevail in natural ecosystems, so that equilibrium may not be reached (Kiczka et al., 2011).

Fig. 5 also highlights that not all of the soils display a vertical Fe redistribution and variations of Fe isotope composition. In general, three main characteristic Fe isotope signatures can so far be ascribed to soils: 1) an enrichment of heavy Fe isotopes in the subsoil, with lower δ^{56}Fe values in the surface soils (Andosols, Acrisols), 2) a depletion of light Fe isotopes in the mineral surface soils (Albeluvisols, Gleysols, Podzols), and 3) no pronounced alteration of δ^{56}Fe values with soil depth (Cambisols, Ferralsol).

The lowest δ^{56}Fe value (−0.52‰, recalculated relative to IRMM-014) of bulk soil in all studied soil profiles was reported in the surface E horizon of an Acrisol (deeply weathered, oxic soil; Fantle and DePaolo, 2004). This Acrisol showed notable differences between the shallow organic-rich and the deeper mineral horizons, where Fe in the organic-rich horizon was significantly isotopically lighter than in the mineral horizons of the profile, likely because plants took up isotopically light Fe from the soil (Table 1) and returned it as above- and belowground litter input to the surface horizons.

The Andosols studied by Thompson et al. (2007) also exhibited lower δ^{56}Fe values (~ +0.04‰) in the surface soils relative to the deeper soil horizons, while the highest δ^{56}Fe value (+0.72‰) was found in the B horizon (Fig. 5). These Andosols experienced annual precipitations ranging from 2200 mm to 4200 mm, which led to increased loss of Fe from the soil profiles due to the enhanced anoxic conditions, leaving heavier Fe isotope compositions in the soil profiles that were directly related to the weathering intensity. In contrast, Ferralsols, which are also deeply weathered tropic/subtropic soils with diffused horizon boundaries and enrichment of Fe oxides, show virtually no vertical Fe isotope fractionation (+0.10 to +0.12‰, Huang

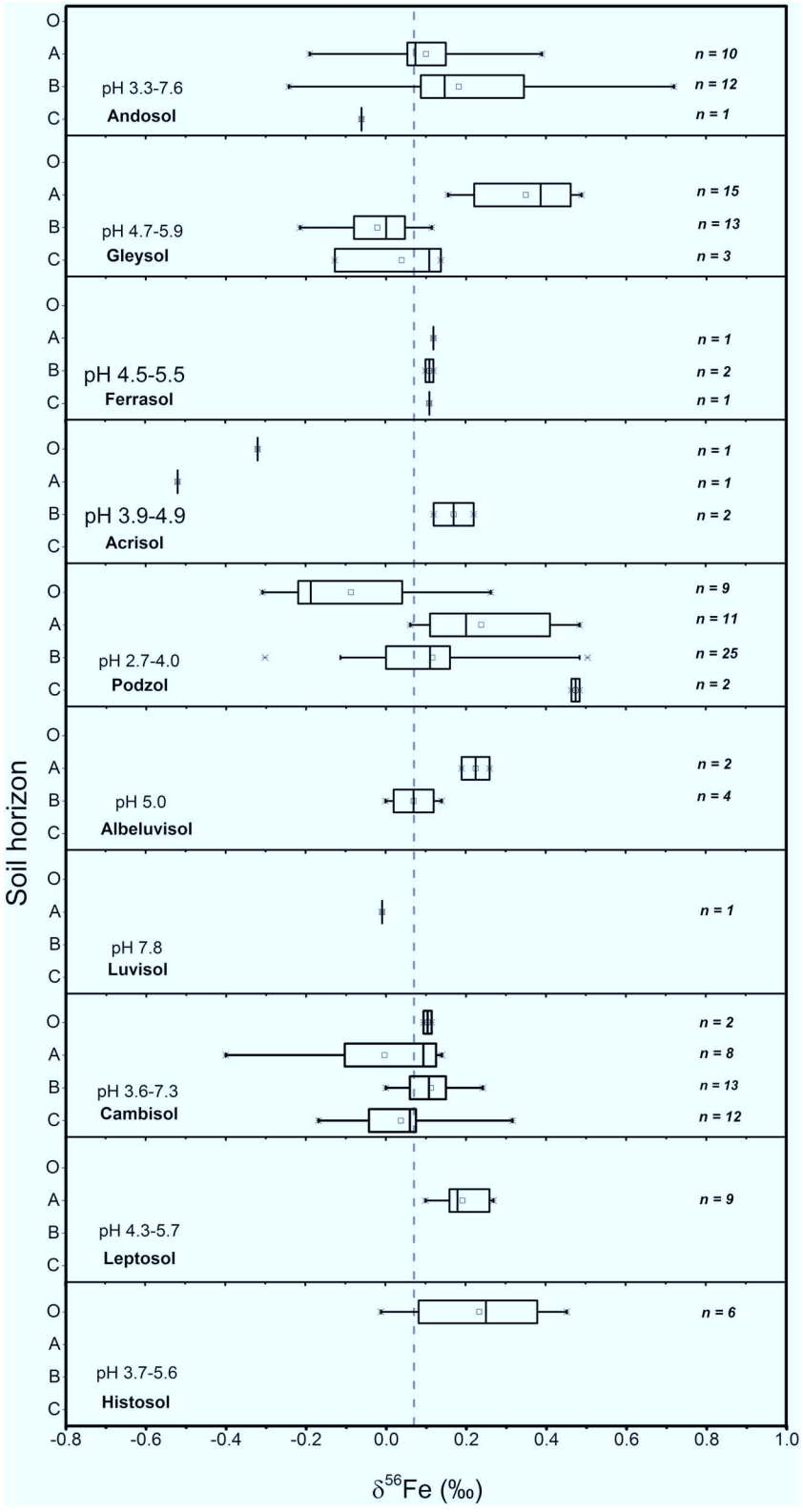

Fig. 5. Depth profile of Fe isotopic signatures in bulk soil (max. depth 140 cm) The soil orders refer to the international soil classification system according to the World Soil Reference Base (IUSS, 2014). If other soil classification systems such as US Soil Taxonomy were applied in the studies, we translated soil names into the WRB system. Soil pH values are referred to $CaCl_2$ extraction wherever given, while those measured in H_2O solution in the literature are assumed 0.6 pH units higher than that measured in $CaCl_2$ solution (Guelke et al., 2010). The number of the data *n* is given on the right side of the whiskered boxes. The gray line at ~0.07% indicates the continental crust mean (Poitrasson, 2006).

et al., 2018b). This reflects the in-situ formation of Fe oxide minerals and a lack of pronounced eluviation processes.

In boreal climate settings, Andosols developed in Iceland showed variable weathering degrees and Fe isotope composition. Limited δ^{56}Fe variations (0.09 ± 0.08‰) were found for Icelandic Haplic Andosol and Gleyic Andosol with low weathering degree, reflecting the Fe isotope signature of the parent basalt. A Histic Andosol in wetland areas with a higher degree of weathering, however, had isotopically heavier Fe at the surface and lighter Fe than the parent basalt below 25 cm depth (Opfergelt et al., 2017). This was attributed to preferential release of light Fe(II) isotopes under poorly drained, i.e., anoxic conditions, followed by quantitative precipitation of Fe oxides during fluctuating oxic conditions as a result of seasonal freeze-thaw cycles. The organic-rich Histosol profile in wetland areas exhibited heavier Fe

isotope composition than the parent basalt, suggesting losses of light Fe isotopes due to reductive dissolution of Fe minerals (Opfergelt et al., 2017). In addition, high contents of organic matter might as well contribute to the Fe isotope variability in the profile.

Albeluvisols are also affected by leaching processes, though to a lower degree than the much older Acrisols or the Andosols receiving much larger amounts of rain. A seasonally water-logged Albeluvisol showed enhanced Fe dissolution and remobilization in both surface and subsurface horizons, leaving the residual soil with decreased Fe concentration and enriched heavy Fe isotopes due to preferential removal of light Fe isotopes (Fekiacova et al., 2013).

The genesis of Gleysols is driven by ground-water induced redoximorphosis. For Gleysols, several studies showed that Fe in the mineral B horizon is considerably isotopically lighter than Fe in the A horizon (Wiederhold et al., 2007a; Mansfeldt et al., 2012; Fekiacova et al., 2013; Akerman et al., 2014). Notably, the authors of these studies offered different interpretations for the isotopic variations between surface and deep horizons. Fekiacova et al. (2013) explained the δ^{56}Fe in the B/C horizon of the Gleysol as a reflection of its parent material due to the presence of large amounts of Si-bound Fe. Mansfeldt et al. (2012), in contrast, attributed the high δ^{56}Fe values in the topsoil primarily to fast ferrihydrite precipitation during aeration immediately after reducing condition which favored heavy Fe isotope to precipitate, while the low δ^{56}Fe values of the Fe-rich horizons (Bg, CrBg) were due to adsorption of dissolved Fe(II) with a light isotope composition onto goethite during capillary rise of the groundwater. The elevated δ^{56}Fe of the Fe-poor subsoil (2Cr) were attributed to silicate-bound Fe rather than to dissolution and precipitation of Fe oxides.

In a successive study, Schuth and Mansfeldt (2016) extracted soil solutions from this Gleysol profile and found that both Fe concentration and Fe isotope composition of the dissolved Fe (< 0.45 μm) strongly varied with the abundance of the soil Fe oxides. In the horizon where Fe oxides were abundant (CrBg), the dissolved Fe was low in amount and exhibited a very low δ^{56}Fe value (-1.7‰), in agreement with the soil data showing adsorption and atom exchange between dissolved Fe(II) and Fe oxides (Schuth and Mansfeldt, 2016). Schuth et al. (2015) used a laboratory experimental design with variable redox potentials to demonstrate that vertical movement of a low-δ solution from the topsoil might result with time in the formation of subsoils with δ values also lower than those of the original topsoil after repeated E_h cycles as common in Gleysols. Rising groundwater levels therewith affect the isotope composition of both aqueous Fe and Fe in soil (Schuth and Mansfeldt, 2016). Such a relation between Fe isotope variation and pronounced redoximorphic features due to water logging can also be observed in Stagnic Cambisols, which exhibit Fe zonation with δ^{56}Fe values at the Fe-depleted zones being higher than those at the Fe-enriched zones (Wiederhold et al., 2007a).

Flooding can also lead to variations of Fe concentrations and isotope compositions in soil and its solution due to change of redox potentials. Compared with dissolved Fe released by floods, colloidal Fe may play an even more important role in defining the Fe isotope composition of the soil solution. In an artificial flooding experiment using carbonatic floodplain topsoil (Calcaric Fluvisol), Kusonwiriyawong et al. (2017) found substantial Fe release as colloidal fractions (0.02–10 μm). These fractions initially showed a light isotope composition due to the precipitation of siderite from dissolved reduced isotopically light $Fe(II)_{aq}$. As the flooding persisted, the difference in δ^{56}Fe values of the dissolved Fe and of colloidal fractions shifted increasingly towards negative values, due to changes in colloid mineralogy, sorption to soil components and/or electron transfer-atom exchange. This study points out the importance of colloids in Fe release from soils to soil solutions.

The formation of Podzols is driven by acid weathering and illuviation processes, which can result in relatively large variations of Fe isotope compositions along the soil profiles (Emmanuel et al., 2005; Wiederhold et al., 2007b; Fekiacova et al., 2017). The main difference in Fe isotope composition is found between the Fe-depleted E horizons and the underlying Bh/Bhs horizons, where Fe in the Bh/Bhs horizon is significantly lighter than Fe in the E and other mineral horizons. The loss of light Fe isotopes from bleached A/E horizons largely explains their elevated δ^{56}Fe values.

Since the Bh horizons in Podzols contain large amount of Fe-organic complexes, the low δ values in these horizons are most likely due to this Fe pool (Wiederhold et al., 2007b). Wiederhold et al. (2007b) proposed that pedogenic vertical Fe translocation was driven by organic ligands at very acidic pH and lighter Fe isotopes were preferentially translocated within the Podzols. However, another Podzol studied by Emmanuel et al. (2005) did not display large differences in Fe isotope variation. This might be due to the fact that the studied samples were not from characteristic eluvial E and illuvial Bh/Bs horizon sections. By studying a unique Podzol chronosequence in Canada, Fekiacova et al. (2017) demonstrated how the podzolization processes evolved successively. After pH values dropped to ~ 4.5 (270 years) due to organic matter accumulation in the surface horizons, the podzolization itself can be a rather fast process (< 50 years). Along this podzolization processes Fe was isotopically fractionated. The heavy Fe isotopic signature of the A/E horizon was a result of mineral dissolution and the light Fe isotope enrichment in illuvial Bh/Bhs horizons was linked with Fe-organic complexes and poorly crystalline Fe oxyhydroxides. However, the authors also pointed out that it was still unclear whether this enrichment was attributed to transport of the light Fe from the surface soil or to preferential incorporation of light Fe into Fe oxides and Fe-organic complexes.

Cambisols are soils that are less affected by vertical Fe translocation than the soils discussed so far, although formation of clay minerals and pedogenetic oxides are diagnostic for the Bw horizon. These processes may alter δ^{56}Fe values on the microscale within the soil horizon and those of soil Fe pools (see Section 3.2), but the variation of Fe isotope composition for the bulk soil can be very limited among different soil horizons. Indeed, for Cambisols in general, Fe isotope compositions along depth profiles vary moderately within a range between 0.0‰ and +0.1‰ for the mean δ^{56}Fe values from O to B horizons (Fig. 5), which is similar to the continental crust mean (~ +0.07‰ relative to IRMM-014, Poitrasson, 2006). The Fe isotope data therewith nicely illustrate that Cambisols are developed under oxic and well-drained conditions under which Fe translocations are limited within the profile and transformations of Fe minerals are localized, so that overall no apparent isotopic effect can be seen (Fekiacova et al., 2013, 2017; Wiederhold et al., 2007b).

The A horizons of Leptosols from a chronosequence of a glacier forefield contained Fe with a heavy isotopic signature with δ^{56}Fe up to +0.27‰, similar to their respective parent materials (granite +0.15‰ and gneiss +0.25‰, Kiczka et al., 2011). Iron speciation analysis of these soils showed a shift from Fe in Fe(II)-bearing phyllosilicates towards Fe in Fe(III)-bearing phyllosilicates and Fe(III) (hydr)oxides with increasing time since deglaciation. This shift did not induce significant variation of the Fe isotope composition of the bulk soil, which ranged between +0.10‰ and +0.27‰ in δ^{56}Fe. However, the Fe isotope composition varied among soil particles: Fe in sand was isotopically heaviest, while Fe in clay was significantly lighter (δ^{56}Fe +0.06 to −0.10‰) than that in bulk soils and became even lighter with increasing time since deglaciation. Based on Fe speciation analysis and particle-size studies, the authors attributed approximately one third of the Fe in the clay size fractions to newly formed Fe(III) (hydr)oxides that were isotopically lighter than the bulk soil and pointed out that the kinetic isotope effect leading to preferential release of light Fe isotope was not a transient phenomenon restricted to the very initial weathering flux, but it could persist over long timescales when Leptosol development proceeded. In such a case, one can expect that, as light Fe isotopes are progressively removed, especially when ligand-controlled or reductive dissolution processes dominate, the residual solid is either increasingly enriched in heavy Fe isotopes over the course of soil weathering (Thompson et al., 2007), or the heavy isotope signature of

the residual solid is “diluted” within the large Fe pool of primary silicate minerals (Kiczka et al., 2011).

To date, only one bulk sample of the A horizon of a Luvisol was studied regarding its isotope composition, showing a near-zero δ^{56}Fe value (Guelke et al., 2010). However, Fe pools in this soil (sequentially extracted by various agents) showed distinct Fe isotope compositions with the so-called “plant-available” Fe pool isotopically the lightest. The Fe pools and their isotope compositions are discussed in detail in Section 3.2.

3.1.2. Deep soil profiles

Soil science usually restricts analyses to 1 to 2 m of soils on earth surface, according to the lower depth of soil classification systems. Very old soils, especially of the tropics, however, are much deeper developed. Also plant roots may go beyond 2 m soil depth, particularly in forests (Canadell et al., 1996).

Deep weathering under wet tropical climates modifies the physicchemical characteristics of the parent rock. The so-called laterites can then form as mineralogical and chemical modified surface material, usually forming Ferralsols in the top meters. The laterite overlies softened bedrock (saprolith) with the original residual bedrock (regolith) usually being found at several meters depth. Laterites may be compacted, are characterized by a rusty-red coloration due to high Fe oxide contents, and can form hard crusts when drying out. The dominant chemical weathering process is hydrolysis which can reach depths even below 80 m. As no bioturbation occurs in these depths, the rock structure is retained and Fe-depleted and Fe-rich areas can be found unmixed side by side (for more details on laterite formation, see, e.g., Aleva, 1994).

Three studies have been carried out to investigate Fe geochemical cycles in deep laterites (either recent or ancient) by using stable Fe isotopes as a tool. The Paleoproterozoic lateritic Hekpoort paleosol (~2.2 Ga) from Gaborone, Botswana, generally showed positive δ^{56}Fe values throughout the profile down to the parent rock at a depth of 128 m, except for a sampling point at around 107 m where the Pallid zone was enriched with light Fe isotopes (Yamaguchi et al., 2007). The δ^{56}Fe value peaked (+1.06‰) at the mottled zone at a depth of ~105 m where Fe was depleted, higher than that in Fe-rich laterites. The authors attributed this phenomenon to Fe mobilization due to multiple alternations of wet and dry seasons during which the groundwater table shifted, leading to relocation of isotopically light Fe $(II)_{aq}$ followed by oxidation and re-precipitation. The positive Fe isotopic signature of this ancient laterite profile thus reflects oxidative weathering of the parent basalt under an atmosphere with relatively high levels of O_2, accompanied by groundwater-induced $Fe(II)_{aq}$ translocation processes. However, the study of Poitrasson et al. (2008) showed little Fe isotope fractionation in recent laterites, despite that strong alternations both in mineralogy and Fe concentration happened during the lateritization process. This may be because, in spite of lateral mobilization and loss, Fe remains mostly in its oxidized form in recent lateritic soils, particularly when a lack in groundwater table shifts is present. As a result, Fe isotope fractionation can be nearly invariable. This is confirmed by the study of Li et al. (2017), who found in a laterite profile obtained from an equatorial rainforest that despite large variation in the concentrations of Fe oxides and dramatic Fe loss, the δ^{56}Fe values differed only in a small range from −0.03‰ in the parent rock (peridotite) to +0.10‰ in the extremely weathered saprolites. In agreement with Poitrasson et al. (2008), the authors suggested that Fe in this laterite profile should have experienced a complete and in situ oxidation prior to Fe translocation. Since Fe(III) is not mobile in water, the possible Fe species to induce significant Fe loss was then expected to be ferric Fe colloids which had a similar Fe isotope composition to the continental crust.

Similarly, a deep saprolite profile which had undergone extreme weathering under oxidizing conditions also showed limited Fe isotope fractionation (Liu et al., 2014). Under oxidizing conditions, Fe is transformed into less mobile Fe(III) and rapidly precipitated as Fe oxides, which is the dominant Fe species in this soil. The authors pointed out that these Fe-oxide rich soils usually showed a relatively heavier Fe isotope composition compared with Fe in the parent rock, while Fe isotope variation along the profile was insignificant. In contrast, when different redox regimes are present in the profile, the Fe isotope fractionation during silicate weathering is redox-controlled and can show substantial variation along the profile as result of the combination of preferential release of light Fe isotopes during primary dissolution and secondary processes such as oxidation, precipitation, as well as complexation with soil organic matter.

A terra rossa developed on dolomite contained Fe with fluctuating isotope signatures along the soil profile and was isotopically lighter than the Fe in the underlying bulk dolomite and the insoluble dolomite residue (Feng et al., 2018). The authors hypothesized that the terra rossa was under the influence of an extraneous input of dissolved Fe with a light isotopic signature and that the dolomite weathering was not the only source of Fe in the terra rossa. The Fe isotope signature in the terra rossa, as well as the relations of Fe, Si, and Al and the contents of their oxides, were resulted from a combined action of extraneous Fe input and redox variations during the early stages of dolomite weathering and terra rossa formation, as well as subsequent desilicification of the terra rossa. Therefore, the authors concluded that the formation mechanism of terra rossa was different from that of the soils developed from weathering products of silicate rocks.

3.1.3. Anthropogenic soils

Paddy soils (Anthrosols) comprise the largest artificial wetlands that feed almost half of the world's population through rice cultivation (Kögel-Knabner et al., 2010). Paddy soils can develop from any pedological soil order, but all soils experience repeated flooding-drainage cycles that lead to specific redoximorphic features. The redox oscillations due to paddy management result in unique Fe dynamics in paddy soils. When waterlogged, paddy soils can contain high amounts of Fe(II) in the pore water as a result of reductive dissolution of Fe(III) minerals mediated by DIR bacteria under low redox potential and anaerobic conditions (Lovley et al., 2004). Poorly crystalline Fe(III) (hydr)oxides (e.g. ferrihydrite) are the main plant-available Fe forms in paddy soils involved in DIR processes. As rice growth progresses, the system becomes oxidative so that Fe(III) (hydr)oxides are re-precipitated. This cycle of dissolution and (re-)precipitation results in a drastic Fe transformation and translocation. In a recent study, Garnier et al. (2017) found that Fe in the pore water was isotopically light (δ^{56}Fe − 1.38‰), and that there was a significant linear correlation between Fe concentration and δ^{56}Fe in pore water due to Rayleigh-type fractionation of the DIR processes in pore water. The study thus confirmed that Fe isotope fractionation between the pore water and the substrate involved three Fe pools (Fe in solution, Fe(II) sorbed at the surface of the substrate, and a reactive Fe(III) pool on the Fe substrate), in agreement with laboratory experiments, e.g. by Crosby et al. (2005). In the studies of paddy chronosequences by Huang et al., 2018a, variation of Fe isotope compositions were firstly investigated with a focus on the impact of long-term anthropedogenesis. The two paddy chronosequences were derived from different parent materials: the one in a plain area developed from calcareous marine sediments, while the other was from highly weathered quaternary red clay on a sloping upland. The non-paddy original soils were classified as Cambisol and Ferralsol, respectively, with significantly different pH values (~8.1 vs. ~5.1), and clay contents (~21% vs. ~54%), but no significant variations of Fe isotope compositions along the profiles for both original soils. Long-term paddy management resulted in increasing profile differentiation of Fe oxides and measurable Fe isotope fractionation compared with the starting soils. The chronosequence located on the sloping upland experienced Fe loss from the surface horizons, and both total Fe and oxide-bound Fe contents decreased with paddy soil age, possibly due to clay particle-facilitated leaching. However, in the other chronosequence, the surface

Fe concentration was relatively constant on a millennial scale with much longer rice cultivation history and the total Fe and Fe oxide-bound Fe contents increased, especially in the first 50 years of rice cultivation. The authors attributed the overall Fe accumulation in this chronosequence to external Fe inputs. Despite these differences, both paddy chronosequences showed enrichment of heavy Fe isotopes in the topsoil while the deeper illuvial horizons were characterized by light Fe isotope compositions, reflecting preferential mobilization of light Fe isotopes.

Mining activities generate mine tailings that are exposed to natural weathering processes, which result in dissolution and (re-)precipitation of minerals and thus affect nearby environments. Stable isotope analysis of these minerals can provide a basis to understand geochemical processes occurring in these tailings, thereby enabling an assessment of their environmental impact. For such purposes, a soil profile through sulfide-bearing tailings at a former copper (Cu) mine in Northern Sweden was studied by Rodríguez et al. (2013), who found no significant difference in δ^{56}Fe values between unoxidized and oxidized zones of the soil profile. However, at the oxidizing front of sulfides the δ^{56}Fe value was the highest (−0.24‰) due to the precipitation of Fe (III) (hydr)oxides, following Fe(II) oxidation, and accompanied by leaching of $Fe(II)_{aq}$. It is noteworthy that the δ^{56}Fe values of this mine tailing profile were generally very negative (average of oxidized and unoxidized zones −0.58 ± 0.06‰ and − 0.49 ± 0.05‰, respectively), and were at the very low end of natural soil profiles (e.g., −0.52‰, Fantle and DePaolo, 2004) that have been studied so far. These negative values may largely be due to the fact that pyrite was the main Fe-sulfide in the unoxidized zone of this profile (Rodríguez et al., 2013), which may have δ^{56}Fe values as low as −3.1‰ (Guilbaud et al., 2011a). Oxidative sulfide weathering in the oxidation zone of the mine tailings in Chañaral in Chili, resulted in Fe(III) (hydr)oxides with positive δ^{56}Fe values, while the Fe-containing sulfide residues were isotopically light (Roebbert et al., 2018).

3.2. Iron isotopic signature of soil iron pools

Weathering processes usually take place locally and do not induce significant Fe translocation (Wiederhold et al., 2007b). Therefore, Fe isotope fractionation may not be revealed by bulk soil analysis, but only presents itself at local scale among different Fe pools. Sequential chemical extraction of soil is usually performed to separate: water-soluble and exchangeable Fe (Fe_{ex}), organically adsorbed and bound Fe (Fe_{org}), poorly crystalline Fe(III) (hydr)oxides ($Fe_{poorly\text{-}cry.\text{-}oxides}$), crystalline Fe (III) (hydr)oxides ($Fe_{cry.\text{-}oxides}$), and Fe sequestered in primary silicate minerals ($Fe_{silicate}$). The distribution of Fe among these pools reflects the type and degree of Fe weathering processes, and their isotopic signatures can be used to track Fe transformation and translocation in soils.

Only a small part of Fe in the soil is plant available due to the low solubility and slow dissolution rates of inorganic Fe compounds (Guelke et al., 2010). Therefore, in order to assess soil Fe fertility in modern agricultural practices, it is indispensable to identify (potentially) plant available Fe in the soil and its transformation processes.

Fig. 6 shows a modified sequential extraction procedure proposed by Guelke et al. (2010) to examine these Fe pools/fractions in soils, especially those associated with plant available Fe. In short, soils are extracted with 1 M $MgCl_2$ solution to access Fe_{ex}, followed by diluted HNO_3 (0.01 M) and H_2O_2 (30%) to release Fe_{org}. The residue is then treated with 0.5 M HCl targeting $Fe_{poorly\text{-}cry.\text{-}oxides}$, prior to the extraction of $Fe_{cry.\text{-}oxides}$ by dithionite-citrate in acetic acid (HAc). The fractions Fe_{ex}, Fe_{org}, and $Fe_{poorly\text{-}cry.\text{-}oxides}$ are considered as plant available Fe, the δ^{56}Fe values of which are thus compared with those of plants to determine the fractionation factor between the plants and the soils where the plants grow in (discussed in Section 5). Guelke et al. (2010) argued that the procedure did not induce significant isotope fractionation if artifacts (see Section 3.3) were eliminated. It is worth noting

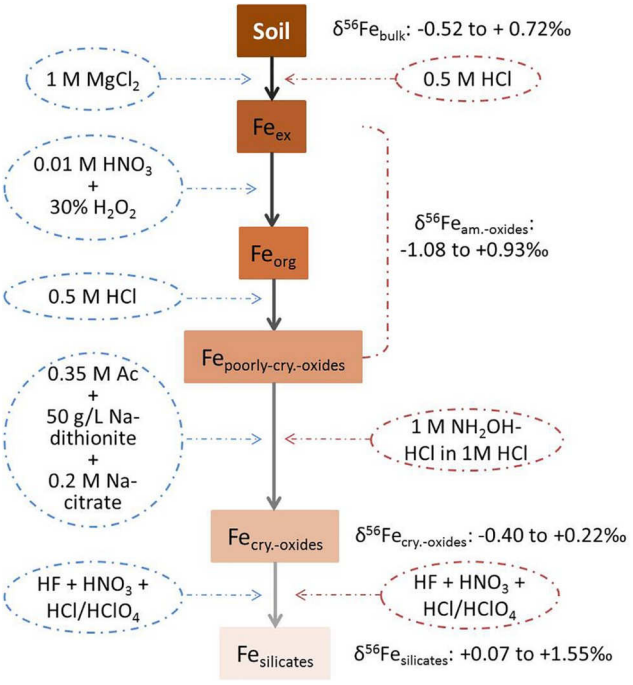

Fig. 6. Sequential chemical extraction procedures proposed by Guelke et al. (2010) (in blue dashed circles) and simplified three-step extraction (in red dashed circles) to study different Fe pools in soil. Fe_{ex}, Fe_{org}, and $Fe_{poorly\text{-}cry\text{-}oxides}$ are together termed as $Fe_{am.\text{-}oxides}$ fraction and claimed as plant-available Fe. Since most studies applied the three-step extraction, we give the range of the δ^{56}Fe values for these Fe pools.

that the concentration of HNO_3 used in the extraction of organically bound Fe may need to be adjusted to bring high pH of soils (e.g. calcareous soils) into the acidic range required in organic matter destruction by H_2O_2 and to prevent secondary precipitation.

Traditionally, in non-isotope studies, poorly crystalline Fe(III) (hydr)oxides are extracted with ammonium oxalate in an acidic solution (usually HCl) at pH 3 (termed as Fe_o) (Schwertmann, 1964, 1991), while total extraction of all Fe oxides is performed with a buffered dithionite-citrate solution (Fe_d) (Mehra and Jackson, 1958; Kiem and Kögel-Knabner, 2002). In addition, Roebbert et al. (2018) proposed to target Fe containing sulfides using $KClO_4$ in 12 M HCl after dithionite and oxalate extraction and claimed no significant Fe isotope fractionation occurred during the extractions. However, as illustrated in a laboratory experiment by Wiederhold et al. (2006), oxalate extraction can result in significant Fe isotope fractionation either through ligand-controlled (in dark) or reductive (in the presence of light) dissolution mechanisms. Therefore, the authors proposed to use diluted HCl to target poorly crystalline Fe oxides as no isotope fractionation was found during the dissolution of goethite by 0.5 M HCl via the proton-promoted mechanism. However, Kiczka et al. (2010a) found negative δ^{56}Fe values when dissolving primary phyllosilicates with diluted HCl, indicating that HCl could attack silicate minerals and release light Fe isotopes leading to isotope fractionation during the dissolution. Whether or not Fe isotope fractionation occurs during dissolution and to which extent depends on the mineralogy of the soil. The possible bias induced by dissolution of Fe from silicate minerals should be considered when studying poorly crystalline Fe oxides using HCl extraction.

Following HCl extraction, hydroxylamine-hydrochloride (NH_2OH-HCl) under acidic condition is applied to access crystalline Fe oxides ($Fe_{crys.\text{-}oxides}$) (Emmanuel et al., 2005; Wiederhold et al., 2007a, 2007b; Guelke et al., 2010). Conversely, Kiczka et al. (2011) used a reversed procedure, i.e. NH_2OH-HCl in HAc to selectively dissolve poorly crystalline Fe oxides, followed by HCl extraction targeting easily leachable Fe from primary Fe(II)-bearing phyllosilicates. These procedures were

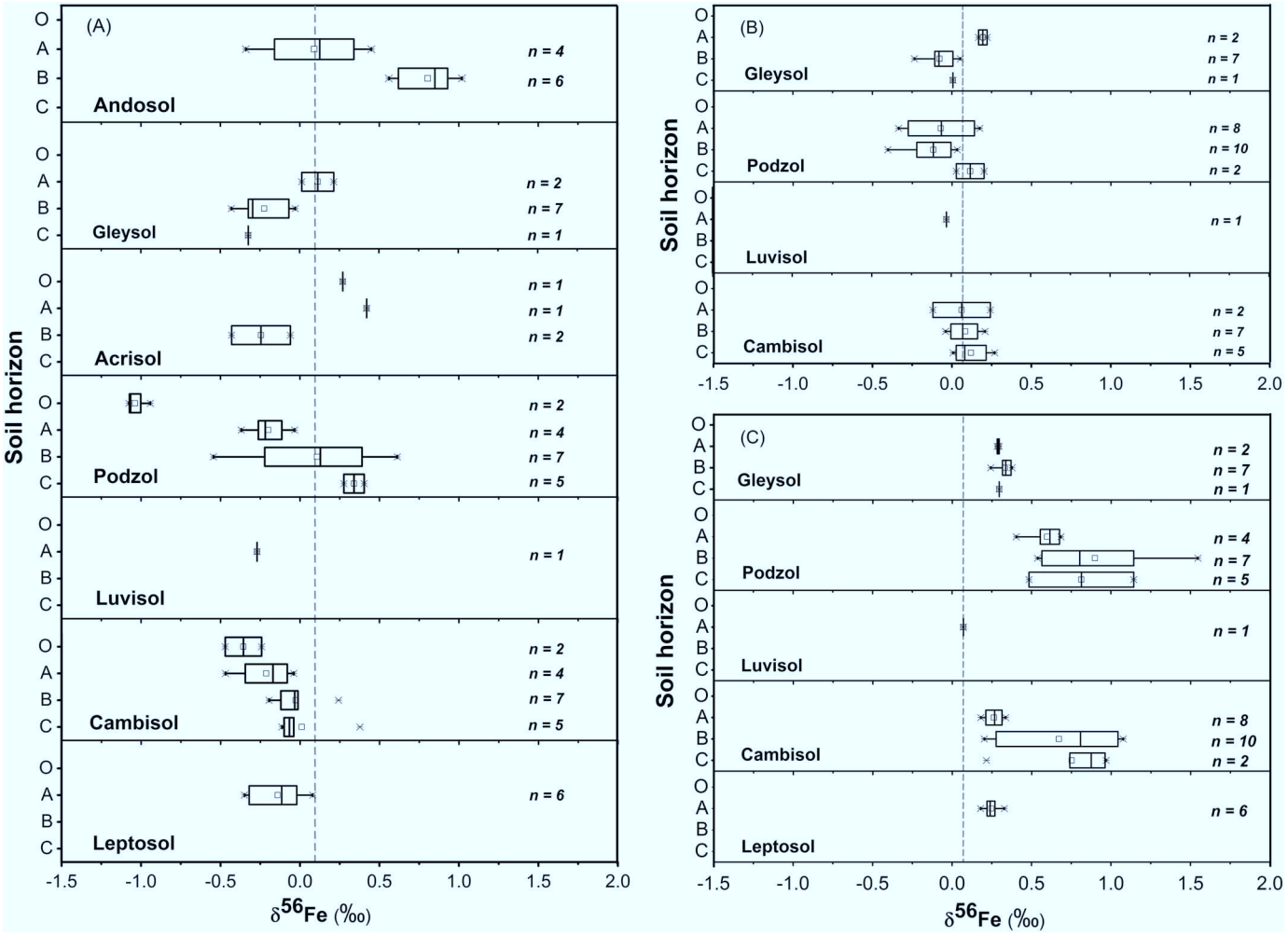

Fig. 7. Depth profile (≤ 140 cm) of isotope compositions of different soil pools: (A) Amorphous Fe oxides ($Fe_{am.\text{-}oxides}$ fraction) are extracted by 0.5 M HCl targeting poorly crystalline Fe (oxyhydr)oxide and adsorbed and organic bound Fe; (B): The $Fe_{cry.\text{-}oxides}$ fraction is extracted by 1 M NH_2OH-HCl in 1 M HCl targeting crystalline Fe oxides; and (C): The $Fe_{silicate}$ fraction is extracted by HF in acidic solution targeting Fe incorporated in silicate minerals. Note that the missing soil orders compared with the bulk soil data (Fig. 5) are due to the lack of Fe isotope data of the Fe pools in these soils. Isotope compositions of soil Fe pools that were extracted differently (e.g. total Fe oxides by dithionite-citrate extraction) were not included in this figure.

based on previous finding that large fractions of Fe (up to 48%) from primary phyllosilicates could be released by diluted HCl which would affect the observed isotopic signature in the leached solution (Kiczka et al., 2011).

In fact, most Fe isotope data in Fe pools in soils are based on extractions by 0.5 M HCl, and then by 1 M NH_2OH-HCl in 1 M HCl followed by HF-acid digestion to obtain Fe fractions of organically adsorbed/bound Fe and poorly-crystalline Fe oxides ($Fe_{am.\text{-}oxides}$, plant available Fe), $Fe_{cry.\text{-}oxides}$ and $Fe_{silicate}$, respectively. Some studies simply applied the extraction by 0.5 M HCl for plant available Fe. Other extraction methods, such as dithionite-citrate extraction of Fe oxides and pyrophosphate extraction of organically bound Fe, are also utilized by several studies. However, these studies either did not analyze Fe isotope composition of the extracts or presented only limited number of $\delta^{56}Fe$ values, Therefore, in Figs. 6 and 7, the $\delta^{56}Fe$ values in different pools are taken from the majority of the data for $Fe_{am.\text{-}oxides}$, $Fe_{cry.\text{-}oxides}$, and $Fe_{silicate}$.

3.2.1. *Water-soluble, exchangeable and organically bound iron*

In aqueous solutions Fe is mobile in its ferrous form at anoxic conditions and at low to neutral pH. In contrast, soil pore water in oxic soils at circumneutral pH generally contains little Fe since Fe is present as Fe(III) whose solubility is very low at pH values above 3 (Stumm and Morgan, 1996). Dissolved organic matter and colloids in soil can enhance the mobility of $Fe(III)_{aq}$ at higher pH values (Henneberry et al., 2012), yet the water-soluble Fe pool is extremely small and only accounts for < 0.01% of total soil Fe. Therefore, this pool is frequently neglected in above-mentioned sequential extraction schemes. Nevertheless, Guelke et al. (2010) managed to analyze the $\delta^{56}Fe$ of water-soluble Fe from the A horizon of a Luvisol showing an isotopically light Fe pool ($\delta^{56}Fe = -0.48‰$) extracted by ultrapure water. The negative values reflect that light Fe isotopes are preferentially dissolved in soil solution, presumably in the form of soluble organic complexes.

Iron that does not remain in soil solution can be rapidly adsorbed in exchangeable forms. The exchangeable Fe pool is obtained by cation exchange of Fe against magnesium (Mg) using $MgCl_2$ solution, which is reported not to fractionate Fe isotopes (Brantley et al., 2004). This Fe pool is also very small and considered to contain ions that have been bound to solid soil surfaces by outer-sphere binding via organic complexes, which may contain slightly light Fe isotopes (e.g., $\delta^{56}Fe = -0.05‰$ for a Luvisol A horizon, Guelke et al., 2010). Nevertheless, we have to bear in mind that due to the low concentration of water-soluble Fe and exchangeable Fe, the isotope measurements can easily be biased, e.g., by the impurities from the Mg salts during the extractions (Guelke et al., 2010). Assessing $\delta^{56}Fe$ values of Fe pools low in absolute Fe amounts should thus carefully rule out any exterior Fe.

As mentioned above, organic ligands play an important role in Fe mobilization in soil, especially in the O horizons, as well as in plant uptake, e.g., in the form of Fe-phytosiderophores. Since soluble Fe is limited in many soils, Fe that is adsorbed, bound or incorporated in such organic ligands is considered to be a major reservoir for plant uptake (Borggaard, 1992). By using diluted HNO_3 and H_2O_2 to oxidize the organics to CO_2, the bound Fe is detached effectively (Tessier et al., 1979). The extraction releases up to a few percent of total Fe, which has also negative δ^{56}Fe values, suggesting a preferential adsorption or complexation of light Fe isotopes with the organic ligands (Guelke et al., 2010).

3.2.2. Iron (hydr)oxides

Iron (hydr)oxides are major weathering products in soils. Their formation, transformation, and dissolution processes have a major influence on soil development and soil properties (Stucki, 1988; Cornell and Schwertmann, 2003). Poorly crystalline Fe(III) (hydr)oxides are usually formed first due to precipitation of $Fe(III)_{aq}$ and then transformed to thermodynamically more stable crystalline Fe oxides such as goethite and hematite (Wiederhold et al., 2007b).

Depending on the soil order, the $Fe_{am.\text{-}oxides}$ fraction, extracted by 0.5 M HCl, can contribute from 2 to 30% of the total Fe (Fe_{total}) in the soil profiles. The organic-rich O and mineral A horizons usually contain more $Fe_{am.\text{-}oxides}$ than the deeper horizons. Specific soil processes such as podzolization and lessiviation can lead to an enrichment of the $Fe_{am.\text{-}oxides}$ fraction by up to 70% of total Fe in illuvial soil horizons underlying the E horizon (Fantle and DePaolo, 2004; Wiederhold et al., 2007b). The remaining $Fe_{crys.\text{-}oxides}$ fraction is a large Fe pool in soils, accounting for 40 to 70% of the total Fe, and is often the major Fe form present in soil horizons except for highly bleached horizons.

In contrast to the bulk soil, the distinctive Fe pools are isotopically more diverse (Fig. 7), indicating that isotope fractionation among the Fe pools occurs. The currently available isotopic data show that poorly crystalline Fe oxides in different soils and in various soil horizons exhibit a wide range of δ^{56}Fe values, varying between −1.08‰ in the O horizon of a Podzol profile to +1.02‰ in the B horizon of an Andosol profile (Fig. 7), i.e., often showing advanced alteration with soil horizon development and pedogenesis.

In the O horizon (surface layers dominated by organic litter), poorly crystalline Fe oxides are mostly fractionated towards a light isotopic signature. Only Fantle and DePaolo (2004) found a δ^{56}Fe value of 0.27‰ in the O horizon of an Acrisol, which, however, was ashed at high temperature prior to the HCl extraction, thus risking changes in Fe mineralogy (Wiederhold et al., 2007b).

In A (and E) horizons, negative δ^{56}Fe values are usually found for poorly crystalline Fe oxides in most soil orders. In a Gleysol profile studied by Wiederhold et al. (2007a), however, the HCl-extracted Fe pool showed a small-degreed fractionation towards relatively heavier isotopic signature compared with its underlying horizons, due to the lower weathering age and the absence of redoximorphic Fe transformations in the oxic upper soil horizons.

In the B and C horizons, the δ^{56}Fe values of Fe(III) (hydr)oxides seem to depend on the soil order. The $Fe_{am.\text{-}oxides}$ fraction was found to be isotopically lighter in Gleysols and Acrisols than in Andosols and Cambisols. Interestingly, a clear trend towards heavier isotope composition is found for the $Fe_{am.\text{-}oxides}$ fraction along the depth profiles of Cambisols, whereas the $Fe_{am.\text{-}oxides}$ fraction becomes isotopically lighter in deeper horizons in Gleysols. In Podzols, the $Fe_{am.\text{-}oxides}$ fraction was the lightest in the illuvial B_h horizon, where the soil is organic rich and the Fe is likely complexed with organic matter, while the $Fe_{am.\text{-}oxides}$ fraction below the B_s horizon was slightly heavier than in the C horizon (Wiederhold et al., 2007b). These finding clearly demonstrate different degree of Fe isotope fractionation along with different mechanisms of pedogenesis (e.g., chemical weathering and goethite formation in Cambisols, capillary rise and redoximorphosis in Gleysols, podzolization in Podzols). In a study of Andosol profiles, which had experienced considerable rainfalls and anoxic conditions, the $Fe_{am.\text{-}oxides}$ fraction in the B horizons was consistently heavier than the Fe fractions that could not be extracted by diluted HCl (Thompson et al., 2007). Meanwhile, the pyrophosphate extracts of these horizons (Fe bound to organic matter) was found enriched in heavy Fe isotopes. The authors explained this phenomenon by light Fe isotopes being preferentially leached from the soil during weathering under reducing conditions, thus leaving behind the residual material with high δ^{56}Fe values.

The isotope composition of the crystalline Fe oxides in soil profiles is less studied compared with that of the poorly crystalline Fe oxides. Nonetheless, the limited data so far confirm a trend towards heavier isotope compositions along the soil profiles for the $Fe_{crys.\text{-}oxides}$ fraction. The mean δ^{56}Fe values of $Fe_{crys.\text{-}oxides}$ fraction are generally more positive than those of the $Fe_{am.\text{-}oxides}$ fraction. However, the $Fe_{crys.\text{-}oxides}$ fraction may not always be isotopically heavier than the $Fe_{am.\text{-}oxides}$ fraction throughout the soil profile. In the subsoil of Podzols, for instance, the $Fe_{crys.\text{-}oxides}$ fraction was lighter than the $Fe_{am.\text{-}oxides}$ fraction by ~0.7‰ in δ^{56}Fe (Wiederhold et al., 2007b). As main weathering products, the Fe oxides including both forms are the lightest in the Fe mineral pools as illustrated by the δ^{56}Fe of the extracts from a dithionite-citrate solution (Guelke et al., 2010).

3.2.3. Iron in silicate minerals

Iron in unweathered silicate minerals is obtained by total digestion of the residues of previous extractions using a combination of hydrofluoric acid (HF), HNO_3, HCl and/or perchloric acid ($HClO_4$). Depending on the weathering age and pedogenic processes, the $Fe_{silicate}$ fraction may represent the major component of the Fe pools or account for as little as ~7% of the Fe_{total} due to intense Fe transformation reactions (Wiederhold et al., 2007b). The δ^{56}Fe values of the $Fe_{silicate}$ fractions published to date are exclusively positive (Fig. 7), indicating that light Fe isotopes are preferentially removed from the primary minerals during weathering leaving the silicate minerals with a heavy Fe isotopic fingerprint.

3.3. Summary

Different processes of pedogenesis may result in different degree of Fe isotope fractionation. Under reducing conditions, such as common in Stagnosols and Gleysols, dissolution of primary Fe-minerals preferentially releases isotopically light Fe(II) into the solution, leaving a weathered residue enriched in heavy Fe isotopes. This light Fe may then be translocated downwards (e.g., via leaching) or upwards (e.g., via capillary rise) within the soil profile or may be exported laterally. Upon oxidation of this light Fe(II) pool and subsequent precipitation of Fe(III) (hydr)oxides when O_2 is present, the oxidized zones can become enriched in Fe with light isotope composition.

Without transient occurrence of reducing conditions, e.g., under permanent oxidizing conditions or moderate soil weathering, Fe isotope fractionation can be limited through the soil profile as shown in Cambisols. On the other hand, advanced weathering may induce clearer gradients towards enrichment with isotopically heavy Fe, as found for Acrisols. Eluviation and illiviation processes may clearly separate Fe-depleted and enriched zones with significant differences in Fe isotope compositions (e.g., Podzols, Albeluvisols). In contrast, other soil processes such as bio-, cryo-, or peloturbation do likely not induce significant isotope fractionation. Yet, Fe isotopic studies in, e.g., Chernozems, Gelisols, or Vertisols, are still lacking, while this knowledge might provide a novel clue to quantify these physical soil alterations.

As a result of pedogenesis, soils usually exhibit pronounced microscale heterogeneity, also encompassing Fe, which prevails in pools with different (bio)availability and turnover. Sequentially and chemically separated soil Fe pools reflect these impacts of pedogenesis and show a larger range of δ^{56}Fe values than the bulk soil. The relatively labile Fe species such as $Fe(II)_{aq}$, organically adsorbed or bound Fe, as well as Fe

(III) (hydr)oxides are generally isotopically lighter than the Fe in unweathered silicate minerals. The Fe oxide fractions, including poorly crystalline and crystalline Fe oxides, as main weathering products are often isotopically the lightest (Fig. 7). The extent of Fe isotope fractionation of each Fe pool depends on the parent material, soil order, and pedogenic processes, and thus on the magnitude of Fe transformation and translocation.

Yet, careful examination of artifacts should be performed when applying sequential extraction procedures for Fe isotope studies. Such artifacts may result from impurity of extractants, incomplete dissolution, alterations of the sample during extraction/treatment, and secondary precipitation or adsorption, leading to possible isotope fractionation during sample preparation (Guelke et al., 2010). Attention should also be paid to the "unwanted" dissolution of silicate minerals when using diluted HCl or dithionite-citrate solution to study Fe oxides (Kiczka et al., 2011). However, if these artifacts can be avoided, the combined analyses of Fe isotope compositions in both bulk soil and in physically and chemically discriminable Fe pools can provide much deeper insights into the mechanisms of terrestrial Fe cycling that are difficult to achieve by other (e.g. concentration and speciation) analyses.

4. Iron isotopic fractionation in plants

Plants have developed two efficient strategies to secure Fe uptake from soil (Roemheld and Marschner, 1986). The sequential acidification-reduction-transport strategy (strategy I) is carried out by all higher plants, except for the graminaceous plants, which use the chelation-based strategy (strategy II) for Fe uptake (Hell and Stephan, 2003). Strategy I plants excrete protons via a plasmalemma AHA H^+-ATPases to acidify the rhizosphere, and then the NADPH-dependent ferric chelate reductase AtFRO2 reduces Fe^{3+} to Fe^{2+} which is then available to plants and can be transported through a plasmalemma by Fe transporter proteins (Hell and Stephan, 2003; Robinson et al., 1999). Strategy II plants release phytosiderophores (PSs) that chelate Fe^{3+} in the rhizosphere. The Fe^{3+}–PS complexes are then channeled into the root by specific plasmalemma transporter proteins (Takagi et al., 1984; Curie et al., 2001; Schaaf et al., 2004). It is generally assumed that the chelation-based strategy is more efficient than the sequential acidification-reduction-transport strategy and allows graminaceous plants to survive under more drastic Fe-deficient conditions (Mori, 1999). Both strategies can induce Fe isotope fractionation between the soil and the plant root, as they basically rely on reductive dissolution and organic compound complexation of Fe. Once Fe is taken up into the plant roots, it is cycled through a variety of biochemical reactions moving from roots to stems, then to leaves and seeds, also leading to fractionation of Fe isotopes within the plant.

4.1. Iron isotope fractionation during root uptake

Iron isotope fractionation during root uptake was first proposed by Guelke and von Blanckenburg (2007), based on that all seven strategy I plants they analyzed were enriched in lighter Fe isotopes and the δ^{56}Fe values decreased from soils to shoots, while strategy II plants had slightly heavier Fe isotope compositions compared with the plant-available Fe in the soil. Even though the Fe isotope composition in roots was not analyzed, the difference in δ^{56}Fe values in the growth medium and the aboveground tissues indicated a clear Fe isotope fractionation. Kiczka et al. (2010) later found a significant fractionation towards negative δ^{56}Fe values within the strategy II plant *Agrostis*. The authors suggested that the Fe isotopic signature of plant biomass depended not only on the Fe uptake strategy, but also on the nutrient availability in the substrate (Kiczka et al., 2010). When Fe is sufficiently available in the growth medium, mechanisms of Fe mobilization are similar for both plant groups, resulting in an isotopically light signature in the plants, whereas when Fe is deficient, the strategy II plants mobilize Fe with Fe-PS complexes leading to no apparent Fe isotope fractionation during uptake (Kiczka et al., 2010). The statement is further consolidated by Guelke-Stelling and von Blanckenburg (2012), who subsequently showed that there was a preferential uptake of lighter Fe isotopes by strategy II plants when growing in non-limiting Fe(III)-EDTA nutrient solution. Furthermore, previous observations showed that the root exudation of siderophores was suppressed under Fe sufficient conditions (Charlson and Shoemaker, 2006; Marschner, 1995), which was probably also the case in the field trials studied by Kiczka et al. (2010).

Charlson and Shoemaker (2006) pointed out that both strategy I and II plant species could possess either all or some genes to acidify and reduce Fe, possibly enabling strategy II plants to also take up Fe through reduction reactions similar to strategy I plants when Fe is sufficient in soils. The strategy II plant rice (*Oryza sativa*) is an example of such a plant that possesses the ferrous transporter OsIRT1, allowing the crop to directly absorb Fe^{2+} from the soil (Kobayashi and Nishizawa, 2012; Arnold et al., 2015), in addition to a PS-mediated Fe (III) transport system (Bughio et al., 2002). This suggests that rice takes up Fe both as Fe(III)-phytosiderophores and Fe(II) ions (Ishimaru et al., 2006), which may result in different extents of Fe isotope fractionation.

Using pot experiments, Arnold et al. (2015) showed that rice shoot and grain contained isotopically light Fe compared with the bulk soil or the leachate of the soil, suggesting possible changes in the redox state of Fe occurring during the uptake and translocation processes. In a paddy soil field study, rice roots were found to be enriched in heavy Fe isotopes with δ^{56}Fe values similar to those of the Fe plaques on its root surface (Garnier et al., 2017). In contrast, the soil pore water had extreme negative δ values, and the plant available soil Fe (0.5 M HCl extracted) was also depleted in heavy Fe isotopes. These Fe isotope composition data indicated that the Fe in the root originated mainly from the Fe plaques, which could not be identified by simply analyzing Fe concentrations or Fe speciation. However, under Fe-rich conditions such as in the studied paddy soils, the mechanisms of how rice roots utilize Fe from the plaques still warrant further attention. Nevertheless, the study of Garnier et al. (2017) clearly indicates that for an understanding of Fe isotope signature in rice plants it is decisive to consider not only the plant and the soil, but also Fe plaques specifically.

Apart from Fe uptake strategies and Fe availability in growth media, Fe isotope compositions in plants may also vary among plant species and within the growing season (Kiczka et al., 2010; Akerman et al., 2014). In addition, plant growth promoting bacteria (PGPR) were found to release lighter Fe isotopes into the living medium indicating that PGPR may have an influence on Fe isotope fractionation during plant uptake in pot experiments (Rodríguez et al., 2014).

4.2. Iron isotope fractionation during translocation

Iron acquisition in plants starts from the apoplast of the root epidermal cells (Sattelmacher, 2001), followed by Fe diffusion through the root apoplast across the plasma membrane to the root symplast. Subsequently, Fe will pass through both xylem and phloem sap bound by chelating compounds (Kim and Guerinot, 2007). To cross the membrane and enter the cells, Fe is mediated by several transporter proteins and ligands (Álvarez-Fernández et al., 2014), such as PSs, nicotianamine (NA) and citrate (Hell and Stephan, 2003).

Moynier et al. (2013) computed the orbital geometries and vibrational frequencies of aqueous Fe(II) and Fe(III) species that are relevant to plants and calculated the corresponding isotope composition. By using such quantum chemical calculations, they estimated the magnitude of equilibrium Fe isotope fractionation among different Fe species [Fe(II)-citrate, Fe(III)-citrate, Fe(II)-NA and Fe(III)-PSs] relevant to Fe transport in higher plants, thereby showing that Fe(II)-NA was by ~3‰ (δ^{56}Fe) isotopically lighter than Fe(III)-PSs. The isotopic variation is due to differences in both Fe redox state and speciation: Fe(III)-PSs are up to 1.5‰ heavier than Fe(III)-citrate and Fe(II)-NA up to 1‰ heavier than Fe(II)-citrate (Moynier et al., 2013). As Fe is stored as Fe(II)-NA in plant seeds (Hell and Stephan, 2003) and likely present as Fe(III)-PSs in

the roots, especially for strategy II plants (Bienfait et al., 1985; Becker et al., 1995), the calculated δ^{56}Fe values for these Fe species may partially explain the often reported isotopically heavier Fe in root than in aboveground tissues.

The translocation of Fe from roots to shoots is similar for plants of both strategies. In the xylem sap, Fe is transported as Fe(III)-citrate (Pich et al., 1994), while in the phloem sap Fe is preferentially transported as Fe(II)-NA (von Wirén et al., 1999). Moreover, processes including xylem loading, transport and unloading, xylem to phloem transfer, phloem loading, transport and unloading (Kim and Guerinot, 2007) are involved in Fe translocation in the aboveground tissues, which may potentially lead to further Fe isotope fractionation in favor of light Fe isotopes in younger leaves (Guelke-Stelling and von Blanckenburg, 2012).

The translocation mechanism of Fe within the aboveground tissues and its relation with Fe isotope fractionation is still uncertain. Younger leaves primarily receive Fe from the phloem where Fe is mostly chelated as Fe(II)-NA, while older leaves acquire Fe from the xylem where Fe is transported as Fe(III)-citrate complexes (Tsukamoto et al., 2008). However, the isotopic difference of Fe(II)-NA and Fe(III)-PSs in the roots of strategy II plants (−3‰ in δ^{56}Fe, Moynier et al., 2013) is much larger than the observed isotopic variations between leaves and roots (Table 1, Fig. 8). Therefore, a mixing between Fe transported by the phloem and the xylem likely controls the extent of Fe isotope fractionation during translocation from roots to shoots (Moynier et al., 2013). It is worth noting that the calculated extent in Fe isotope fractionation by Moynier et al. (2013) was due to an equilibrium effect, while processes in plant uptake and translocation are more likely kinetically controlled. Therefore, the values given above should be carefully examined when comparing them with the observed Fe isotope variation in plants.

It is also possible that “dilution effects” during the maturation of the leaves can alter Fe isotopic composition. Besides, plants can also remobilize Fe from older leaves prior to litterfall to avoid Fe losses. This process can also lead to changes in the final Fe isotope ratio determined in the leaves. In addition, other types of ligands such as Fe transport protein (ITP) may be involved in isotope fractionation during translocation into younger leaves. At the cellular level, chloroplast and mitochondria use the largest amount of Fe in plant cells and represent crucial sites for Fe biosynthesis. However, their contribution to Fe isotope fractionation still remains unexplored and deserves further investigation in order to understand the mechanisms of Fe translocation and transformation in plants.

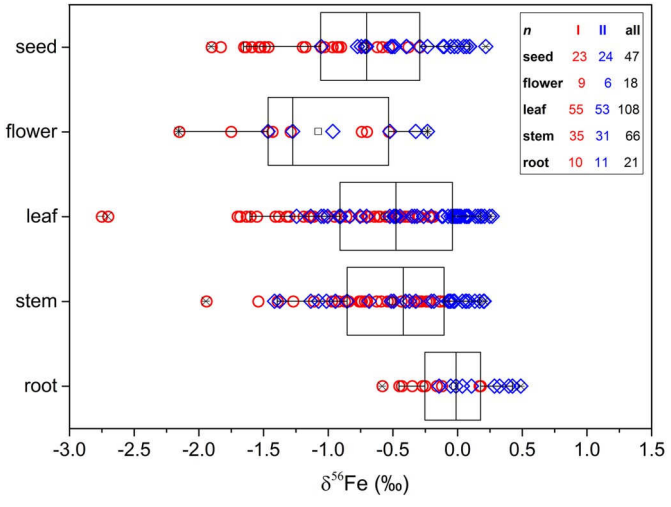

Fig. 8. Iron isotope variation in different tissues of plants with Fe uptake strategy I (red circles) and strategy II (blue diamonds). The black boxplots show the δ^{56}Fe value distribution of all plants that have to date been studied. The number of the data *n* is given with respective colors.

4.3. Fe isotope composition in different plant tissues

Fig. 8 shows the range of δ^{56}Fe values in different plant tissues that have to date been studied for Fe isotopes, including 12 species of strategy I plants [bean (*Phaseolus vulgaris* L.), lettuce (*Valerianella locusta* L.), spinach (*Spinaci oleracea* L.), rape (*Brassica napus* L.), pea (*Pisum sativum* L.), amaranth (*Amaranthus hybridus* L.), soybean (*Glycine* max L.), lentil (*Lens culinaris*), mountain sorrel (*Oxyria digyna*), French sorrel (*Rumex scutatus*), umbrella tree (*Musanga cecropioides*), and West African piassava palm (*Raphia vinifera*)] and 10 species of strategy II plants [black bent (*Agrostis gigantea*), oat (*Avena sativa* L.), maize (*Zea mays* L. convar. *Sacharata*), wheat (*Triticum aestivum* L.), wild rye (*Elymus virginicus*), Johnsongrass (*Sorghum halepense*), Kentucky bluegrass (*Poa pratensis*), river oat (*Uniola latifolia*), Indian goosegrass (*Eleusine indica*) and rice (*Oryza sativa* L. cv. Oochikara)]. It clearly indicates that Fe in plants is isotopically lighter than in soils (Figs. 5, 7, and 8). Compared with strategy II plants, strategy I plants are enriched in light Fe isotopes with median δ^{56}Fe of −0.72‰ vs. −0.10‰ (strategy II) for the whole plants (including root and aboveground tissues). For both types of plants, aboveground tissues possess lighter Fe isotopes compared with that in the roots, with the lightest Fe being found in flowers with mean δ^{56}Fe of −1.26 ± 0.53‰ and − 0.96 ± 0.63‰, respectively. It is hypothesized that roots may be enriched in relatively heavy Fe isotopes, as light Fe isotopes are transported into younger plant (aboveground) parts (Guelke-Stelling and von Blanckenburg, 2012). However, it is worth noting that Fe isotope fractionation due to plant uptake should be interpreted relative to Fe isotope composition of the Fe source (e.g. nutrient solution, plant available Fe in soil), which has not been carried out in every study. Nevertheless, we can summarize that Fe isotopic data in soils and plants demonstrate that the processes of uptake and translocation of Fe can lead to significant isotope fractionation, which is controlled by changes of redox state and the binding ligands for Fe (von Blanckenburg et al., 2009).

5. Iron isotope fractionation in freshwaters

As a limiting micronutrient in many aquatic ecosystems, Fe plays a critical role in regulating concentrations and bioavailability of a variety of other elements also in water bodies (Martin and Fitzwater, 1988). On a global scale, climate change leading to, e.g., enhanced run-off from glacier melting, is expected to have great impact on riverine and oceanic Fe cycles and thus on the productivity of the aquatic ecosystems (e.g. Gerringa et al., 2012). An increasing number of studies have focused on identifying Fe source, speciation, mobility, and Fe partitioning in different particle size fractions of the water systems. Additional attention is paid to the waterbodies in areas with intensive industrial or mining activities in order to assess anthropogenic impacts on the Fe cycle, as well as to groundwater systems that naturally bear elevated Fe concentrations and other species with public health concerns. Nevertheless, the total range of Fe isotopic signature of freshwater systems is still poorly defined (Escoube et al., 2009). The following sections aim to systemize Fe isotopic signatures in freshwater environments as a proxy for: i) Fe behavior with redox variation; ii) the partitioning of Fe between dissolved, colloidal (< 1 μm) and suspended particulate fractions (> 1 μm); iii) different Fe inputs to both fresh- and seawaters; as well as iv) Fe associations with co-existing pollutants. It is worth noting that the definition of colloids for particles < 1 μm follows that used in colloid chemistry (e.g., Lead and Wilkinson, 2007). Most freshwater studies conventionally used water filtration cut-offs of 0.45 μm or 0.22 μm to isolate what is then mostly termed the “dissolved” fraction. Some studies apply further filtration steps, but nomenclature of the isolated size fractions is inconsistent among studies (please also see SI3 and SI4 on water sampling and size fraction nomenclature).

5.1. Freshwater environments with redox variation

In waters and sediments that show different redox conditions at the surface and at depth, Fe isotope fractionation is most pronounced at the oxic-anoxic interface. At this interface, dissolved Fe(II) was reported to be isotopically lighter than the suspended Fe(III) (hydr)oxides as a result of equilibrium isotope fractionation effect during the cycles of oxidation of Fe(II), precipitation and re-dissolution of Fe(III) oxides, as well as due to the adsorption of dissolved Fe(II) on the surface of Fe(III) oxides (Malinovsky et al., 2005). In sediments, Malinovsky et al. (2005) found the largest concentration of Fe oxide with the most positive δ^{56}Fe values at the oxic-anoxic interface, while below the interface, Liu et al. (2015) found isotopically heavier Fe(III) (hydr)oxides compared with $Fe(II)_{aq}$, $Fe(III)_{aq}$ and sorbed Fe(II). The depth profile of the water column in the anoxic and ferruginous Lac Pavin (France) showed a remarkable increase in concentration and δ^{56}Fe values of dissolved Fe (II) (from −2.14‰ to +0.31%) across the oxic-anoxic interface to the lake bottom due to partial oxidation of $Fe(II)_{aq}$ (Busigny et al., 2014). Sulfate reduction occurred at this interface, leading to Fe sulfide formation with limited Fe isotope fractionation, which eventually determined the Fe isotope composition of pyrite in the lake sediments containing isotopically light Fe isotopes compared with that in the sediment in the oxic zone. In Lake Nyos (Cameroon), negative δ^{56}Fe values (−1.25‰) were observed for dissolved Fe(II) at the oxic–anoxic interface, whereas precipitation of Fe(II) as siderite at the bottom of the lake led to isotopically heavy dissolved Fe(II) in the bottom water (Teutsch et al., 2009).

In a contaminated artificial lake in China, seasonal variations in Fe isotope of the suspended particulate matter (SPM) were observed (Song et al., 2011). In winter, the SPM Fe in the lake was isotopically homogeneous, while the δ^{56}Fe shifted significantly to lower values in both surface layer and bottom strata during summer stratification. The authors suggested that these ^{56}Fe-depletions of the SPM in the lake in summer reflected tributary inputs of organically-bound Fe colloids leached from topsoils during the peak water discharge. The lower δ^{56}Fe values in bottom strata were attributed to “ferrous wheel” cycling (microbial reductive dissolution of fluvial Fe-oxides) near the redox boundary.

Redox cycling of Fe can also happen in subterranean estuaries influenced by anoxic groundwater. When encountering O_2 in the sediment pore water, the groundwater-borne Fe(II) is fastly oxidized, precipitated and adsorbed on Fe-oxides coated sediment sands and can result in the dissolved Fe(II) in the pore water being strongly depleted in heavy Fe isotopes (Rouxel et al., 2008).

5.2. Partitioning of iron in particle size fractions

One important aspect to consider when determining the Fe isotope composition of water samples is the choice of size fraction to be analyzed and the respective chemical Fe pools. Most studies on Fe isotopes in freshwater analyzed either unfiltered bulk samples (Fantle and DePaolo, 2004; Poitrasson et al., 2014) or samples passed through (precleaned) 0.22 µm (Malinovsky et al., 2005; Escoube et al., 2009; Guo et al., 2013; Akerman et al., 2014; Chen et al., 2014; Schuth and Mansfeldt, 2016; Garnier et al., 2017) or 0.45 µm filters (Teutsch et al., 2005; Bergquist and Boyle, 2006; Teutsch et al., 2009; Schroth et al., 2011; Castorina et al., 2013; dos Santos Pinheiro et al., 2013, 2014; Xie et al., 2014; Song et al., 2011; Zhang et al., 2015; Schuth and Mansfeldt, 2016) on site. Filtrates were stabilized through acidification to prevent Fe oxide precipitation prior to analysis. Three studies performed elaborate fractionation schemes using filter cascades, some on site, to separate different size fractions (Ilina et al., 2013; Escoube et al., 2015; Mulholland et al., 2015a). In all cases accurate sample processing was paramount to avoid artifacts due to adsorption to suspended (organic) particles (mostly in the case of bulk samples), belated precipitation of Fe (hydr)oxides in the sampling bottles, or biodegradation of organically complexed Fe-colloids, especially in the case of filtration cascades. Therefore, we distilled a recommendation for aerobic freshwater sampling separation procedure for particle-size fractions with the purpose of Fe isotope analysis, which can be found in the SI2 and 3.

Ilina et al. (2013) used a 12-step-filtration cascade starting at 100 µm down to 1 kDa. Frontal ultrafiltration was carried out for the 100, 10 and 1 kDa fractions. Escoube et al. (2015) filtered samples on site using filter sizes of 5, 2.5, 0.45 and 0.22 µm. They further compared two ultrafiltration techniques (frontal ultrafiltration and in-situ dialysis) for the 100, 10 and 1 kDa sizes. Mulholland et al. (2015a) used frontal filtration with 0.45 µm pore size and tangential-flow ultrafiltration with cutoffs of 0.22 µm and 5 kDa. So far, there is unfortunately a lack of consistent naming of these isolated fractions. Ilina et al. (2013) simply referred to (ultra)filtrates or retentates of a specific size for fractions below or above a given pore size. Escoube et al. (2015) called all fractions below 0.45 µm or 0.22 µm dissolved Fe, fractions below 100 or 10 kDa colloidal and fractions below 1 kDa truly dissolved or soluble. Mulholland et al. (2015a) termed their fractions particulate (> 0.22 µm), dissolved (< 0.22 µm), colloidal (5 kDa < x < 0.22 µm) and truly dissolved (< 5 kDa) (Fig. SI3).

Fig. 9 compiles δ^{56}Fe values in freshwater that have so far been reported and shows that the spread of δ^{56}Fe values tends to increase with decreasing particle size. This spread is wider in < 0.45 µm fractions and below than in larger sized particles. There is a trend to more positive δ^{56}Fe values with decreasing fraction size. In fact, this trend can be found in some (but not all) individual studies. Ilina et al. (2013) found a systematic enrichment in heavy Fe isotopes with decreasing size fraction and decreasing Fe/organic-carbon ratio in several organic-rich boreal rivers in Russia. Small sized, organic-rich, but Fe-poor

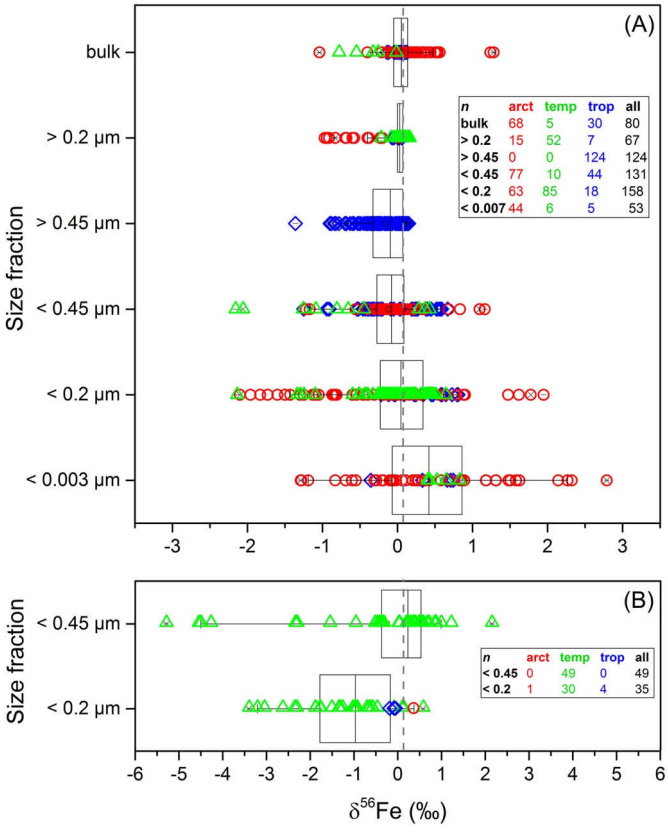

Fig. 9. Iron isotope compositions in surface freshwater samples (A) and in groundwater and hyporheic samples (B) grouped by size fractions. Black boxplots: waters from all regions; red circles: waters from arctic/subarctic areas; green triangles: waters from temperate regions; blue diamonds: waters from tropical regions. The number of data *n* is given accordingly. The gray line at ~0.07% indicates the continental crust mean (Poitrasson, 2006).

fractions were isotopically heavier than the large sized mineral-rich fractions. The authors hypothesized that this variation indicated differences in the chemical bonding of Fe with Fe-O-C bonds likely dominating in the low molecular weight organic carbon-rich fractions, and Fe-O-Fe bonds in the Fe-rich high molecular weight fractions.

Escoube et al. (2015) found that the < 0.22 μm fractions of Northern European and Siberian rivers were isotopically heavier in Fe than the continental crust, especially when samples were derived from stagnant waters or semi-permanent streams. At one sampling location, δ^{56}Fe values increased with decreasing fraction size in rivers and semi-permanent streams, and decreased in the stagnant waters. However, such a systematic variation in δ^{56}Fe values was not found for different size fractions from boreal-forested areas of the Copper River catchment in Alaska. The authors attributed these differences to the varied contents of dissolved organic carbon (DOC) in these rivers. Similarly, Mulholland et al. (2015a) found contrasting Fe isotope partitioning in rivers of the Amazon Basin with different organic content and particulate load. In the organic-rich tributary river, Fe in the particulate matter (> 0.45 μm or > 0.22 μm) was isotopically lightest and Fe in the smaller sized fractions (< 0.22 μm) had more positive δ^{56}Fe values. By contrast, the particulate-rich tributary river contained Fe mainly in suspended particles with δ^{56}Fe values close to the continental crust mean and the smaller sized Fe was enriched in light Fe isotopes. The authors attributed the isotopically heavier colloidal Fe in the organic-rich river to organic ligands (Fe–O–C bonds), while the isotopically light colloidal Fe was assigned to Fe(III)-oxyhydroxides (O–Fe–O bonds) in the particulate-rich river.

In a recent study of water samples from different European streams by Gottselig et al. (2017), 30–76% of riverine Fe was frequently found in size fractions < 1 μm. In filtered water (< 0.2 μm) of Icelandic rivers, 26 to 56% of Fe was found to be colloidal (10 kD to 0.2 μm), which were characterized with variable Fe isotope compositions (Opfergelt et al., 2017). These studies demonstrated that, in order to identify underlying processes, one should isolate and pay close attention to the smaller-sized fractions. Yet, little is known on redistribution of Fe isotopes among these fractions during sample storage and transport. Therefore, care has to be taken to prevent, e.g., CO_2 degassing and aeration when analyzing pH- and redox-sensitive water bodies. It should also be acknowledged that the pool size of each size fraction is different and thus the contribution of each size fraction to the bulk water Fe isotope composition should be weighted.

5.3. Iron input from freshwaters to seawater

In one of the first studies, Fantle and DePaolo (2004) investigated the Fe isotope composition of bulk waters, which deliver a large amount of suspended sediments to the Pacific Ocean and subarctic seas. Rivers with high particle loads contained Fe with an isotope composition similar to that of the continental crust, while rivers with low particle loads generally showed negative δ^{56}Fe values.

In estuaries, about 90% of river-borne dissolved and colloidal Fe (< 0.45 μm) is precipitated due to flocculation (Boyle et al., 1977). The flocculation process, however, produces minimal isotope fractionation of the dissolved Fe (< 0.22 μm), suggesting that the isotope composition of the coastal oceanic dissolved Fe pool can represent that of the riverine Fe (Escoube et al., 2009). On the other hand, studies show that many rivers carry large amounts of SPM to the oceans with the Fe isotope composition of the river water similar to that of the continental crust (e.g. Fantle and DePaolo, 2004; Escoube et al., 2015; Poitrasson et al., 2014). This particulate Fe pool becomes isotopically heavier upon flocculation due to the mixing of river-borne particles, coagulated river colloids and detrital Fe derived from coastal area (Escoube et al., 2009).

5.3.1. Arctic and subarctic river systems

Glacial meltwater runoff and iceberg calving are generally considered to be one of the main inputs of both dissolved Fe and particulate Fe to oceans, and thus they receive particular attention for understanding oceanic productivity (Gerringa et al., 2012). However, according to Zhang et al. (2015), > 80% of the dissolved Fe could be lost during transport through the proglacial environment, so that with the additional losses upon mixing of the fresh water with the saline water in the estuary, < 2% of the dissolved Fe in the meltwater reached the boreal estuary. The analyzed δ^{56}Fe values in the river formed by the meltwaters of cold-based glaciers were close to the continental crust mean, indicating no significant Fe isotope fractionation during dissolution under the glacier before entering the river. The small amount of Fe that finally entered the open ocean was considered to be truly soluble and stable over days and weeks. Therefore, the data in this study did not support the previous hypothesis of the glacial meltwater being an important source to the oceanic dissolved Fe pool.

Compared with glacial meltwater, boreal forested riverine Fe was found to be associated with larger concentrations of dissolved organic matter owing to the input of groundwater- and/or soil water-derived Fe. These riverine systems exhibited light Fe isotopic signatures (Schroth et al., 2011). Similar as discussed for soils, the δ^{56}Fe values of water bodies therefore changed with Fe speciation, here mostly in the presence of organic complexes. With further evolution of glacial recession and mass loss in the subarctic landscape, the contribution of the boreal forested riverine Fe to the ocean may play an increasingly important role. Assuming a continued subarctic warming, such catchments may eventually evolve to boreal forest-dominated areas and cause a fundamental shift in the riverine Fe chemistry, where mostly Fe (III) (hydr)oxides in the form of Fe colloids and particles will then be delivered to the ocean.

Large rivers, such as Ob' and Lena (Escoube et al., 2015), which discharge vast amounts of freshwaters into the Arctic Ocean, were found to contain dissolved Fe (< 0.45 μm) with limited isotope fractionation (i.e. Fe isotope composition similar to that of the continental crust). In contrast, organic-rich, small rivers were characterized with a larger range in δ^{56}Fe of the dissolved Fe. In particular, these small rivers contained larger portions of smaller particle sized fractions enriched in heavy Fe isotopes. As a result, in spite of lower discharges, smaller rivers can contribute disproportional amounts of dissolved Fe with strongly fractionated Fe isotopes of both isotopically light (dissolved, organic complexed) and heavy Fe (bound to small particles) into the Arctic Ocean (Escoube et al., 2015).

It is worth noting that there are also seasonal variations in Fe concentrations and Fe isotope compositions in river systems. In the Kalix River in Northern Sweden, for instance, both the concentrations and δ^{56}Fe values of suspended matter (> 0.45 μm) decreased concurrently upon flood events in May every year, but increased thereafter until the next flood event (Ingri et al., 2006). The authors assigned variations in both Fe concentration and isotope composition to temporal mixing of different Fe species: i) detrital particles stemming from abrasive rock erosion with low Fe concentration and δ^{56}Fe values close to zero, ii) organically-complexed colloidal Fe (< 10 kDa) with negative δ^{56}Fe values, and iii) Fe-oxyhydroxide particulate-colloidal matter (> 10 kDa) precipitated from inflowing anaerobic groundwater enriched in dissolved Fe(II). The authors argued that organically-complexed colloids were less prone to precipitation in the estuary zone than Fe-oxyhydroxides or detrital particles due to their lower specific density, i.e., the organically-complexed colloids might exhibit a more conservative transport within the river mouth. Upon storm events and spring snow melts, these organically-complexed colloids could thus be flushed to the open ocean in substantial amounts (Ingri et al., 2006).

In a follow-up study, Ingri et al. (2018) partly identified the Fe sources during winter base flow and spring flood by analyzing the Fe isotopes of the Kalix River and a further long-term monitored forested first-order stream in the same boreal landscape in Northern Sweden. The bulk waters of both stream types had opposite δ^{56}Fe values during winter base flow, with the Kalix river having a heavy isotopic signature around +0.5‰ and the first-order stream having a light isotopic

signature around −0.5‰. Sampling soil water from lysimeters installed in the riparian zone of the first-order stream showed that the Fe input in the first-order stream was mainly fed by a narrow dominant source layer (DSL) responsible for most of the Fe export from the riparian zone. This DSL was located close to the groundwater level and Fe transport was mainly controlled by groundwater advection. The δ^{56}Fe values around the groundwater table showed a very steep gradient from −0.1‰ (below) to +0.9‰ (above), which led to instantly changing isotope signals when the water table rose. During spring flood in April/May the δ^{56}Fe values of the Kalix and the first-order stream transiently decreased respectively to around −0.1‰. Relying on the results and conclusions from Ilina et al. (2013), Ingri et al. (2018) hypothesized that the dominating colloids in the dissolved fraction (< 0.22 µm) of the first-order stream changed throughout the sampling with large sized mineral-rich colloids, with negative δ^{56}Fe values, dominating the base flow and large amounts of small sized organic-rich colloids, with positive δ^{56}Fe values, being flushed in during spring flood due to the activation of the shallow organic-rich soil layers above the groundwater table. Using the investigated forested first-order stream as a proxy for similar forested headwater streams feeding the Kalix, the authors concluded that, as spring snowmelt in the forests always preceded snowmelt in the mountains, riparian soils as main Fe source of first-order streams were the primary Fe source of the Kalix during spring flood. During base flow, however, forest soils could be excluded as primary Fe source for the Kalix River. This was consistent with low total organic carbon (TOC) and Fe_{bulk} ratios in the Kalix during base flow, indicating Fe-oxyhydroxides as dominant phase, and high TOC/Fe_{bulk} ratios during spring flood, suggesting Fe(II)(III)-organic carbon aggregates as dominant phase.

Compiling the δ^{56}Fe values from Arctic/subarctic rivers published so far, Fig. 10 confirms that freshwater filtrates with elevated DOC concentrations tend to have heavier Fe isotope compositions relative to the continental crust, likely due to isotopically heavy Fe(III) linked with organic ligands (Fe–O–C bonds). In contrast, filtrates with low DOC concentrations preferably display a light Fe isotope composition (with the exception of arctic filtrates < 100 kDa), reflecting the release of light Fe isotopes during dissolution of Fe-bearing minerals.

5.3.2. *The Amazon Basin*

While arctic ecosystems usually comprise young soils, old landscapes frequently prevail in the tropical environment (see also Section 3.1.2). The Amazon River basin is one of the most intensive weathering systems in the world (Bergquist and Boyle, 2006), and one of the largest freshwater and SPM inputs to oceans (Gaillardet et al., 1997; Meade et al., 1985). Overall, the Amazon River delivers approximately $34 \cdot 10^6$ tons of Fe to the Atlantic Ocean every year, with a bulk Fe isotope composition similar to that of the continental crust mean (Poitrasson et al., 2014).

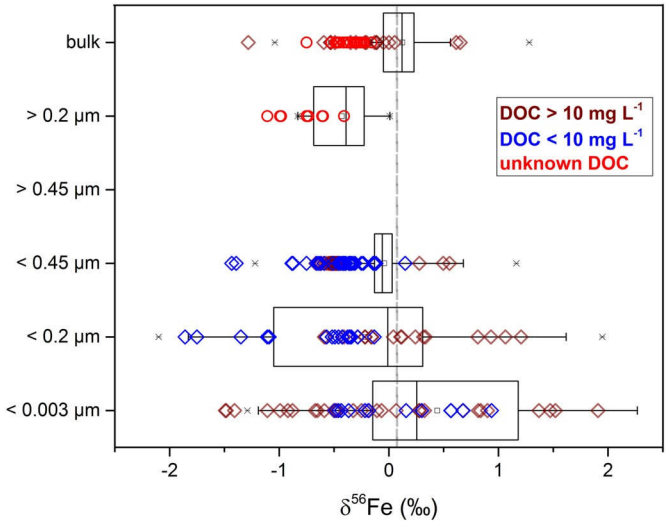

Fig. 10. Iron isotope compositions in freshwater samples from Arctic/subarctic areas grouped by size fractions, showing that Fe in rivers with higher DOC contents is isotopically heavier than that in rivers with lower DOC contents. The gray line at ~0.07% indicates the continental crust mean (Poitrasson, 2006).

The Amazon River receives discharges from two types of tributaries: the white waters with large discharge and SPM loads (> 0.45 µm), such as the Solimões River and the Rio Madeira, and the black waters with small discharge, low SPM load and high organic matter contents, like the Negro River. These two chemically distinct tributary types also vary in Fe species and isotope compositions. The Solimões River contains isotopically light Fe both in the dissolved (~5% of the Fe load) and the particulate fractions, while the Negro River exhibited isotopically heavier Fe in the dissolved fractions (~50% of the Fe load) mixed with light particulate Fe fractions (Bergquist and Boyle, 2006). The overall Fe load of the Amazon River is dominated by inputs from the Solimões River and similar to or slightly lighter in δ^{56}Fe than the continental crust mean (Bergquist and Boyle, 2006; dos Santos Pinheiro et al., 2013). Whether (Escoube et al., 2009) and to which degree (Bergquist and Boyle, 2006) subsequent Fe isotope fractionations happen in the estuary upon mixing with the riverine water, still warrants further clarification for these tropical regions.

The total Fe concentrations in the Amazon River and its tributaries reveal pronounced spatial and temporal variation. The spatial variability in Fe isotope composition of the SPM in these rivers, however, was found to be relatively small and did not exceeded 0.1‰ in δ^{56}Fe, indicating that mechanical weathering rather than chemical fractionation likely controlled Fe concentrations and isotope compositions (dos Santos Pinheiro et al., 2013). In contrast, temporal variations in the δ^{56}Fe of the SPM were found to be substantial, particularly in the Negro River, where the most negative δ^{56}Fe values occurred during the period when the river experienced minimal precipitation (dos Santos Pinheiro et al., 2014). This variation of Fe isotope compositions was attributed to seasonal fluctuations of Fe inputs from the catchment soils that were rich in organic matter.

Upon extreme weather events, as the centennial flood in May 2009 and the great drought in September to October 2010, the Amazon River systems experienced drastic hydrological and physicochemical changes. During the low water season, a tremendous Fe loss (~50%) was found at the confluence of the tributaries to the Amazon River through flocculation and sedimentation, compared with 25% of Fe lost during the high water period (Poitrasson et al., 2014). Nevertheless, Poitrasson et al. (2014) found that in spite of the Fe loss and variation of water properties, the Fe isotope compositions of the bulk waters (< 300 µm) from the Amazon River and its tributaries were within a limited range of ± 0.2‰ in δ^{57}Fe (~ ± 0.13 in δ^{56}Fe) across both low and high water periods, with the white waters displaying δ^{56}Fe of the continental crust mean and the organic-rich black waters being slightly isotopically light corresponding to an also light Fe in the sediment. Considering that the absolute contribution of the (seasonally variable) Fe flux of black water rivers to the Fe budget is small on the Amazon Basin scale, their isotope influence on the Amazon River is negligible (Poitrasson et al., 2014).

5.4. *Riparian zones*

In semi-terrestrial soils and riparian zones, i.e., soils in close contact with freshwater systems, studying the changes in Fe isotope compositions may potentially complement the understanding of processes that are learned from the analyses of whole soil profiles. In a swamp zone of a watershed in Cameroon, formed by an organic-rich stream and surrounding Gleysols, the topsoil of the Gleysols was enriched in heavy Fe isotopes, as a result of chemical weathering followed by lateral drainage leading to the loss of light Fe isotopes (Akerman et al., 2014). The

lost Fe was oxidized and further complexed with soil organic matter after humification, and then entered the stream water in the form of soluble humic-Fe(III) complexes. Intriguingly, the light isotopic signature of the lost Fe from the soil profiles was not mirrored in the stream waters. Instead, the dissolved Fe (< 0.22 μm) in the stream water showed a heavy signature along the stream flow with the heaviest being observed at the watershed's outlet, indicating a significant impact of biological Fe recycling on stream water Fe isotope compositions. Mass balance calculations of Fe contents on the watershed scale revealed that the overall Fe loss from both lateritic uphill and the swamp zone would have δ^{56}Fe values close to 0‰, in agreement with the studies of larger tropic water systems (e.g. the Amazon Basin, see above), delivering Fe to the ocean with isotopic signature indistinguishable to the continental crust mean.

As discussed for the Amazon River, there may also be a pronounced seasonal variation in δ^{56}Fe values of riparian zones and corresponding semi-terrestrial ecosystems. The Fe outflow from soils to neighboring streams occurs as both dissolved and colloidal Fe, but mainly at high groundwater level (e.g., after rainfall). At ascending groundwater level, the Fe in soil solution was found to be mostly adsorbed on Fe oxide surfaces or precipitated when encountering elevated redox potentials, so that low concentrations of dissolved Fe with very low δ^{56}Fe value remained with limited Fe outflow (Schuth and Mansfeldt, 2016).

5.5. Peculiarities through anthropogenic impacts on Fe isotope compositions in freshwaters

In contrast to pristine systems, freshwaters that are affected by human activities are less studied regarding Fe cycling and Fe isotope composition. These water systems may carry an anthropogenic surplus flux of Fe or exhibit large redox variations and thus can have an impact on the local Fe cycle.

Repeated precipitation/dissolution cycles induced by industrial activities in a groundwater in Italy, for instance, resulted in large variations of Fe isotope compositions, showing an extremely wide range of δ^{56}Fe values from −5.29‰ to +2.15‰ for the dissolved Fe (< 0.45 μm) of the low-salinity and brackish waters (Castorina et al., 2013). By combining Fe and Zn isotopic studies, Chen et al. (2014) demonstrated that the human-impacted Seine River carried a mixture of dissolved Fe from both anthropogenic and natural sources with different isotope compositions. The dissolved Fe pool of natural origin was mainly associated with organic colloids and enriched in heavy Fe isotopes, while anthropogenically derived dissolved Fe corresponded to Fe-oxyhydroxide or sulfide colloids with a light Fe isotopic signature. However, this isotopic difference was “diluted” in the bulk water by the SPM fractions (> 0.2 μm) which accounted for 99% of the total Fe transport to the ocean and exhibited a similar isotope composition for both Fe sources. Therefore, the Fe from anthropogenic sources in this case could not be traced in the flush to the oceans. This study also highlights the pool-size and reservoir effect on Fe isotope composition.

5.6. Case studies using δ^{56}Fe as proxy for Fe cycling in arsenic enriched groundwater

Arsenic (As) is enriched in many groundwaters worldwide. As its fate is closely linked to Fe cycling in the aquifers, several studies assessed the Fe isotope composition to trace different biogeochemical processes of Fe and As cycling in these groundwaters (Guo et al., 2013; Xie et al., 2014; Wang et al., 2014). According to Guo et al. (2013), the groundwaters of As-enriched shallow aquifers in Northern China were isotopically light in dissolved Fe, while heavy Fe isotopes prevailed in the sediments similar to the Fe isotope composition of the continental crust. An exception was found at the oxic-anoxic interface, where negative δ^{56}Fe values reflected the redox changes. In addition, the δ^{56}Fe values of the groundwaters showed a positive relationship to the As concentration. The authors identified three pathways for Fe cycling in shallow groundwater: i) dissimilatory reduction of Fe oxides, resulting in light δ^{56}Fe values and elevated As concentration in groundwater under anoxic conditions, ii) re-adsorption of Fe(II) leading to further enrichment of light Fe isotopes in the water under anoxic–suboxic conditions, accompanied by As re-adsorption decreasing As concentration, and iii) precipitation of pyrite and siderite under strongly reducing conditions, increasing groundwater δ^{56}Fe values, with a simultaneous decrease in As concentrations via co-precipitation.

These pathways were also identified to control Fe isotope compositions and As concentrations at different depths in a hyporheic zone of the Datong basin in Northern China, where the Fe cycling in the upper sections of the sediments and in the hyporheic zone was governed by microbial dissimilatory reduction of Fe(III) oxides forming non-sulfidic Fe(II) minerals, concurrent with a mobilization of As (Xie et al., 2014). Apart from microbially mediated DIR, abiotic reduction of Fe(III) by HS^-, adsorption of Fe(II) on Fe(II) sulfides precipitates, and/or SO_4^{2-} reduction were considered to drive Fe isotope fractionation in the middle section of the sediments. At the bottom, however, microbial SO_4^{2-} reduction was limited, and microbially mediated DIR determined the δ^{56}Fe values of both the water and the sediments.

In agreement with Guo et al. (2013) and Xie et al. (2014), Wang et al. (2014) confirmed that the groundwaters with elevated As concentrations exhibited also higher δ^{56}Fe and $\delta^{34}S_{SO4}$ values but lower δ^{13}C values. They came to the conclusion that microbial reduction of amorphous Fe oxides alone could not explain As concentration in the water that exceeded 50 μg L^{-1}. For such large As concentrations, additional As release appeared to be also caused by microbial reduction of Fe-sulfate (as a product of HS^- abiotic reduction of crystalline Fe oxides) coupled to the oxidation of organic carbon and/or the formation of As—S components.

6. Conclusions and perspectives

The overall stock of Fe in soils and sediments is large, frequently in the range of 30–150 tons per ha, but only small Fe fluxes up to a few kg per ha are available, e.g., for plant uptake (Blume et al., 2016). Many processes of the terrestrial Fe cycle in soils and freshwater systems are accompanied by stable isotope fractionation. Seasonal variations in Fe dynamics may thus affect the δ^{56}Fe values of the aqueous phase in soil solution, groundwater, lacustrine and riverine systems. In addition, abundant microscale variations in Fe isotope composition exist between aqueous phase and adjacent surfaces of colloids or larger particles, as well as among different Fe species or minerals. Similarly, Fe isotope compositions of unfiltered water samples did not register Fe biogeochemical cycling in the water, but rather reflected the Fe isotopic signatures from the river headwater terranes. However, dissolved Fe fractions are usually isotopically lighter than particle-bound ones. Also Fe uptake by and translocation within plants often show a light Fe isotope signature in the plant compared with the growing media. In this regard, it appears that most processes that are involved in Fe losses of dissolved Fe mainly affect the light Fe isotopes. However, Fe losses in form of nanoparticles may differ in isotope compositions, which still warrants further attention.

Overall, processes involved in the terrestrial Fe cycle may result in variation of δ^{56}Fe values of up to ~4‰ (Table 1). Across real ecosystem compartments, the most extreme δ^{56}Fe values recorded so far have been even as low as ~ −6‰, while the largest differences in δ^{56}Fe values was found for different sized colloids, followed by plants and Fe pools in soils. Therefore, tracing Fe isotope ratios can provide a tool to potentially identify the mechanisms by which Fe has been released into or has accumulated within a given environmental compartment. The true challenge, however, is to differentiate kinetic from equilibrium fractionation processes, and to disentangle apparent fractionations when several processes prevail at the same time. To do the latter, it is inevitable to i) maintain pH and redox potential after sampling until processing, and ii) to extend stable δ^{56}Fe analyses on the

spatiotemporal, microscale heterogeneity of different Fe pools and bonding forms in the environment. This includes a tracing of fine Fe colloids and nanoparticles in water bodies as well as their allocation within larger soil and sediment particles.

Within a given terrestrial subsystem, elucidating Fe isotope fluxes may help to trace the origin and turnover of Fe in soil and water bodies. In soils, variations in Fe isotope signatures can potentially be used, for instance, to differentiate the contribution of different pedogenic processes to the overall Fe cycle, as advanced weathering with Fe loss can result in slow enrichment of heavy Fe isotopes, while turbation processes likely do not involve significant Fe fractionation. In sediments and water bodies, Fe from riverbank erosion could retain the isotope signature of the Fluvisols, while redox-mediated Fe release should alter its isotope compositions in both dissolved and colloidal fractions. In plants, δ^{56}Fe values can provide a clue to assessing uptake mechanisms and possibly even uptake depth, provided that the roots enter zones with different natural δ^{56}Fe values of the source materials, like Fe in organic surface layers or deeper subsoils.

Future work is now needed to link changes in Fe isotope signatures quantitatively to different Fe fluxes, to combine Fe isotope tracing with biogeochemical modelling in order to disentangle complex interactions of various processes within the studied systems, as well as to understand the range of Fe isotope fractionation for a given process under variable environmental conditions (e.g., across different climates and thus different degree of soil weathering), or within given environmental compartments, such as plants. However, particularly when linked with other stable isotope tracing of related element cycles in environment, as performed, for instance, for S in aquifers, and when linking temporal variations in δ^{56}Fe signatures with spatial variations in Fe pools, using stable Fe isotopes will continue to provide very valuable information to detangle the complexity of Fe cycling in terrestrial ecosystems.

Acknowledgements

We highly appreciate the professional editing and insightful and constructive comments by Dr. Olivier Rouxel, Dr. Jan G. Wiederhold, and another anonymous reviewer of Earth Sci. Reviews. This work was supported by the German Federal Ministry of Education and Research (BMBF) in the framework of the funding initiative “Soil as a Sustainable Resource for the Bioeconomy – BonaRes”, project “BonaRes (Module A): Sustainable Subsoil Management - Soil^3; subproject 3” [grant number 031B0026C, 2015], as well as by German Research Foundation (DFG) project [grant number 391749090].

Appendix A. Supplementary data

Supplementary data to this article can be found online at https://doi.org/10.1016/j.earscirev.2018.12.012.

References

Akerman, A., Poitrasson, F., Oliva, P., Audry, S., Prunier, J., Braun, J.-J., 2014. The isotopic fingerprint of Fe cycling in an equatorial soil–plant–water system: The Nsimi watershed, South Cameroon. Chem. Geol. 385, 104–116. https://doi.org/10.1016/j.chemgeo.2014.07.003.

Aleva, G.J.J., 1994. Laterites: Concepts, Geology, Morphology and Chemistry. International Soil Reference and Information Centre, Wageningen (ISBN: 90-6672-053-0).

Álvarez-Fernández, A., Díaz-Benito, P., Abadía, A., López-Millán, A.-F., Abadía, J., 2014. Metal species involved in long distance metal transport in plants. Front. Plant Sci. 5, 105. https://doi.org/10.3389/fpls.2014.00105.

Amor, M., Busigny, V., Louvat, P., Gélabert, A., Cartigny, P., Durand-Dubief, M., Ona-Nguema, G., Alphandéry, E., Chebbi, I., Guyot, F., 2016. Mass-dependent and –independent signature of Fe isotopes in magnetotactic bacteria. Science 352, 705–708. https://doi.org/10.1126/science.aad7632.

Amor, M., Busigny, V., Louvat, P., Tharaud, M., Gélabert, A., Cartigny, P., Carlut, J., Isambert, A., Durand-Dubief, M., Ona-Nguema, G., Alphandéry, E., Chebbi, I., Guyot, F., 2018. Iron uptake and magnetite biomineralization in the magnetotactic bacterium Magnetospirillum magneticum strain AMB-1: an iron isotope study. Geochim. Cosmochim. Acta 232, 225–243. https://doi.org/10.1016/j.gca.2018.04.020.

Anbar, A.D., 2004. Iron stable isotopes: beyond biosignatures. Earth Planet. Sci. Lett. 217, 223–236. https://doi.org/10.1016/S0012-821X(03)00572-7.

Anbar, A.D., Roe, J.E., Barling, J., Nealson, K.H., 2000. Nonbiological fractionation of iron isotopes. Science 288, 126–128. https://doi.org/10.1126/science.288.5463.126.

Anbar, A.D., Jarzecki, A.A., Spiro, T.G., 2005. Theoretical investigation of iron isotope fractionation between $Fe(H_2O)_6^{3+}$ and $Fe(H_2O)_6^{2+}$: Implications for iron stable isotope geochemistry. Geochim. Cosmochim. Acta 69, 825–837. https://doi.org/10.1016/j.gca.2004.06.012.

Arnold, T., Markovic, T., Kirk, G.J.D., Schönbächler, M., Rehkämper, M., Zhao, F.J., Weiss, D.J., 2015. Iron and zinc isotope fractionation during uptake and translocation in rice (*Oryza sativa*) grown in oxic and anoxic soils. Comptes Rendus Geosci. 347, 397–404. https://doi.org/10.1016/j.crte.2015.05.005.

Balci, N., Bullen, T.D., Witte-Lien, K., Shanks, W.C., Motelica, M., Mandernack, K.W., 2006. Iron isotope fractionation during microbially stimulated Fe(II) oxidation and Fe(III) precipitation. Geochim. Cosmochim. Acta 70, 622–639. https://doi.org/10.1016/j.gca.2005.09.025.

Beard, B.L., Johnson, C.M., 2004. Fe isotope variations in the modern and ancient earth and other planetary bodies. Rev. Mineral. Geochem. 55, 319–357. https://doi.org/10.2138/gsrmg.55.1.319.

Beard, B.L., Johnson, C.M., Cox, L., Sun, H., Nealson, K.H., Aguilar, C., 1999. Iron isotope biosignatures. Science 285, 1889–1892. https://doi.org/10.1126/science.285.5435.1889.

Beard, B.L., Johnson, C.M., Skulan, J.L., Nealson, K.H., Cox, L., Sun, H., 2003. Application of Fe isotopes to tracing the geochemical and biological cycling of Fe. Chem. Geol. 195, 87–117. https://doi.org/10.1016/S0009-2541(02)00390-X.

Beard, B.L., Handler, R.M., Scherer, M.M., Wu, L., Czaja, A.D., Heimann, A., Johnson, C.M., 2010. Iron isotope fractionation between aqueous ferrous iron and goethite. Earth Planet. Sci. Lett. 295, 241–250. https://doi.org/10.1016/j.epsl.2010.04.006.

Becker, R., Fritz, E., Manteuffel, R., 1995. Subcellular localization and characterization of excessive iron in the nicotianamine-less tomato mutant chloronerva. Plant Physiol. 108, 269–275. https://doi.org/10.1104/pp.108.1.269.

Bergquist, B.A., Boyle, E.A., 2006. Iron isotopes in the Amazon River system: Weathering and transport signatures. Earth Planet. Sci. Lett. 248, 54–68. https://doi.org/10.1016/j.epsl.2006.05.004.

Bienfait, H.F., van den Briel, W., Mesland-Mul, N.T., 1985. Free space iron pools in roots generation and mobilization. Plant Physiol. 78, 596–600. https://doi.org/10.1104/pp.78.3.596.

Bigeleisen, J., Mayer, M.G., 1947. Calculation of equilibrium constants for isotopic exchange reactions. J. Chem. Phys. 15, 261–267. https://doi.org/10.1063/1.1746492.

Blume, H.-P., Brümmer, G.W., Fleige, H., Horn, R., Kandeler, E., Kögel-Knabner, I., Kretzschmar, R., Stahr, K., Wilke, B.-M., 2016. Scheffer/Schachtschabel Soil Science, 1st English Edition. Springer-Verlag, Berlin Heidelberg. https://doi.org/10.1007/978-3-642-30942-7. ISBN: 978-3-642-30941-0 (PB), ISBN: 978-3-642-30942-7 (E-Book).

Borggaard, O.K., 1992. Dissolution of poorly crystalline iron-oxides in soils by EDTA and oxalate. J. Plant Nutr. Soil Sci. 155, 431–436. https://doi.org/10.1002/jpln.19921550513.

Bowell, R.J., 1994. Sorption of arsenic by iron oxides and oxyhydroxides in soils. Appl. Geochem. 9, 279–286. https://doi.org/10.1016/0883-2927(94)90038-8.

Boyle, E.A., Edmond, J.M., Sholkovitz, E.R., 1977. The mechanism of iron removal in estuaries. Geochim. Cosmochim. Acta 41, 1313–1324.

Brantley, S.L., Liermann, L., Bullen, T.D., 2001. Fractionation of Fe isotopes by soil microbes and organic acids. Geology 29, 535–538. https://doi.org/10.1130/0091-7613(2001)029<0535:FOFIBS>2.0.CO;2.

Brantley, S.L., Liermann, L.J., Guynn, R.L., Anbar, A., Icopini, G.A., Barling, J., 2004. Fe isotopic fractionation during mineral dissolution with and without bacteria. Geochim. Cosmochim. Acta 68, 3189–3204. https://doi.org/10.1016/j.gca.2004.01.023.

Briat, J.-F., Curie, C., Gaymard, F., 2007. Iron utilization and metabolism in plants. Curr. Opin. Plant Biol. 10, 276–282. https://doi.org/10.1016/j.pbi.2007.04.003.

Bughio, N., Yamaguchi, H., Nishizawa, N.K., Nakanishi, H., Mori, S., 2002. Cloning an iron-regulated metal transporter from rice. J. Exp. Bot. 53, 1677–1682. https://doi.org/10.1093/jxb/erf004.

Bullen, T.D., White, A.F., Childs, C.W., Vivit, D.V., Schulz, M.S., 2001. Demonstration of significant abiotic iron isotope fractionation in nature. Geology 29, 699–702. https://doi.org/10.1130/0091-7613(2001)029<0699:DOSAII>2.0.CO;2.

Busigny, V., Planavsky, N.J., Jézéquel, D., Crowe, S., Louvat, P., Moureau, J., Viollier, E., Lyons, T.W., 2014. Iron isotopes in an Archean ocean analogue. Geochim. Cosmochim. Acta 133, 443–462. https://doi.org/10.1016/j.gca.2014.03.004.

Butler, I.B., Archer, C., Vance, D., Oldroyd, A., Rickard, D., 2005. Fe isotope fractionation on FeS formation in ambient aqueous solution. Earth Planet. Sci. Lett. 236, 430–442. https://doi.org/10.1016/j.epsl.2005.05.022.

Canadell, J., Jackson, R.B., Ehleringer, J.R., Mooney, H.A., Sala, O.E., 1996. Maximum rooting depth of vegetation types at the global scale. Oecologia 108, 583–595. https://doi.org/10.1007/BF00329030.

Castorina, F., Petrini, R., Galic, A., Slejko, F.F., Aviani, U., Pezzetta, E., Cavazzini, G., 2013. The fate of iron in waters from a coastal environment impacted by metallurgical industry in Northern Italy: hydrochemistry and Fe-isotopes. App. Geochem. 34, 222–230. https://doi.org/10.1016/j.apgeochem.2013.04.003.

Chapman, J.B., Weiss, D.J., Shan, Y., Lemburger, M., 2009. Iron isotope fractionation during leaching of granite and basalt by hydrochloric and oxalic acids. Geochim. Cosmochim. Acta 73, 1312–1324. https://doi.org/10.1016/j.gca.2008.11.037.

Charlson, D.V., Shoemaker, R.C., 2006. Evolution of iron acquisition in higher plants. J. Plant Nutr. 29, 1109–1125. https://doi.org/10.1080/01904160600689266.

Chen, Y., Barak, P., 1982. Iron nutrition of plants in calcareous Soils. Adv. Agron. 35, 217–240. https://doi.org/10.1016/S0065-2113(08)60326-0.

Chen, J.-B., Busigny, V., Gaillardet, J., Louvat, P., Wang, Y.-N., 2014. Iron isotopes in the Seine River (France): Natural versus anthropogenic sources. Geochim. Cosmochim. Acta 128, 128–143. https://doi.org/10.1016/j.gca.2013.12.017.

Cornell, R.M., Schwertmann, U., 2003. The Iron Oxides — Structure, Properties, Reactions, Occurrence and Uses. Wiley-VGH Verlag GmbH & Co. KGaA, Weinheim. https://doi.org/10.1002/3527602097. ISBN: 3-527-30274-3.

Croal, L.R., Johnson, C.M., Beard, B.L., Newman, D.K., 2004. Iron isotope fractionation by Fe(II)-oxidizing photoautotrophic bacteria. Geochim. Cosmochim. Acta 68, 1227–1242. https://doi.org/10.1016/j.gca.2003.09.011.

Crosby, H.A., Johnson, C.M., Roden, E.E., Beard, B.L., 2005. Coupled Fe(II)-Fe(III) electron and atom exchange as a mechanism for Fe isotope fractionation during dissimilatory iron oxide reduction. Environ. Sci. Technol. 39, 6698–6704. https://doi.org/10.1021/es0505346.

Crosby, H.A., Roden, E.E., Johnson, C.M., Beard, B.L., 2007. The mechanisms of iron isotope fractionation produced during dissimilatory Fe(III) reduction by *Shewanella putrefaciens* and *Geobacter sulfurreducens*. Geobiology 5, 169–189. https://doi.org/10.1111/j.1472-4669.2007.00103.x.

Curie, C., Panaviene, Z., Loulergue, C., Dellaporta, S.L., Briat, J.F., Walker, E.L., 2001. Maize yellow stripe1 encodes a membrane protein directly involved in Fe(III) uptake. Nature 409, 346–349. 10.1038/35053080.

Dauphas, N., Rouxel, O., 2006. Mass spectrometry and natural variations of iron isotopes. Mass Spectrom. Rev. 25, 515–550. https://doi.org/10.1002/mas.20078.

Dauphas, N., Schauble, E., 2016. Mass fractionation laws, mass-independent effects, isotopic anomalies. Ann. Rev. Earth Planet Sci. 44, 709–783. https://doi.org/10.1146/annurev-earth-060115-012157.

Dauphas, N., John, S., Rouxel, O., 2017. Iron isotope systematics. Rev. Mineral. Geochem. 82, 415–510. https://doi.org/10.2138/rmg.2017.82.11.

Dideriksen, K., Baker, J.A., Stipp, S.L.S., 2008. Equilibrium Fe isotope fractionation between inorganic aqueous Fe(III) and the siderophore complex, Fe(III)-desferrioxamine B. Earth Planet. Sci. Lett. 269, 280–290. https://doi.org/10.1016/j.epsl.2008.02.022.

Emerson, D., Fleming, E.J., McBeth, J.M., 2010. Iron-oxidizing bacteria: An environmental and genomic perspective. Annu. Rev. Microbiol. 64, 561–583. https://doi.org/10.1146/annurev.micro.112408.134208.

Emerson, D., Roden, E., Twining, B.S., 2012. The microbial ferrous wheel: iron cycling in terrestrial, freshwater, and marine environments. Front. Microbiol. 3, 383. https://doi.org/10.3389/fmicb.2012.00383.

Emmanuel, S., Erel, Y., Matthews, A., Teutsch, N., 2005. A preliminary mixing model for Fe isotopes in soils. Chem. Geol. 222, 23–34. https://doi.org/10.1016/j.chemgeo.2005.07.002.

Escoube, R., Rouxel, O.J., Sholkovitz, E., Donard, O.F.X., 2009. Iron isotope systematics in estuaries: The case of North River, Massachusetts (USA). Geochim. Cosmochim. Acta 73, 4045–4059. https://doi.org/10.1016/j.gca.2009.04.026.

Escoube, R., Rouxel, O.J., Pokrovsky, O.S., Schroth, A., Holmes, R.M., Donard, O.F.X., 2015. Iron isotope systematics in Arctic rivers. C. R. Geoscience 347, 377–385. https://doi.org/10.1016/j.crte.2015.04.005.

Eusterhues, K., Rennert, T., Knicker, H., Schwertmann, U., 2011. Fractionation of organic matter due to reaction with ferrihydrite: coprecipitation versus adsorption. Environ. Sci. Technol. 45, 527–533. https://doi.org/10.1021/es1023898.

Fantle, M.S., DePaolo, D.J., 2004. Iron isotopic fractionation during continental weathering. Earth Planet. Sci. Lett. 228, 547–562. https://doi.org/10.1016/j.epsl.2004.10.013.

Fekiacova, Z., Pichat, S., Cornu, S., Balesdent, J., 2013. Inferences from the vertical distribution of Fe isotopic compositions on pedogenetic processes in soils. Geoderma 209–210, 110–118. https://doi.org/10.1016/j.geoderma.2013.06.007.

Fekiacova, Z., Vermeire, M.L., Bechon, L., Cornelis, J.T., Cornu, S., 2017. Can Fe isotope fractionations trace the pedogenetic mechanisms involved in podzolization? Geoderma 296, 38–46. https://doi.org/10.1016/j.geoderma.2017.02.020.

Feng, J.-L., Pei, L.-L., Zhu, X., Ju, J.-T., Gao, S.-P., 2018. Absolute accumulation and isotope fractionation of Si and Fe during dolomite weathering and terra rossa formation. Chem. Geol. 476, 340–351. https://doi.org/10.1016/j.chemgeo.2017.11.030.

Fernandez, A., Borrok, D.M., 2009. Fractionation of Cu, Fe, and Zn isotopes during the oxidative weathering of sulfide-rich rocks. Chem. Geol. 264, 1–12. https://doi.org/10.1016/j.chemgeo.2009.01.024.

Frierdich, A.J., Beard, B.L., Reddy, T.R., Scherer, M.M., Johnson, C.M., 2014. Iron isotope fractionation between aqueous Fe(II) and goethite revisited: new insights based on a multi-direction approach to equilibrium and isotopic exchange rate modification. Geochim. Cosmochim. Acta 139, 383–398. https://doi.org/10.1016/j.gca.2014.05.001.

Gaillardet, J., Dupré, B., Allègre, C.J., Négrel, P., 1997. Chemical and physical denudation in the Amazon River Basin. Chem. Geol. 142, 141–173. https://doi.org/10.1016/S0009-2541(97)00074-0.

Garnier, J., Garnier, J.-M., Vieira, C.L., Akerman, A., Chmeleff, J., Ruiz, R.I., Poitrasson, F., 2017. Iron isotope fingerprints of redox and biogeochemical cycling in the soil-water-rice plant system of a paddy field. Sci. Total Environ. 574, 1622–1632. https://doi.org/10.1016/j.scitotenv.2016.08.202.

Gerringa, L.J.A., Alderkamp, A.C., Laan, P., Thuroczy, C.E., De Baar, H.J.W., Mills, M.M., van Dijken, G.L., van Haren, H., Arrigo, K.R., 2012. Iron from melting glaciers fuels the phytoplankton blooms in Amundsen Sea (Southern Ocean): iron bio-geochemistry. Deep-Sea Res. II Top. Stud. Oceanogr. 71–76, 16–31. https://doi.org/10.1016/j.dsr2.2012.03.007.

Gottselig, N., Bol, R., Nischwitz, V., Vereecken, H., Amelung, W., Klumpp, E., 2014. Distribution of phosphorus-containing fine colloids and nanoparticles in stream water of a forest catchment. Vadose Zone J. 13. https://doi.org/10.2136/vzj2014.01.0005.

Gottselig, N., Amelung, W., Kirchner, J.W., Bol, R., Eugster, W., Granger, S.J., Hernández-Crespo, C., Herrmann, F., Keizer, J.J., Korkiakoski, M., Laudon, H., Lehner, I., Löfgren, S., Lohila, A., Macleod, C.J.A., Mölder, M., Müller, C., Nasta, P., Nischwitz, V., Paul-Limoges, E., Pierret, M.C., Pilegaard, K., Romano, N., Sebastià, M.T., Stähli, M., Voltz, M., Vereecken, H., Siemens, J., Klumpp, E., 2017. Elemental composition of natural nanoparticles and fine colloids in European forest stream waters and their role as phosphorus carriers. Global Biogeochem. Cycles 31, 1592–1607. https://doi.org/10.1002/2017GB005657.

Guelke, M., von Blanckenburg, F., 2007. Fractionation of stable iron isotopes in higher plants. Environ. Sci. Technol. 41, 1896–1901. https://doi.org/10.1021/es062288j.

Guelke, M., von Blanckenburg, F., Schoenberg, R., Staubwasser, M., Stuetzel, H., 2010. Determining the stable Fe isotopic signature of plant-available iron in soils. Chem. Geol. 277, 269–280. https://doi.org/10.1016/j.chemgeo.2010.08.010.

Guelke-Stelling, M., von Blanckenburg, F., 2012. Fe isotope fractionation caused by translocation of iron during growth of bean and oat as models of strategy I and II plants. Plant Soil 352, 217–231. https://doi.org/10.1007/s11104-011-0990-9.

Guilbaud, R., Butler, I.B., Ellam, R.M., 2011a. Abiotic pyrite formation produces a large Fe isotope fractionation. Science 332, 1548–1551. https://doi.org/10.1126/science.1202924.

Guilbaud, R., Butler, I.B., Ellam, R.M., Rickard, D., Oldroyd, A., 2011b. Experimental determination of the equilibrium Fe isotope fractionation between Fe^{2+}_{aq} and FeS_m (mackinawite) at 25 and 2 °C. Geochim. Cosmochim. Acta 75, 2721–2734. https://doi.org/10.1016/j.gca.2011.02.023.

Guo, H., Liu, C., Lu, H., Wanty, R.B., Wang, J., Zhou, Y., 2013. Pathways of coupled arsenic and iron cycling in high arsenic groundwater of the Hetao basin, Inner Mongolia, China: An iron isotope approach. Geochim. Cosmochim. Acta 112, 130–145. https://doi.org/10.1016/j.gca.2013.02.031.

Hedrich, S., Schlömann, M., Johnson, D.B., 2011. The iron-oxidizing proteobacteria. Microbiology 157, 1551–1564. https://doi.org/10.1099/mic.0.045344-0.

Hell, R., Stephan, U.W., 2003. Iron uptake, trafficking and homeostasis in plants. Planta 216, 541–551. https://doi.org/10.1007/s00425-002-0920-4.

Henneberry, Y.K., Kraus, T.E.C., Nico, P.S., Horwath, W.R., 2012. Structural stability of coprecipitated natural organic matter and ferric iron under reducing conditions. Org. Geochem. 48, 81–89. https://doi.org/10.1016/J.ORGGEOCHEM.2012.04.005.

Herbel, M.J., Fendorf, S., 2006. Biogeochemical processes controlling the speciation and transport of arsenic within iron coated sands. Chem. Geol. 228, 16–32. https://doi.org/10.1016/j.chemgeo.2005.11.016.

Hill, P.S., Schauble, E.A., Shahar, A., Tonui, E., Young, E.D., 2009. Experimental studies of equilibrium iron isotope fractionation in ferric aquo–chloro complexes. Geochim. Cosmochim. Acta 73, 2366–2381. https://doi.org/10.1016/j.gca.2009.01.016.

Hill, P.S., Schauble, E.A., Young, E.D., 2010. Effects of changing solution chemistry on Fe^{3+}/Fe^{2+} isotope fractionation in aqueous Fe–Cl solutions. Geochim. Cosmochim. Acta 74, 6669–6689. https://doi.org/10.1016/j.gca.2010.08.038.

Huang, L.-M., Jia, X.-X., Zhang, G.-L., Thompson, A., Huang, F., Shao, M.-A., Cheng, L.-M., 2018a. Variations and controls of iron oxides and isotope compositions during paddy soil evolution over a millennial time scale. Chem. Geol. 476, 340–351. https://doi.org/10.1016/j.chemgeo.2017.11.030.

Huang, L.-M., Shao, M.-A., Huang, F., Zhang, G.-L., 2018b. Effects of human activities on pedogenesis and iron dynamics in paddy soils developed on Quaternary red clays. Catena 166, 78–88. https://doi.org/10.1016/j.catena.2018.03.019.

Icopini, G.A., Anbar, A.D., Ruebush, S.S., Tien, M., Brantley, S.L., 2004. Iron isotope fractionation during microbial reduction of iron: The importance of adsorption. Geology 32, 205–208. https://doi.org/10.1130/G20184.1.

Ilina, S.M., Poitrasson, F., Lapitskiy, S.A., Alekhin, Y.V., Viers, J., Pokrovsky, O.S., 2013. Extreme iron isotope fractionation between colloids and particles of boreal and temperate organic-rich waters. Geochim. Cosmochim. Acta 101, 96–111. https://doi.org/10.1016/j.gca.2012.10.023.

Ingri, J., Malinovsky, D., Rodushkin, I., Baxter, D.C., Widerlund, A., Andersson, P., Gustafsson, Ö., Forsling, W., Öhlander, B., 2006. Iron isotope fractionation in river colloidal matter. Earth Planet. Sci. Lett. 245, 792–798. https://doi.org/10.1016/j.epsl.2006.03.031.

Ingri, J., Conrad, S., Lidman, F., Nordblad, F., Engström, E., Rodushkin, I., Porcelli, D., 2018. Iron isotope pathways in the boreal landscape: Role of the riparian zone. Geochim. Cosmochim. Acta 239, 49–60. https://doi.org/10.1016/j.gca.2018.07.030.

Ishimaru, Y., Suzuki, M., Tsukamoto, T., Suzuki, K., Nakazono, M., Kobayashi, T., Wada, Y., Watanabe, S., Matsuhashi, S., Takahashi, M., Nakanishi, H., Mori, S., Nishizawa, N.K., 2006. Rice plants take up iron as an Fe^{3+}-phytosiderophore and as Fe^{2+}. Plant J. 45, 335–346. https://doi.org/10.1111/j.1365-313X.2005.02624.x.

IUSS Working Group WRB, 2014. World Reference Base for Soil Resources 2014. International soil classification system for naming soils and creating legends for soil maps. In: World Soil Resources Reports No. 106. FAO, Rome.

Jang, J.-H., Mathur, R., Liermann, L.J., Ruebush, S., Brantley, S.L., 2008. An iron isotope signature related to electron transfer between aqueous ferrous iron and goethite. Chem. Geol. 250, 40–48. https://doi.org/10.1016/j.chemgeo.2008.02.002.

Jiang, J.-H., Mathur, R., Liermann, L.J., Ruebush, S., Brantley, S.L., 2008. An iron isotopic signature related to electron transfer between aqueous ferrous iron and goethite. Chem. Geol. 250, 40–48. https://doi.org/10.1016/j.chemgeo.2008.02.002.

Johnson, C.M., Beard, B.L., 2006. Fe isotopes: An emerging technique for understanding modern and ancient biogeochemical cycles. GSA Today 16, 4–10. https://doi.org/10.1130/GSAT01611A.1.

Johnson, C.M., Skulan, J.L., Beard, B.L., Sun, H., Nealson, K.H., Braterman, P.S., 2002. Isotopic fractionation between Fe(III) and Fe(II) in aqueous solutions. Earth Planet. Sci. Lett. 195, 141–153. https://doi.org/10.1016/S0012-821X(01)00581-7.

Johnson, C.M., Beard, B.L., Beukes, N.J., Klein, C., O'Leary, J.M., 2003. Ancient geochemical cycling in the Earth as inferred from Fe isotope studies of banded iron formations from the Transvaal Craton. Contrib. Mineral. Petrol. 144, 523–547. https://doi.org/10.1007/s00410-002-0418-x.

Johnson, C.M., Beard, B.L., Roden, E.E., Newman, D.K., Nealson, K.H., 2004. Isotopic constraints on biogeochemical cycling of Fe. Rev. Mineral. Geochem. 55, 359–408. https://doi.org/10.2138/gsrmg.55.1.359.
Johnson, C.M., Roden, E.E., Welch, S.A., Beard, B.L., 2005. Experimental constraints on Fe isotope fractionation during magnetite and Fe carbonate formation coupled to dissimilatory hydrous ferric oxide reduction. Geochim. Cosmochim. Acta 69, 963–993. https://doi.org/10.1016/j.gca.2004.06.043.
Johnson, C.M., Beard, B.L., Roden, E.E., 2008. The iron isotope fingerprints of redox and biogeochemical cycling in the modern and ancient Earth. Ann. Rev. Earth Planet. Sci. 36, 457–493. https://doi.org/10.1146/annurev.earth.36.031207.124139.
Kappler, A., Straub, K.L., 2005. Geomicrobiological cycling of iron. Rev. Mineral. Geochem. 59, 85–108. https://doi.org/10.2138/rmg.2005.59.5.
Kappler, A., Johnson, C.M., Crosby, H.A., Beard, B.L., Newman, D.K., 2010. Evidence for equilibrium iron isotope fractionation by nitrate-reducing iron(II)-oxidizing bacteria. Geochim. Cosmochim. Acta 74, 2826–2842. https://doi.org/10.1016/j.gca.2010.02.017.
Kavner, A., Bonet, F., Shahar, A., Simon, J., Young, E., 2005. The isotopic effects of electron transfer: an explanation for Fe isotope fractionation in nature. Geochim. Cosmochim. Acta 69, 2971–2979. https://doi.org/10.1016/j.gca.2005.01.014.
Kavner, A., Shahar, A., Black, J., Young, E.D., 2009. Iron isotope electroplating: diffusion-limited fractionation. Chem. Geol. 267, 131–138. https://doi.org/10.1016/j.chemgeo.2009.04.018.
Kendall, B., Anbar, A.D., Kappler, A., Konhauser, K.O., 2012. The global iron cycle. In: Knoll, A.H., Canfield, D.E., Konhauser, K.O. (Eds.), Fundamentals of Geobiology, First Edition. Wiley-Blackwell Publishing Ltd. (ISBN: 978-1-4051-8752-7).
Kiczka, M., Wiederhold, J.G., Frommer, J., Kraemer, S.M., Bourdon, B., Kretzschmar, R., 2010a. Iron isotope fractionation during proton- and ligand-promoted dissolution of primary phyllosilicates. Geochim. Cosmochim. Acta 74, 3112–3128. https://doi.org/10.1016/j.gca.2010.02.018.
Kiczka, M., Wiederhold, J.G., Kraemer, S.M., Bourdon, B., Kretzschmar, R., 2010b. Iron isotope fractionation during plant uptake and translocation in alpine plants. Environ. Sci. Technol. 44, 6144–6150. https://doi.org/10.1021/es100863b.
Kiczka, M., Wiederhold, J.G., Frommer, J., Voegelin, A., Kraemer, S.M., Bourdon, B., Kretzschmar, R., 2011. Iron speciation and isotope fractionation during silicate weathering and soil formation in an alpine glacier forefield chronosequence. Geochim. Cosmochim. Acta 75, 5559–5573. https://doi.org/10.1016/j.gca.2011.07.008.
Kiem, R., Kögel-Knabner, I., 2002. Refractory organic carbon in particle-size fractions of arable soils: II. Organic carbon in relation to mineral surface area and iron oxides in fractions < 6 μm. Org. Geochem. 33, 1699–1713. https://doi.org/10.1016/S0146-6380(02)00112-2.
Kim, S.A., Guerinot, M.L., 2007. Mining iron: Iron uptake and transport in plants. FEBS Lett. 581, 2273–2280. https://doi.org/10.1016/j.febslet.2007.04.043.
Kobayashi, T., Nishizawa, N.K., 2012. Iron uptake, translocation, and regulation in higher plants. Annu. Rev. Plant Biol. 63, 131–152. https://doi.org/10.1146/annurev-arplant-042811-105522.
Kögel-Knabner, I., Amelung, W., Cao, Z., Fiedler, S., Frenzel, P., Jahn, R., Kalbitz, K., Kölbl, A., Schloter, M., 2010. Biogeochemistry of paddy soils. Geoderma 157, 1–14. https://doi.org/10.1016/j.geoderma.2010.03.009.
Kusonwiriyawong, C., Bigalke, M., Abgottspon, F., Lazarov, M., Schuth, S., Weyer, S., Wilcke, W., 2017. Isotopic variation of dissolved and colloidal iron and copper in a carbonatic floodplain soil after experimental flooding. Chem. Geol. 459, 13–23. https://doi.org/10.1016/j.chemgeo.2017.03.033.
Lead, J.R., Wilkinson, K.J., 2007. Environmental colloids and particles: current knowledge and future developments. In: Lead, J.R., Wilkinson, K.J. (Eds.), Environmental Colloids and Particles Behaviour, Separation and Characterisation. IUPAC Series on Analytical and Physical Chemistry of Environmental Systems. vol. 10 John Wiley & Sons, Ltd, West Sussex. https://doi.org/10.1002/9780470024539. ISBN: 9780470024324 (PB), ISBN: 9780470024539 (E-book).
Li, M., He, Y.-S., Kang, J.-T., Yang, X.-Y., He, Z.-W., Yu, H.-M., Huang, F., 2017. Why was iron lost without significant isotope fractionation during the lateritic process in tropical environments? Geoderma 290, 1–9. https://doi.org/10.1016/j.geoderma.2016.12.003.
Liu, S.-A., Teng, F.-Z., Li, S., Wei, G.-J., Ma, J.-L., Li, D., 2014. Copper and iron isotope fractionation during weathering and pedogenesis: Insights from saprolite profiles. Geochim. Cosmochim. Acta 146, 59–75. https://doi.org/10.1016/j.gca.2014.09.040.
Liu, K., Wu, L., Couture, R.-M., Li, W., Van Cappellen, P., 2015. Iron isotope fractionation in sediments of an oligotrophic freshwater lake. Earth Planet. Sci. Lett. 423, 164–172. https://doi.org/10.1016/j.epsl.2015.05.010.
Lovley, D.R., Holmes, D.E., Nevin, K.P., 2004. Dissimilatory Fe(III) and Mn(IV) reduction. Adv. Microb. Physiol. 49, 219–286. https://doi.org/10.1016/S0065-2911(04)49005-5.
Malinovsky, D.N., Rodyushkin, I.V., Shcherbakova, E.P., Ponter, C., Öhlander, B., Ingri, J., 2005. Fractionation of Fe isotopes as a result of redox processes in a basin. Geochem. Int. 43, 797–803.
Mandernack, K.W., Bazylinski, D.A., Shanks, W.C., Bullen, T.D., 1999. Oxygen and Iron Isotope Studies of Magnetite Produced by Magnetotactic Bacteria. Science 285, 1892–1896. https://doi.org/10.1126/science.285.5435.1892.
Mansfeldt, T., Schuth, S., Häusler, W., Wagner, F.E., Kaufhold, S., Overesch, M., 2012. Iron oxide mineralogy and stable iron isotope composition in a Gleysol with petrogleyic properties. J. Soils Sediments 12, 97–114. https://doi.org/10.1007/s11368-011-0402-z.
Marschner, H., 1995. Mineral Nutrition of Higher Plants. Academic Press, London (ISBN: 9780124735439 (PB), ISBN: 9780080571874 (Ebook)).
Martin, J.M., Fitzwater, S.E., 1988. Iron deficiency limits phytoplankton growth in the north-East Pacific subarctic. Nature 331, 341–343. https://doi.org/10.1038/331341a0.
Matthews, A., Zhu, X.-K., O'Nions, K., 2001. Kinetic iron stable isotope fractionation between iron (-II) and (-III) complexes in solution. Earth Planet. Sci. Lett. 192, 81–92. https://doi.org/10.1016/s0012-821x(01)00432-0.
Meade, R.H., Dunne, T., Richey, J.E., De, M., Santos, U., Salati, E., 1985. Storage and remobilization of suspended sediment in the lower Amazon River of Brazil. Science 228, 488–490. https://doi.org/10.1126/science.228.4698.488.
Mehra, O.P., Jackson, M.L., 1958. Iron oxide removal from soils and clays by a dithionite-citrate system buffered with sodium bicarbonate. Clay Clay Miner. 7, 317–327. https://doi.org/10.1016/B978-0-08-009235-5.50026-7.
Melton, E.D., Swanner, E.D., Behrens, S., Schmidt, C., Kappler, A., 2014. The interplay of microbially mediated and abiotic reactions in the biogeochemical Fe cycle. Nature Rev. Microbiol. 12, 797–808. https://doi.org/10.1038/nrmicro3347.
Michel, F.M., Barrón, V., Torrent, J., Morales, M.P., Serna, C.J., Boily, J.-F., Liu, Q., Ambrosini, A., Cismasu, A.C., Brown Jr., G.E., 2010. Ordered ferrimagnetic form of ferrihydrite reveals links among structure, composition, and magnetism. PNAS 107, 2787–2792. https://doi.org/10.1073/pnas.0910170107.
Mikutta, C., Wiederhold, J.G., Cirpka, O.A., Hofstetter, T.B., Bourdon, B., Von Gunten, U., 2009. Iron isotope fractionation and atom exchange during sorption of ferrous iron to mineral surfaces. Geochim. Cosmochim. Acta 73, 1795–1812. https://doi.org/10.1016/j.gca.2009.01.014.
Morgan, J.L.L., Wasylenki, L.E., Nuester, J., Anbar, A.D., 2010. Fe Isotope Fractionation during Equilibration of Fe − Organic Complexes. Environ. Sci. Technol. 44, 6095–6101. https://doi.org/10.1021/es100906z.
Mori, S., 1999. Iron acquisition by plants. Curr. Opin. Plant Biol. 2, 250–253. https://doi.org/10.1016/S1369-5266(99)80043-0.
Moynier, F., Fujii, T., Wang, K., Foriel, J., 2013. Ab initio calculations of the Fe (II) and Fe (III) isotopic effects in citrates, nicotianamine, and phytosiderophore, and new Fe isotopic measurements in higher plants. Compt. Rendus Geosci. 345, 230–240. https://doi.org/10.1016/j.crte.2013.05.003.
Mulholland, D.S., Poitrasson, F., Boaventura, G.R., Allard, T., Vieira, L.C., Santos, R.V., Mancini, L., Seyler, P., 2015a. Insights into iron sources and pathways in the Amazon River provided by isotopic and spectroscopic studies. Geochim. Cosmochim. Acta 150, 142–159. https://doi.org/10.1016/j.gca.2014.12.004.
Mulholland, D.S., Poitrasson, F., Shirokova, L.S., González, A.G., Pokrovsky, O.S., Boaventura, G.R., Vieira, L.C., 2015b. Iron isotope fractionation during Fe(II) and Fe (III) adsorption on cyanobacteria. Chem. Geol. 400, 24–33. https://doi.org/10.1016/j.chemgeo.2015.01.017.
Nie, N.X., Dauphas, N., Greenwood, R.C., 2017. Iron and oxygen isotope fractionation during iron UV photo-oxidation: Implications for early Earth and Mars. Earth Planet. Sci. Lett. 458, 179–191. https://doi.org/10.1016/j.epsl.2016.10.035.
Nikolic, M., Römheld, V., 2007. The dynamics of iron in the leaf apoplast. In: Sattelmacher, B., Horst, W.J. (Eds.), The Apoplast of Higher Plants: Compartment of Storage, Transport and Reactions. Springer, Netherlands (ISBN: 978-1-4020-5842-4 (PB), ISBN: 978-1-4020-5843-1 (Ebook)).
Opfergelt, S., Williams, H.M., Cornelis, J.T., Guicharnaud, R.A., Georg, R.B., Siebert, C., Gislason, S.R., Halliday, A.N., Burton, K.W., 2017. Iron and silicon isotope behaviour accompanying weathering in Icelandic soils, and the implications for iron export from peatlands. Geochim. Cosmochim. Acta 217, 273–291. https://doi.org/10.1016/j.gca.2017.08.033.
Patrick Jr., W.H., Khalid, R.A., 1974. Phosphate release and sorption by soils and sediments: effect of aerobic and anaerobic conditions. Science 186, 53–55. https://doi.org/10.1126/science.186.4158.53.
Peretyazhko, T., Sposito, G., 2005. Iron(III) reduction and phosphorous solubilization in humid tropical forest soils. Geochim. Cosmochim. Acta 69, 3643–3652. https://doi.org/10.1016/j.gca.2005.03.045.
Pich, A., Scholz, G., Stephan, U.W., 1994. Iron-dependent changes of heavy metals, nicotianamine, and citrate in different plant organs and in the xylem exudate of two tomato genotypes. Nicotianamine as possible copper translocator. Plant Soil 165, 189–196. https://doi.org/10.1007/BF00008061.
Poitrasson, F., 2006. On the iron isotope homogeneity level of the continental crust. Chem. Geol. 235, 195–200. https://doi.org/10.1016/j.chemgeo.2006.06.010.
Poitrasson, F., Freydier, R., 2005. Heavy iron isotope composition of granites determined by high resolution MC-ICP-MS. Chem. Geol. 222, 132–147. https://doi.org/10.1016/j.chemgeo.2005.07.005.
Poitrasson, F., Viers, J., Martin, F., Braun, J.-J., 2008. Limited iron isotope variations in recent lateritic soils from Nsimi, Cameroon: Implications for the global Fe geochemical cycle. Chem. Geol. 253, 54–63. https://doi.org/10.1016/j.chemgeo.2008.04.011.
Poitrasson, F., Vieira, L.C., Seyler, P., dos Santos Pinheiro, G.M., Mulholland, D.S., Bonnet, M.-P., Martinez, J.-M., Lima, B.A., Boaventura, G.R., Chmeleff, J., Dantas, E.L., Guyot, J.-L., Mancini, L., Pimentel, M.M., Santos, R.V., Sondag, F., Vauchel, P., 2014. Iron isotope composition of the bulk waters and sediments from the Amazon River Basin. Chem. Geol. 377, 1–11. https://doi.org/10.1016/j.chemgeo.2014.03.019.
Polyakov, V.B., 1997. Equilibrium fractionation of the iron isotopes: Estimation from Mössbauer spectroscopy data. Geochim. Cosmochim. Acta 61, 4213–4217. https://doi.org/10.1016/S0016-7037(97)00204-4.
Polyakov, V.B., Mineev, S.D., 2000. The use of Mössbauer spectroscopy in stable isotope geochemistry. Geochim. Cosmochim. Acta 64, 849–865. https://doi.org/10.1016/S0016-7037(99)00329-4.
Raiswell, R., Canfield, D.E., 2012. The iron biogeochemical cycle past and present. Geochem. Perspect. 1, 1–232. https://doi.org/10.7185/geochempersp.1.1.
Reddy, T.R., Frierdich, A.J., Beard, B.L., Johnson, C.M., 2015. The effect of pH on stable iron isotope exchange and fractionation between aqueous Fe(II) and goethite. Chem. Geol. 397, 118–127. https://doi.org/10.1016/j.chemgeo.2015.01.018.

Robinson, N.J., Procter, C.M., Connolly, E.L., Guerinot, M.L., 1999. A ferric-chelate reductase for iron uptake from soils. Nature 397, 694–697. https://doi.org/10.1038/17800.
Rodríguez, N.P., Engström, E., Rodushkin, I., Nason, P., Alakangas, L., Öhlander, B., 2013. Copper and iron isotope fractionation in mine tailings at the Laver and Kristineberg mines, northern Sweden. Appl. Geochem. 32, 204–215. https://doi.org/10.1016/j.apgeochem.2012.10.012.
Rodríguez, N.P., Langella, F., Rodushkin, I., Engström, E., Kothe, E., Alakangas, L., Öhlander, B., 2014. The role of bacterial consortium and organic amendment in Cu and Fe isotope fractionation in plants on a polluted mine site. Environ. Sci. Pollut. Res. 21, 6836–6844. https://doi.org/10.1007/s11356-013-2156-1.
Rodríguez, N.P., Khoshkhoo, M., Sandström, Å., Rodushkin, I., Alakangas, L., Öhlander, B., 2015. Isotopic signature of Cu and Fe during bioleaching and electrochemical leaching of a chalcopyrite concentrate. Int. J. Miner. Process. 134, 58–65. https://doi.org/10.1016/j.minpro.2014.11.010.
Rodushkin, I., Stenberg, A., Andrén, H., Malinovsky, D., Baxter, D.C., 2004. Isotopic fractionation during diffusion of transition metal Ions in solution. Anal. Chem. 76, 2148–2151. https://doi.org/10.1021/ac035296g.
Roe, J.E., Anbar, A.D., Barling, J., 2003. Nonbiological fractionation of Fe isotopes: evidence of an equilibrium isotope effect. Chem. Geol. 195, 69–85. https://doi.org/10.1016/S0009-2541(02)00389-3.
Roebbert, Y., Rabe, K., Lazarov, M., Schuth, S., Schippers, A., Dold, B., Weyer, S., 2018. Fractionation of Fe and Cu isotopes in acid mine tailings: Modification and application of a sequential extraction method. Chem. Geol. 493, 67–79. https://doi.org/10.1016/j.chemgeo.2018.05.026.
Roemheld, V., Marschner, H., 1986. Evience for a specific uptake system for iron phytosiderophores in roots of grasses. Plant Physiol. 80, 175–180. https://doi.org/10.1104/pp.80.1.175.
Rouxel, O., Dobbek, N., Ludden, J., Fouquet, Y., 2003. Iron isotope fractionation during oceanic crust alteration. Chem. Geol. 202, 155–182. https://doi.org/10.1016/j.chemgeo.2003.08.011.
Rouxel, O., Sholkovitz, E., Charette, M., Edwards, K.J., 2008. Iron isotope fractionation in subterranean estuaries. Geochim. Cosmochim. Acta 72, 3413–3430. https://doi.org/10.1016/j.gca.2008.05.001.
Rouxel, O., Toner, B., Germain, Y., Glazer, B., 2018. Geochemical and iron isotopic insights into hydrothermal iron oxyhydroxide deposit formation at Loihi Seamount. Geochim. Cosmochim. Acta 220, 449–482. https://doi.org/10.1016/j.gca.2017.09.050.
Rue, E.L., Bruland, K.W., 1997. The role of organic complexation on ambient iron chemistry in the equatorial Pacific Ocean and the response of a mesoscale iron addition experiment. Limnol. Oceanogr. 42, 901–910. https://doi.org/10.4319/lo.1997.42.5.0901.
dos Santos Pinheiro, G.M., Poitrasson, F., Sondag, F., Vieira, L.C., Pimentel, M.M., 2013. Iron isotope composition of the suspended matter along depth and lateral profiles in the Amazon River and its tributaries. J. S. Am. Earth Sci. 44, 35e44. https://doi.org/10.1016/j.jsames.2012.08.001.
dos Santos Pinheiro, G.M., Poitrasson, F., Sondag, F., Cochonneau, G., Vieira, L.C., 2014. Contrasting iron isotopic compositions in river suspended particulate matter: the Negro and the Amazon annual river cycles. Earth Planet. Sci. Lett. 394, 168–178. https://doi.org/10.1016/j.epsl.2014.03.006.
Sattelmacher, B., 2001. The apoplast and its significance for plant mineral nutrition. New Phytol. 149, 167–192. https://doi.org/10.1046/j.1469-8137.2001.00034.x.
Schaaf, G., Ludewig, U., Erenoglu, B.E., Mori, S., Kitahara, T., von Wirén, N., 2004. ZmYS1 functions as a proton-coupled symporter for phytosiderophore- and nicotianamine-chelated metals. J. Biol. Chem. 279, 9091–9096. https://doi.org/10.1074/jbc.M311799200.
Schauble, E.A., 2004. Applying stable isotope fractionation theory to new systems. Rev. Mineral. Geochem. 55, 65–111. https://doi.org/10.2138/gsrmg.55.1.65.
Schauble, E.A., Rossman, G.R., Taylor Jr., H.P., 2001. Theoretical estimates of equilibrium Fe-isotope fractionations from vibrational spectroscopy. Geochim. Cosmochim. Acta 65, 2487–2497. https://doi.org/10.1016/S0016-7037(01)00600-7.
Schroth, A.W., Crusius, J., Chever, F., Bostick, B.C., Rouxel, O.J., 2011. Glacial influence on the geochemistry of riverine iron fluxes to the Gulf of Alaska and effects of deglaciation. Geophys. Res. Let. 38, L16605. https://doi.org/10.1029/2011GL048367.
Schuth, S., Mansfeldt, T., 2016. Iron isotope composition of aqueous phases of a lowland environment. Environ. Chem. 13, 89–101. https://doi.org/10.1071/EN15073.
Schuth, S., Hurraß, J., Münker, C., Mansfeldt, T., 2015. Redox-dependent fractionation of iron isotopes in suspensions of a groundwater-influenced soil. Chem. Geol. 392, 74–86. https://doi.org/10.1016/j.chemgeo.2014.11.007.
Schwertmann, U., 1964. Differenzierung der Eisenoxide des Bodens durch Extraktion mit Ammoniumoxalat-Lösung. In: Zeitschrift für Pflanzenernährung und Bodenkunde 105, pp. 194–202. https://doi.org/10.1002/jpln.3591050303.
Schwertmann, U., 1991. Solubility and dissolution of iron oxides. Plant Soil 130, 1–25. https://doi.org/10.1007/BF00011851.
Shi, B., Liu, K., Wu, L., Li, W., Smeaton, C.M., Beard, B.L., Johnson, C.M., Roden, E.E., Van Cappellen, P., 2016. Iron isotope fractionations reveal a finite bioavailable Fe pool for structural Fe(III) reduction in nontronite. Environ. Sci. Technol. 50, 8661–8669. https://doi.org/10.1021/acs.est.6b02019.
Skulan, J.L., Beard, B.L., Johnson, C.M., 2002. Kinetic and equilibrium Fe isotope fractionation between aqueous Fe(III) and hematite. Geochim. Cosmochim. Acta 2002 (66), 2995–3015. https://doi.org/10.1016/S0016-7037(02)00902-X.
Song, L., Liu, C.-Q., Wang, Z.-L., Zhu, X., Teng, Y., Liang, L., Tang, S., Li, J., 2011. Iron isotope fractionation during biogeochemical cycle: Information from suspended particulate matter (SPM) in Aha Lake and its tributaries, Guizhou. China. Chem. Geol. 280, 170–179. https://doi.org/10.1016/j.chemgeo.2010.11.006.
Straub, K.L., Benz, M., Schink, B., Widdel, F., 1996. Anaerobic, nitrate-dependent microbial oxidation of ferrous iron. Appl. Environ. Microbiol. 62, 1458–1460.
Stucki, J.W., 1988. Structural iron in smectites. In: Stucki, J.W., Goodman, B.A., Schwertmann, D. (Eds.), Iron in Soils and Clay Minerals. Reidel Publishing Company, Dordrecht, pp. 625–675 (ISBN: 978-94-010-8278-5 (PB), ISBN: 978-94-009-4007-9 (Ebook)).
Stumm, W., 1992. Chemistry of the Solid-Water Interface: Processes at the Mineral Water and Particle-Water Interface in Natural Systems. Wiley, New York (ISBN: 978-0-471-57672-3).
Stumm, W., Morgan, J.J., 1996. Aquatic Chemistry: Chemical Equilibria and Rates in Natural Waters. John Wiley & Sons, New York (ISBN: 978-0-471-51185-4).
Sun, R., Wang, B., 2018. Iron isotope fractionation during uptake of ferrous ion by phytoplankton. Chem. Geol. 481, 65–73. https://doi.org/10.1016/j.chemgeo.2018.01.031.
Swanner, E.D., Bayer, T., Wu, W., Hao, L., Obst, M., Sundman, A., Byrne, J.M., Michel, F.M., Kleinhanns, I.C., Kappler, A., Schoenberg, R., 2017. Iron isotope fractionation during Fe(II) oxidation mediated by the oxygen-producing marine cyanobacterium *Synechococcus* PCC 7002. Environ. Sci. Technol. 51, 4897–4906. https://doi.org/10.1021/acs.est.6b05833.
Swanner, E.D., Wu, W., Schoenberg, R., Byrne, J., Michel, F.M., Pan, Y., Kappler, A., 2015. Fractionation of Fe isotopes during Fe(II) oxidation by a marine photoferrotroph is controlled by the formation of organic Fe-complexes and colloidal Fe fractions. Geochim. Cosmochim. Acta 165, 44–61. https://doi.org/10.1016/j.gca.2015.05.024.
Takagi, S., Nomoto, K., Takemoto, T., 1984. Physiological aspect of mugineic acid, a possible phytosiderophore of graminaceous plants. J. Plant Nutr. 7, 469–477. https://doi.org/10.1080/01904168409363213.
Teng, F.-Z., Dauphas, N., Helz, R.T., 2008. Iron isotope fractionation during magmatic differentiation in Kilauea Iki Lava Lake. Science 320, 1620–1622. https://doi.org/10.1126/science.1157166.
Tessier, A., Campbell, P.G.C., Bisson, M., 1979. Sequential extraction procedure for the speciation of particulate trace-metals. Anal. Chem. 51, 844–851. https://doi.org/10.1021/ac50043a017.
Teutsch, N., von Gunten, U., Porcelli, D., Cirpka, O.A., Halliday, A.N., 2005. Adsorption as a cause for iron isotope fractionation in reduced groundwater. Geochim. Cosmochim. Acta 69, 4175–4185. https://doi.org/10.1016/j.gca.2005.04.007.
Teutsch, N., Schmid, M., Müller, B., Halliday, A.N., Bürgmann, H., Wehrli, B., 2009. Large iron isotope fractionation at the oxic–anoxic boundary in Lake Nyos. Earth Planet. Sci. Lett. 285, 52–60. https://doi.org/10.1016/j.epsl.2009.05.044.
Thompson, A., Ruiz, J., Chadwick, O.A., Titus, M., Chorover, J., 2007. Rayleigh fractionation of iron isotopes during pedogenesis along a climate sequence of Hawaiian basalt. Chem. Geol. 238, 72–83. https://doi.org/10.1016/j.chemgeo.2006.11.005.
Tsukamoto, T., Nakanishi, H., Uchida, H., Watanabe, S., Matsuhashi, S., Mori, S., Nishizawa, N.K., 2008. ^{52}Fe translocation in barley as monitored by a positron-emitting tracer imaging system (PETIS): evidence for the direct translocation of Fe from roots to young leaves via phloem. Plant Cell Physiol. 50, 48–57. https://doi.org/10.1093/pcp/pcn192.
van Breemen, N., Buurman, P., 2002. Soil Formation. Kluwer Academic Publishers, The Netherlands (ISBN: 978-0-306-48163-5).
Vanhaecke, F., Degryse, P., 2012. Isotopic analysis: fundamentals and applications using ICP-MS. In: Wiley-VCH Verlag & Co. KGaA, Weinheim (ISBN: 978-3-527-32896-3).
von Blanckenburg, F., von Wirén, N., Guelke, M., Weiss, D.J., Bullen, T.D., 2009. Fractionation of metal stable isotopes by higher plants. Elements 5, 375–380. https://doi.org/10.2113/gselements.5.6.375.
von Wirén, N., Klair, S., Bansal, S., Briat, J.-F., Khodr, H., Shioiri, T., Leigh, R.A., Hider, R.C., 1999. Nicotianamine chelates both Fe^{III} and Fe^{II}. Implications for metal transport in plants. Plant Physiol. 119, 1107–1114. https://doi.org/10.1104/pp.119.3.1107.
Wang, Y., Xie, X., Johnson, T.M., Lundstrom, C.C., Ellis, A., Wang, X., Duan, M., Li, J., 2014. Coupled iron, sulfur and carbon isotope evidences for arsenic enrichment in groundwater. J. Hydrol. 519, 414–422. https://doi.org/10.1016/j.jhydrol.2014.07.028.
Wasylenki, L.E., Anbar, A.D., Liermann, L.J., Mathur, R., Gordona, G.W., Brantley, S.L., 2007. Isotope fractionation during microbial metal uptake measured by MC-ICP-MS. J. Anal. At. Spectrom. 22, 905–910. https://doi.org/10.1039/b705476a.
Weber, K.A., Achenbach, L.A., Coates, J.D., 2006. Microorganisms pumping iron: anaerobic microbial iron oxidation and reduction. Nature 4, 752–764. https://doi.org/10.1038/nrmicro1490.
Welch, S.A., Beard, B.L., Johnson, C.M., Braterman, P.S., 2003. Kinetic and equilibrium Fe isotope fractionation between aqueous Fe(II) and Fe(III). Geochim. Cosmochim. Acta 67, 4231–4250. https://doi.org/10.1016/S0016-7037(03)00266-7.
Wiederhold, J.G., 2015. Metal stable isotopic signatures as tracers in environmental geochemistry. Environ. Sci. Technol. 2015 (49), 2606–2624. https://doi.org/10.1021/es504683e.
Wiederhold, J.G., Kraemer, S.M., Teutsch, N., Borer, P.M., Halliday, A.N., Kretzschmar, R., 2006. Iron isotope fractionation during proton-promoted, ligand-controlled, and reductive dissolution of goethite. Environ. Sci. Technol. 40, 3787–3793. https://doi.org/10.1021/es052228y.
Wiederhold, J.G., Teutsch, N., Kraemer, S.M., Halliday, A.N., Kretzschmar, R., 2007a. Iron isotope fractionation during pedogenesis in redoximorphic soils. Soil Sci. Soc. Am. J. 71, 1840–1850. https://doi.org/10.2136/sssaj2006.0379.
Wiederhold, J.G., Teutsch, N., Kraemer, S.M., Halliday, A.N., Kretzschmar, R., 2007b. Iron isotope fractionation in oxic soils by mineral weathering and podzolization. Geochim. Cosmochim. Acta 71, 5821–5833. https://doi.org/10.1016/j.gca.2007.07.023.
Wiesli, R.A., Beard, B.L., Johnson, C.M., 2004. Experimental determination of Fe isotope fractionation between aqueous Fe(II), siderite and “green rust” in abiotic systems.

Chem. Geol. 211, 343–362. https://doi.org/10.1016/j.chemgeo.2004.07.002.
Wolfe, A.L., Stewart, B.W., Capo, R.C., Liu, R., Dzombak, D.A., Gordon, G.W., Anbar, A.D., 2016. Iron isotope investigation of hydrothermal and sedimentary pyrite and their aqueous dissolution products. Chem. Geol. 427, 73–82. https://doi.org/10.1016/j.chemgeo.2016.02.015.
Wu, L., Beard, B.L., Roden, E.E., Johnson, C.M., 2009. Influence of pH and dissolved Si on Fe isotope fractionation during dissimilatory microbial reduction of hematite. Geochim. Cosmochim. Acta 73, 5584–5599. https://doi.org/10.1016/j.gca.2009.06.026.
Wu, L., Beard, B.L., Roden, E.E., Kennedy, C.B., Johnson, C.M., 2010. Stable Fe isotope fractionations produced by aqueous Fe(II)-hematite surface interactions. Geochim. Cosmochim. Acta 74, 4249–4265. https://doi.org/10.1016/j.gca.2010.04.060.
Wu, L., Beard, B.L., Roden, E.E., Johnson, C.M., 2011. Stable iron isotope fractionation between aqueous Fe(II) and hydrous ferric oxide. Environ. Sci. Technol. 45, 1847–1852. https://doi.org/10.1021/es103171x.
Wu, L., Druschel, G., Findlay, A., Beard, B.L., Johnson, C.M., 2012a. Experimental determination of iron isotope fractionations among Fe^{2+}_{aq}–FeS_{aq}–Mackinawite at low temperatures: Implications for the rock record. Geochim. Cosmochim. Acta 89, 46–61. https://doi.org/10.1016/j.gca.2012.04.047.
Wu, L., Percak-Dennett, E.M., Beard, B.L., Roden, E.E., Johnson, C.M., 2012b. Stable iron isotope fractionation between aqueous Fe(II) and model Archean ocean Fe–Si co-precipitates and implications for iron isotope variations in the ancient rock record. Geochim. Cosmochim. Acta 84, 14–28. https://doi.org/10.1016/j.gca.2012.01.007.
Xie, X., Johnson, T.M., Wanga, Y., Lundstrom, C.C., Ellis, A., Wang, X., Duan, M., Li, J., 2014. Pathways of arsenic from sediments to groundwater in the hyporheic zone: evidence from an iron isotope study. J. Hydrol. 511, 509–517. https://doi.org/10.1016/j.jhydrol.2014.02.006.
Yamaguchi, K.E., Johnson, C.M., Beard, B.L., Beukes, N.J., Gutzmer, J., Ohmoto, H., 2007. Isotopic evidence for iron mobilization during Paleoproterozoic lateritization of the Hekpoort paleosol profile from Gaborone, Botswana. Earth Planet. Sci. Lett. 256, 577–587. https://doi.org/10.1016/j.epsl.2007.02.010.
Zhang, R., John, S.G., Zhang, J., Ren, J., Wu, Y., Zhu, Z., Liu, S., Zhu, X., Marsay, C.M., Wenger, F., 2015. Transport and reaction of iron and iron stable isotopes in glacial meltwaters on Svalbard near Kongsfjorden: from rivers to estuary to ocean. Earth Planet. Sci. Lett. 424, 201–211. https://doi.org/10.1016/j.epsl.2015.05.031.